Dynamic Analysis of Musculoskeletal System Performances during Human Standing and Walking

Chen, Lin

Awarding institution:
King's College London

Title: Dynamic Analysis of Musculoskeletal System Performances during Human Standing and Walking

Author: Lin Chen

KING'S College LONDON

University of London

Dynamic Analysis of Musculoskeletal System Performances during Human Standing and Walking

Lin CHEN

A dissertation submitted in fulfillment of the requirements for the degree of

Doctor of Philosophy in Mechanical Engineering

Division of Engineering, King's College London, University of London

December 2012

Abstract

The objective of this thesis is to develop the computational methodologies for investigating the musculoskeletal system performance during human standing and walking, which can lead to a better understanding of the musculoskeletal functions in standing balance and locomotion, and hence to improve clinical diagnosis, treatments and also rehabilitation interventions.

Firstly, an improved Hill-type muscle model was developed to describe the dynamic response of a musculotendon unit subjected to neural excitation by considering more physiological characteristics of skeletal muscles. The dynamic process from neural input through to muscular force generation was represented using two processes: neural excitation dynamics and muscle activation dynamics. The improved muscle model has been used throughout the thesis for musculoskeletal analysis.

An inverted pendulum model driven by a pair of antagonistic muscles was developed to simulate human standing in the sagittal plane. A set of dynamic simulations has been used to investigate the effect of muscle intrinsic properties on system stability. It is found that the force-velocity relationship of the muscle contractile element has the most significant impact on the dynamic stability of the musculoskeletal system.

Thereafter, a musculoskeletal model with six ankle flexor and extensor muscles, which was combined with a multi-objective optimization scheme had been constructed to investigate the interplay between energy cost and body stability during standing balance. The simulation results suggest that there is a very strong dependence between energy expenditure and body stability during standing postural control, and energy expenditure appears to be a primary consideration in standing balance.

To simulate human walking biomechanics, a three-dimensional musculoskeletal model with 13 body segments and 98 muscle groups was constructed using OpenSim software. The gait measurement database provided by Grant Challenge Competition was used to support the modelling. A set of bone scaling and inverse kinematics procedures was used to refine the model to fit to the subject-specific anthropometric and kinematic dataset. The refined model generated reasonable muscle moment arm and net muscle moment data over a complete walking cycle.

Finally, a novel computational framework has been developed to evaluate the mechanical loadings at each individual skeletal muscle group during human walking by integrating a forward dynamics formulation of the muscle contraction dynamics into an inverse dynamics based static optimization scheme. The experimental validation against the measured force sensor data suggested that the approach proposed here provided more accurate estimation of the muscular loadings than the conventional static optimization method and also the OpenSim software.

Acknowledgement

Firstly, I wish to thank my supervisors Professor Jian S Dai and Dr. Lei Ren for their supervisions during these four years. I am especially grateful to Dr Lei Ren for his encouraging support, patient guidance and personal attention throughout this research. His invaluable constructive suggestions and numerous exhaustive long discussions have been a driving force and formed a solid basis to the fulfillment of the goals of this work.

I would like to extend many thanks to my colleagues and friends, particularly to Dr. Qi Zhong, Dr. Jining Sun, Ms. Amaraporn Boonpratatong, Dr. Lei Cui, Dr. Helge wuerdemann, Dr. Peng Yu and many others at King's College London and University of Manchester.

Huge thanks go to my parents, my grandparents and my uncle, for their love, their generosity and their selflessness. Without their unwavering support throughout this period, my work would not have been completed. To them, I dedicate this thesis.

The work is sponsored by China Scholarship Council, and their support is gratefully acknowledged.

CONTENTS

LIST OF FIGURES

LIST OF TABLES

Nomenclature

q_a	output of calcium release and re-uptake process
x_a	output of calcium binding to troponin process
a_a, m, k	Parameter from calcium release and re-uptake and calcium binding to troponin process
C_n	${C_a}^{2+}$ complex
R_i	parameter for accounting for the non-linear summation
P_0	maximum isometric force in Hill muscle model
a_H	coefficient of shortening heat in Hill muscle model
V_0	maximum velocity (when $P = 0$) in Hill muscle model
b	variable dependent on a, V_0, P_0 in Hill muscle model
P	muscle force in Hill muscle model
B, K	constant in Fenn muscle model
V_{0f}	shortening velocity of an unload muscle in Fenn muscle model
P_f	muscle force in Fenn muscle model
V^M	muscle contraction velocity in Thelen muscle model
a_T	muscle activation in Thelen muscle model
V_{max}^M	the maximum contraction velocity in Thelen muscle model
$\bar{F}^M$	normalized muscle force in Thelen muscle model
f_{lT}	muscle force at the current muscle length in Thelen muscle model
b_T	muscle shorting velocity parameter
$\bar{F}_{len}^M$	maximum normalized muscle force when the muscle is lengthening in Thelen muscle model
A_f	force-velocity shape factor in Thelen muscle model
L_O^M	optimal muscle fibre length in Anderson muscle model
$\tilde{V}_{max}$	maximum contraction velocity in Anderson muscle model
$\tilde{F}_V^M$	the muscle force generated when muscle contracts in Anderson muscle model
$\dot{L}^M$	muscle contraction velocity in Anderson muscle model
F_{ce}	contractile element force
a	muscle activation
f_l	force from force-length relation
f_v	force from force-velocity relation
F_m	total muscle force
F_{pe}	parallel element force
M	system mass matrix
C	centrifugal and coriolis loading
G	gravitational loading
E	external forces
R	muscle moment arms
F_{MT}	muscle forces
U, E, A	neural input, neural excitation and muscle activation
T_{ne} , T_a	time constant of neural excitation and muscle activation
TI	time step

F_{f-l}	normalized force from force-length relationship
L_m	muscle fibre length
L_f	muscle fibre belly length
L_{mo}	optimal muscle fibre length
F_{mo}	maximum isometric muscle fibre force
α	pennation angle
L_{fo}	the muscle fibre belly length corresponding to the muscle fibre length L_{mo}
F_{f-v}	normalized force from force-velocity relationship
v_m	muscle contraction velocity
$v_{\max}$	maximum muscle shortening velocity
F_t	series elastic element force
L_t	series elastic element length
SE_{sh}, SE_{xm}	mechanical parameters, varying as tendon type differs
w	weight for multi-objective optimization
x_i^{exp}	experimental position of marker i
x_i	the position of the corresponding marker on the model
q_j^{exp}	experimental value for coordinate j
w_i	the i^{th}marker weight
ω_j	the j^{th} coordinate weight
τ	vector of generalized forces
a_m	activation level of muscle
F_m^0	maximum isometric force
$r_{m,j}$	the i^{th} moment arm about the j^{th} joint axis
τ_j	the generalized force acting about the j^{th} joint axis
p	constant in objective function
F_{moo}	maximum isometric muscle fibre force from the scaled model in OpenSim
R_m	muscle moment arms
T_m	net muscle moments
L_{sto}	slack tendon length scaled by geometrical method in OpenSim
$PCSA_i$	the i^{th} muscle's Physiological Cross-sectional Area
V_m	The i^{th} muscle's volume
$\vec{F}_{con}$	knee joint contact force
$\vec{F}_{m,i}$	summation of individual muscle forces at knee joint
$\vec{F}_{res}$	knee joint resultant force

Chapter 1. Introduction

1.1 Background

As an interdisciplinary subject, biomechanics of human movement appeals researchers for it involves the knowledge of bioscience, mathematics, physics, chemistry and anatomy, being implemented ranging from orthopaedics, rehabilitation, therapy to sports and medical sciences. For example, the study of human athletic performance has been revolutionized by the motion analysis equipment and software, which makes it possible to analyze complex three-dimensional movement. From rugby to cricket to swimming to pole vaulting, the kinematics and kinetics in human movement have been examined for improving human performance (Bartlett, 1997).

A wide variety of human movements had been explored since centuries ago, dating back to ancient Greece when the first book about biomechanics of movement of animals, On the Motion of Animals, was written by Aristotle (Ross and Smith, 1912). It opens the door to the venture that discovers the secret of human locomotion, which has led plenty of famous scientists and researchers to dedicate to explore the mysteries in human movement. During Renaissance period, Leonardo Da Vinci, who had kept close eyes on the application of mechanics to biological problems, studied the flight of birds to find means by which human could fly (Mason, 1962). In 19th century, human locomotion was scientifically investigated by Étienne-Jules Marey, and a great deal about human gait was hypothesized by the German brothers, Ernst Heinrich Weber and Wilhelm Eduard Weber (Matin, 1999).

As the development of mathematics and mechanics, the contemporary biomechanics research has not only implemented more advanced techniques to measure and describe the human movement, but the mathematical modelling and the simulation are employed for analyzing and interpreting a broad range of human locomotion as well. The most frequently used method to measure the human movement involves placing the reflective markers on the skin. The relative movements between segments can be captured by high resolution camera with the purpose of defining the movement of the joint. However, the limitation of the skin-based marker system is the skin movement relative to the underlying bone which will decrease the precision of the trajectory of the segment (Benedetti and Cappozzo, 1994). It is recently reported that the point cluster technique (PCT) employs excessive markers on each segment to minimize the artifice from skin (Andriacchi et al., 1998). The PCT furthest reduces the negative influence from skin movement by using the optimization method, and the error induced by the deformation of the segment is corrected as well. In the modern-day research, models are believed to play an important role in predicting the information that is not measurable. For example, the understanding of how musculoskeletal system is activated, generates force and drives body to accomplish movement is important to scientists and engineers, who wish to theoretically analyze and explain the human movements and design equipments for medical and therapeutic use. The process stated above could be realized in the model and simulated virtually. The mathematical representation of muscle mechanics has been improved since the first muscular model was developed by Hill (Hill, 1938). Currently, various modified musculoskeletal models have been applied in analyzing human locomotion, and more physiological and biological properties are involved in the models as well.

There has been a tremendous growth in the application of the study of human movement. Particularly, the gait measurement data of patient with neuromuscular disorders is analyzed to assist the diagnoses before treatment. For example, specialists use data to monitor the progress of the disease and complete the surgery for children with cerebral palsy. The effect of the treatment would be observed by further measurement for improving the outcome of surgery. In addition, the research of coordinated movement is studied in robotics. The roboticist develops computer programs to produce coordinated movements in a robot. On the other hand, the motor control researcher measures coordinated movements in order to understand what the 'neural program' is (Kutz, 2003). In neuroscience research, by considering the mechanics of muscles, skeletons and bodies, we could understand the activity of neural circuit. For example, with the help of the Electromyography (EMG) and infrared camera system, researchers could detect the neural disorder happened in the abnormal gait and posture, and work out solutions to improve behaviour in human movement (Andriacchi, 1998). The ergonomics study has been promoted by biomechanics of human movement as well. Both the development of human-machine interfaces and minimizing industrial injuries require knowledge of human kinematics and kinetics.

Although most of the secret of human movement has been revealed by the effort of bio-scientists and mechanical engineers, the evaluation of dynamic loading during human standing and walking are still need to be emphasized. The concept of a simple muscle stiffness balance control during quiet standing has been introduced by Winter (Winter et al., 2001), and the argument on the feasibility of balance control solely by ankle muscle stiffness during standing was addressed by Morasso (Morasso and

Sanguineti, 2002). However, most of the investigators simplified the function of muscle as a spring-like mechanism, which could provide a resultant stiffness to stabilize human body, and few had concerned about the individual muscle's mechanics as well as the control strategy from central neural system. Unlike the studies on human standing, more research on the estimation of dynamic loading during human walking has been employed in biomechanical community, and the individual muscle's response was analyzed in detail (Zajac et al, 2003). Developing more advanced algorithm that includes muscle physiological characteristic and adjustment from central neural system, especially the algorithm with lower computational cost and higher precious result, is still a hot topic in this field (Erdemir et al., 2007).

In the following chapters, the dynamic loading during human standing and walking will be explicitly discussed and explained by the outcome of the research.

1.2 Objectives

The musculoskeletal system, as an interface between Central Neural System (CNS) and human behaviour, plays a vital role in human postural stability and movement. To perform a plethora of coordinated movements, the musculoskeletal systems are excited by the CNS, and then develop and transmit the forces to generate the movements. The understanding of how such an interface is activated, generates force and drives body to accomplish movement is quite important. Particularly, the mathematical modelling of the musculoskeletal system, which is used for estimating the intersegment forces, moments and predicting movement has been an effective method to analyze the dynamic responses in human locomotion.

The main objectives of this research are as follows,

● Chapter 2 is to undertake the literature reviews on mathematical modelling of muscle mechanics, dynamic muscular loading in human standing and walking.

● Chapter 3 is to construct a novel muscle model for analyzing the mechanical behaviour of skeletal muscles.

● Chapter 4 is to analyze the influence of intrinsic muscle properties on postural stability and the trade-off between stability and energy consumption in human standing.

● Chapter 5 is to develop a three-dimensional human walking musculoskeletal model, where the model parameters are from the Grand Challenge Competition 2010.

● The primary objective of chapter 6 is to develop the methodologies for estimating the individual lower limb muscle forces during human walking by using optimization schemes, which are based on muscle forces and combined 'force-length & force-velocity' relationships. This combined computational and experimental methodology is illustrated in Figure 1.1.

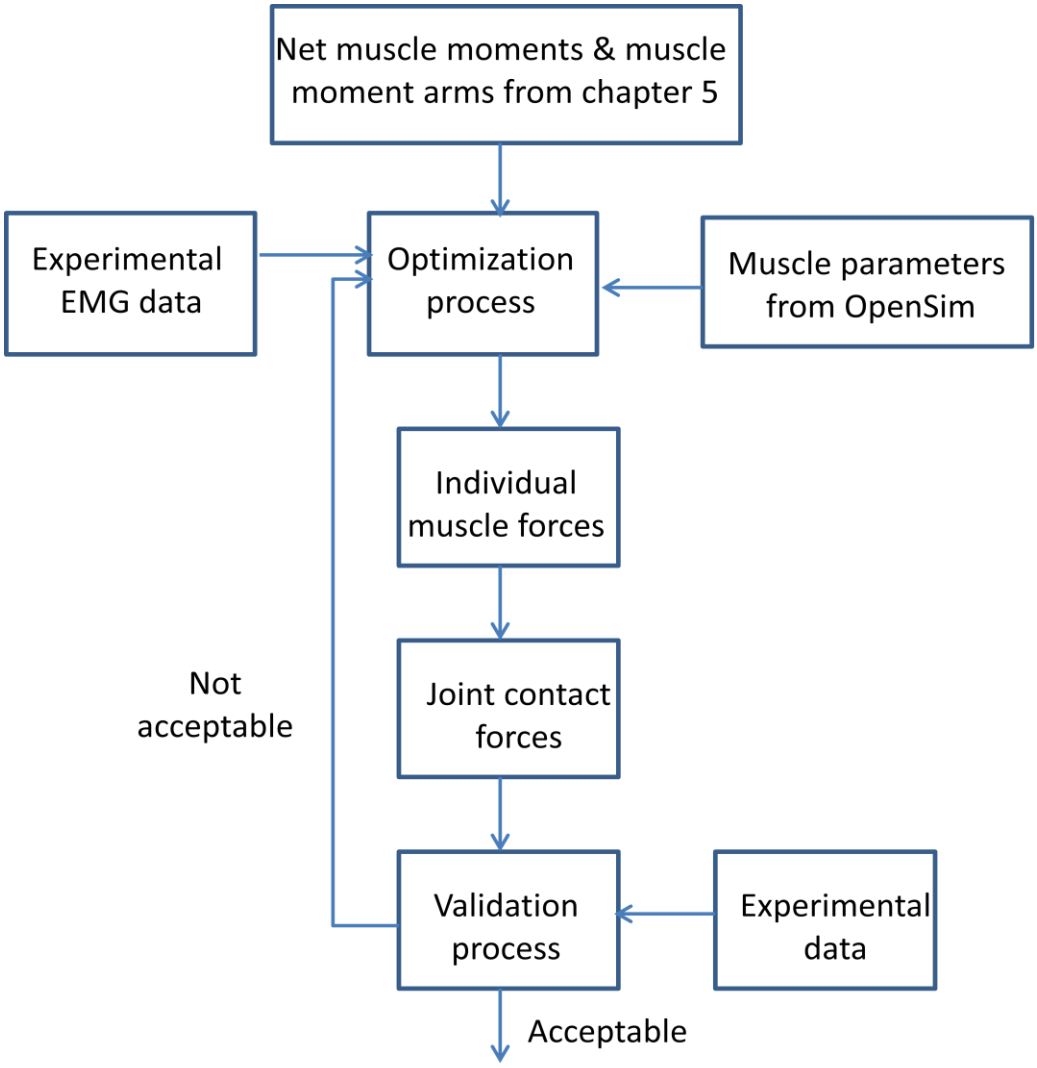

Fig. 1.1The combined computational and experimental methodology for individual muscle forces evaluation

1.3 Thesis overview

The thesis is divided into seven chapters. The first chapter briefly reviews the human movement biomechanics and the current research on the evaluation of human dynamic loading during standing and walking. The objectives of the research in this thesis are introduced in Chapter 1 as well. The remaining six chapters are arranged as: Chapter 2 provides a literature review on human musculoskeletal modelling and the evaluation of dynamic muscular loading, Chapter 3 to 6 present the core work of the

thesis, and Chapter 7 concludes the thesis by summarizing the whole thesis work and suggesting the future work. Below is a breakdown of the whole thesis by reviewing the main content of each of the constituent chapters.

Chapter 2 presents a literature survey on the research of skeletal muscle modelling and the musculoskeletal system performance during standing and walking. The chapter commences with the review of the traditional ways of single skeletal muscle modelling, especially the model developed by Hill in 1938 and its other derivatives. Afterwards, the current status of the assessment of the musculoskeletal system performance during standing and walking is reviewed. It includes the effect of the muscle intrinsic properties on postural stability, the relationship between postural stability and muscle energy consumption and the evaluation of individual muscular loadings during walking.

Chapter 3 proposes an improved Hill-type model to represent the mechanical behaviour of a single skeletal muscle by integrating the latest knowledge based on muscle physiology. The model includes two core dynamic processes: the activation dynamics and the contraction dynamics. The muscle intrinsic properties in the contractile element include a force-length relation and a force-velocity relation, and the non-linear elasticity of the parallel element and the series elastic element. A set of isometric contraction simulations is conducted, which produces very reasonable muscle force histories compared with the literature data.

In Chapter 4, two musculoskeletal models with different model configurations are developed to investigate the musculoskeletal system performances during standing

posture. Based on the simulation studies, the influence of intrinsic muscle properties on the stability of the musculoskeletal system is analyzed systematically, and furthermore the interplay between stability and energy consumption in postural control is quantitatively assessed by using a multiple-objective optimization scheme.

A three-dimensional musculoskeletal model with 13 body segments and 98 muscle groups is constructed to simulate human walking in Chapter 5. The anthropometric data and gait measurement data provided by the Grand Challenge Competition is used to support the modelling process. By using scaling and inverse kinematics methods, the model is developed to fit for the subject-specific data provided. The muscle moment arms and net muscle moments in a complete walking cycle are calculated, which can be used to investigate the musculoskeletal functions during human gait.

In Chapter 6, a novel computational framework to evaluate the individual muscle forces during human walking is developed, which includes a specially designed subject-specific calibration process to identify the key model parameters and a novel formulation for the load sharing problem by integrating a time-dependent muscular dynamic process with an inverse dynamics based optimisation scheme. The simulation results are experimentally validated against the measured force sensor data and are also compared with the results generated by the conventional static optimisation method and those produced by a widely used software package.

Chapter 7 draws the conclusions from this research and makes a brief review of each constituent chapter by summarising the main points. Chapter 7 also consolidates the methodologies employed in this thesis: a computational framework for evaluating the

dynamic loadings during standing and walking, which may also find applications in other areas of biomechanics. Finally, some suggestions for future work are proposed.

Chapter 2. Literature Review

2.1 Muscle anatomy and physiology

The anatomical structure of skeletal muscles is fundamental to understand the muscle mechanics. As shown in Figure 2.1, a skeletal muscle is made up of bundles of fascicles which consist of a huge amount of muscle fibres. Perimysium and blood vessels are found between different fascicle bundles. Muscle fibre is multinucleate cell and is lined in parallel with each other. Synaptic junction, motor axon and motor end plate exist in muscle fibre which is stimulated by neural input to generate muscle forces. A muscle fibre is about 100 μm in diameter, and the muscle fibres are connected by soft tissues (Winter, 2009).

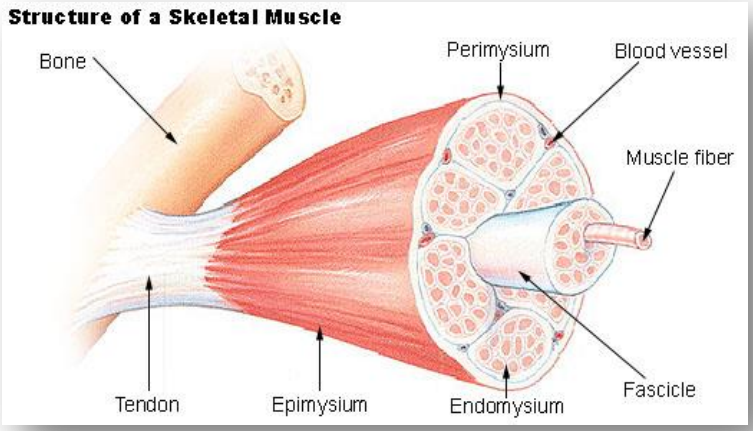

Fig. 2.1 The structure of a skeletal muscle

Digital image <http://training.seer.cancer.gov/anatomy/muscular/structure.html >

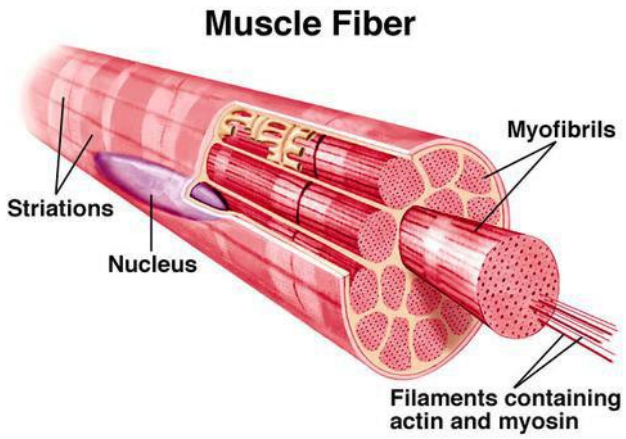

Fig. 2.2 The structure of a muscle fibre

Digital image < http://www.nvo.com/jin/homepage8/ >

Myofibril, the primary component of muscle fibre, is about 1 μm in diameter. Like muscle fibre in fascicle, myofibrils are arranged in bundles as well. Under an electron microscope, filaments, the basic mechanical structures are seen, which contain two primary types of protein - actin and myosin. Filaments are serialised by many repeating sections termed sarcomeres, which are shown in Figure 2.2 (Winter, 2009).

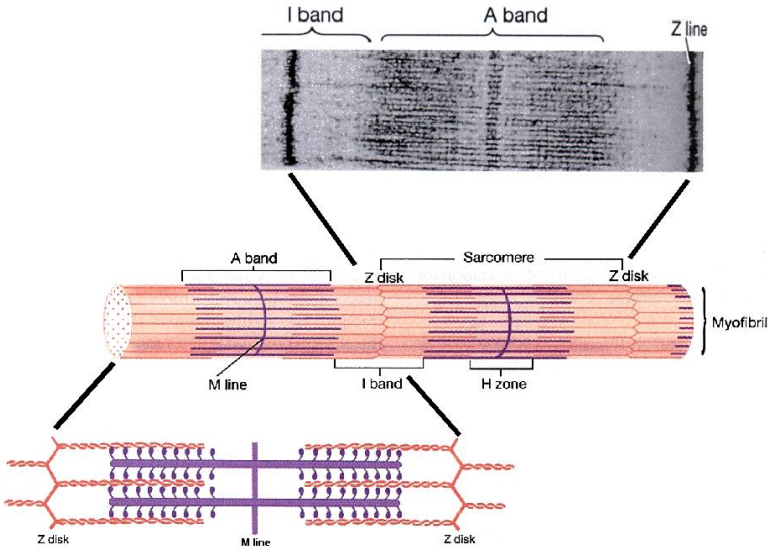

Fig. 2.3 The structure of sarcomeres

Digital image <http://physioweb.uvm.edu/muscle/berger2.htm>

In Figure 2.3, the sarcomere is defined as the myofibril segment between two ‘Z lines’ or ‘Z disks’, where the ‘Z line’ appears as a dark line under the electron microscope. ‘A band’ is named for the entire length of a single thick filament in sarcomere, and correspondingly, ‘I band’ is the zone that is solely occupied by the thin filaments. Within the ‘A band’, it is clearly found that a region termed ‘H zone’ is much lighter than the region beside it, because thick filament is not superimposed by thin filament in this area. A thin ‘M line’ is formed of cross-connecting elements of the cytoskeleton inside the ‘H zone’. In the magnified schematic diagram of the sarcomere, cross-bridge structures are found between the thin filaments (orange area in Figure 2.3) and the thick filaments (purple area in Figure 2.3). Tension is created at the cross-bridge structure where the muscle shortening and lengthening take place. During muscle contraction, the sarcomere length could vary from 1.5 μm to 4.0 μm between which the rest length is about 2.5 μm. In contrast, the length of ‘A band’ does not change, whereas ‘I band’ and ‘H zone’ shorten respectively. This causes two ‘Z line’s come closer.

It is well known that muscle contraction is caused by neural stimulation and regulated by Ca^{2+}, the calcium ion, which is the key factor in muscle contraction in molecular level. At rest, the myosin head is bound to an ATP molecule in a low-energy configuration and is unable to access the cross bridge binding sites on the actin. However, the myosin head can hydrolyze ATP into adenosine diphosphate (ADP) and an inorganic phosphate ion (Pi). In the absence of stimulation, calcium ions are accumulated in sarcoplasmic reticulum (SR), and the protein tropomyosin covers the myosin binding sites of the actin molecules, blocking the access of to the binding sites.

During stimulation of the muscle cells, the action potential from the motor neuron changes the permeability of the SR, allowing the flow of calcium ions get into the sarcomere. The calcium ions bind with the tropomyosin and alter its structure, resulting in the access of the binding sites unblocked. Then myosin binds to actin in a strong binding stage, forming a cross-bridge structure between thick filament and thin filament. ADP and inorganic phosphate are tightly coupled to the power stroke. This will pull the Z-bands towards each other, thus shortening the sarcomere and the I-band. The energy is released as the myosin heads pull the thin filament to move forward; meanwhile, the ADP and Pi dissociate from myosin as well. The myosin remains attached to actin until a new ATP binds the myosin head. This binding of ATP to myosin releases the actin by cross-bridge dissociation. The ATP-associated myosin is ready for another cycle, beginning with hydrolysis of the ATP. The entire working cycle is illustrated in Figure 2.4. Obviously, without the stimulation from neural system, the calcium ions will be pumped back to SR, and the protein tropomyosin will change back to its original state and block the access of the binding sites. Therefore, such cycle is unable to occur, and it is impossible to enforce muscles to do any contraction either (Cacioppo, et al., 2007; Shwedyk et al., 1977).

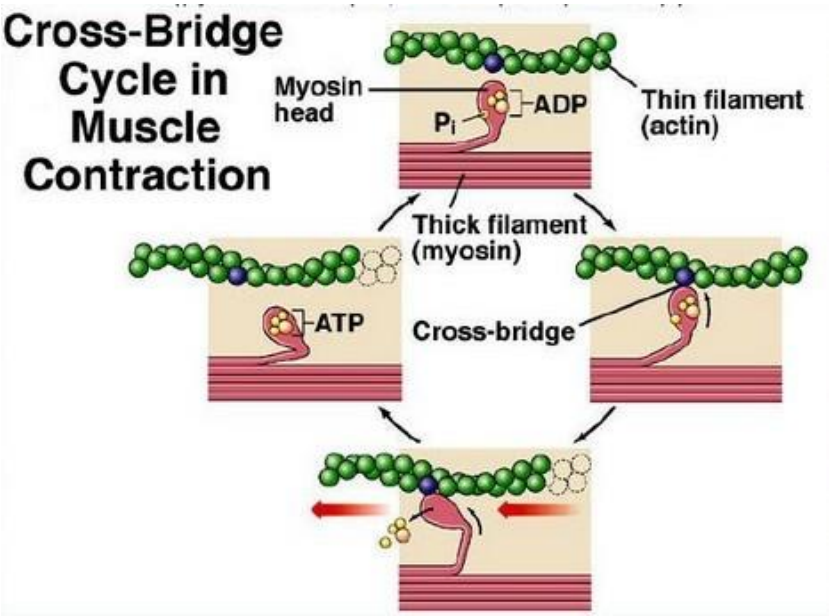

Fig. 2.4The molecular mechanism of muscle contraction

Digital image <http://www.coa.edu/stodd/oceanweb/bio2/bio2lectures/Lecture7/sld029.htm>

If a muscle is given a single and short pulse, a response known as twitch will be produced. Such contraction rapidly generates a force and then the force gradually decreases for a longer period. If a second stimulus inputs before the response decline to zero, a mechanical summation will make the peak of the response force higher than the single twitch's. If a muscle receives a repetitive stimulus which is more than a certain frequency, it will respond as a smooth and stable force with the highest plateau. Such certain frequency is named fusion frequency, and the response is termed tetanus. Figure 2.5 shows the twitch and tetanus, where fast train and slow train represent high frequency and low frequency stimulus respectively.

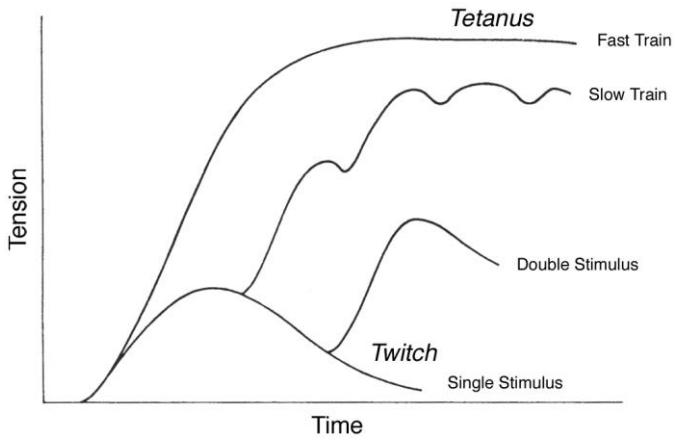

Fig. 2.5 Time course of a muscle twitch (Winter, 2009)

The force generated is not only controlled by the frequency of stimulus, and the size of the stimulus gives impact on the tension amplitude as well. With higher stimulations, more motor units will be fired to generate force. In addition, the order for activating motor units is not random but obeys the rule which is called size principle. Small motor units get recruited earlier than large units' recruitment (see Figure 2.6). Such recruit order makes sense that low forces are controlled by small motor units, but to produce large force, larger units begin firing and dominate the change of tension levels.

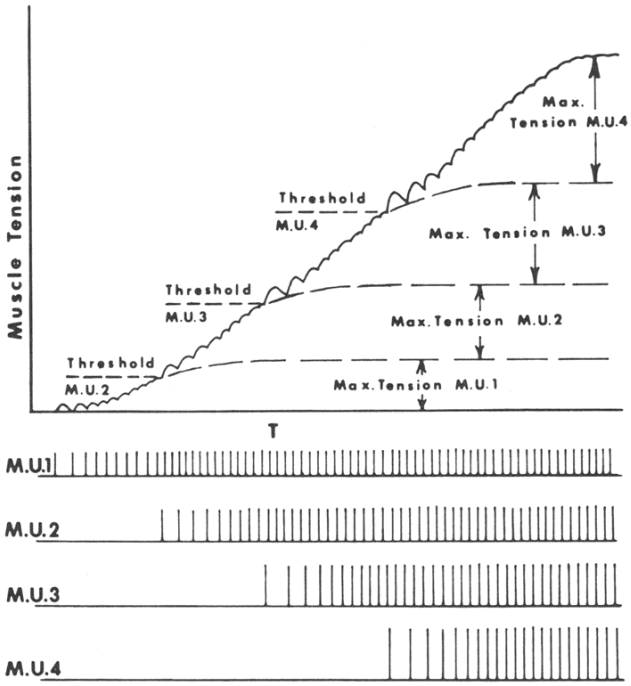

Fig. 2.6 Size principle of recruitment of motor unit (Winter, 2009)

However, if two muscles are activated by the same size and frequency of stimulus, the twitch speeds are not the same indeed. It is revealed by experiments that fast-twitch and slow-twitch fibres in muscle hold different twitch response time. Fast twitch fibres are used for rapid burst of activities but fatigue very quickly. In contrast, slow twitch fibres could continuously generate force for long period but with insignificant fatigue. In micrographs, the colour of fast twitch fibres is much lighter than the slow twitch fibres' (see Figure 2.7).

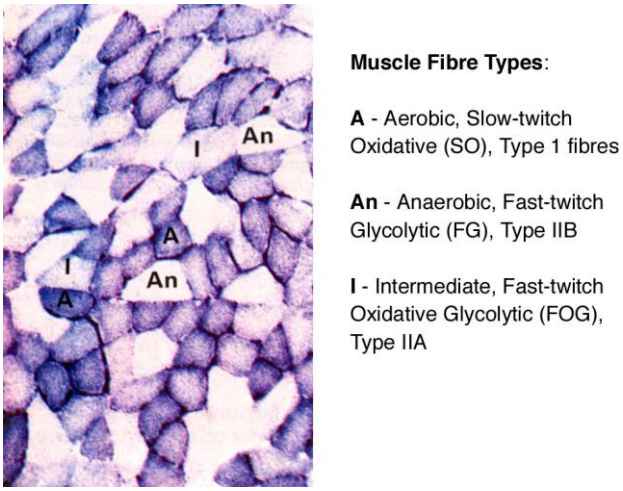

Fig. 2.7 The dark slow-twitch fibres and light fast-twitch fibres (Winter, 2009)

The directional arrangement of muscle fibres also plays an important role in muscle mechanics. The muscle fibre direction is not always the same as the direction for muscle contraction. We call it pennate when the line of action force does not match the direction of muscle fibre, and the angle between such two directions is named as pennation angle. Another physical definition in muscle structure is physiological cross-sectional area (PCSA), which influences the force magnitude generated by muscle. In non-pennated muscle, the PCSA is the same as the area the middle part of muscle which is perpendicular to the line of action. In pennated muscles, in order to involve as many muscle fibres as possible, the PCSA is considered as the area that is perpendicular to the average direction of muscle fibres. Figure 2.8 shows the pennation angle and PCSA in muscle.

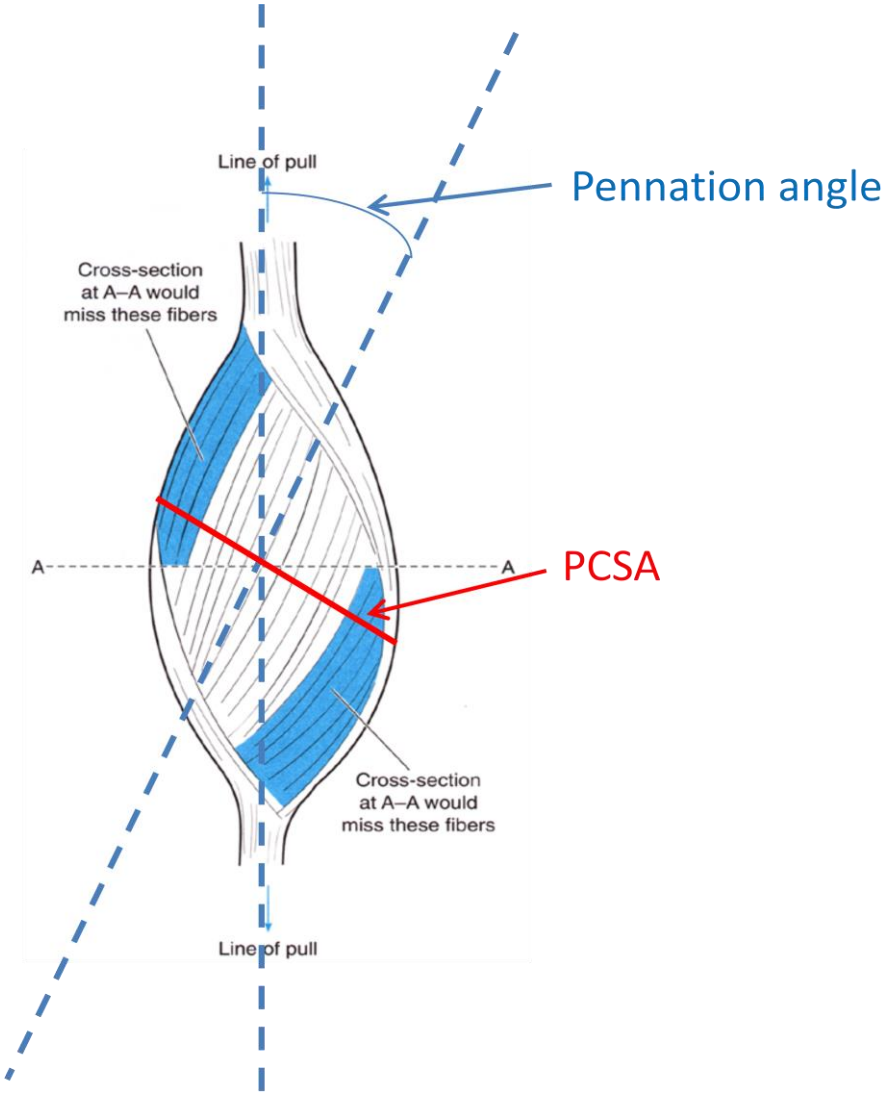

Fig. 2.8 The muscle pennation angle and PCSA (McGinnis, 1999)

2.2 Muscle mechanics

The musculotendon complexes, as an interface between Central Neural System (CNS) and human skeletal system, play a vital role in human postural control and locomotion. In musculotendon unit, muscle is the only controllable element that dynamically coupled with neural system, and it contracts given the activations from neural system. Subsequently, tendons, the connection between muscles and bones, deliver the forces generated by muscles to control the body's posture or enforce the movement of the

skeletal system. The process could be expressed in a model and simulated virtually. The mathematical representation of muscle mechanics has been improved since the first muscular model was developed by Hill in 1938 (Hill, 1938). Currently, various modified musculotendon unit models involving more physiological and biological properties have been applied in analyzing human motions.

The muscle dynamic process can be divided into activation dynamics and contraction dynamics. Activation dynamics corresponds to the process from neural excitation to activation of muscle tissue, and muscle contraction dynamics is the transformation from muscle activation to muscle force. In Figure 2.9, those two dynamic transitions are shown sequentially (Zajac, 1989).

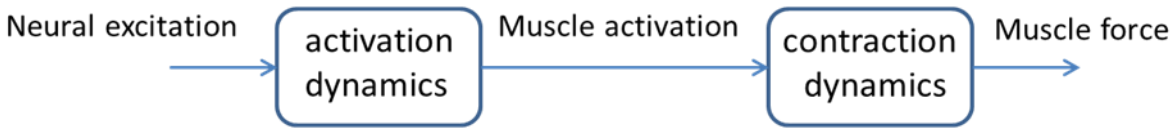

Fig. 2.9 The working process of muscle mechanics

2.2.1 Activation dynamics

Each motor unit in a muscle fibre is controlled by a separate nerve ending. As shown in Figure 2.10, the neural excitation is coupled to the contractile machinery, going through an intermediate connection called muscle activation. It often leads to a time delay by calcium pumping out of the sarcoplasmic reticulum to travelling down the T-tubule system and binding to troponin. Such biochemical process is shown in Figure 2.10 (Zajac, 1989).

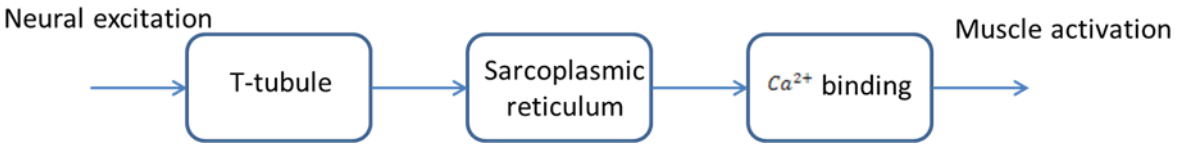

Fig. 2.10 The chemical process in activation dynamics

It was reported that the activation dynamics used to be treated as a linear system due to its simplicity in the analysis, although such simplification would give rise to some errors for detailed analysis (Chapman and Harrower, 1977). Since Mannard and Stein found out that a nerve-muscle system could be described as a family of input-based second order systems, researchers have developed many linear second order systems to represent the activation dynamics (Mannard and Stein, 1973). For example, Baratta and Solomon worked out a linear second order system with double real poles and a pure time delay (Baratta and Solomonow, 1990). The pole values are able to tell the muscles' differences. At the same time, Bobet and his colleague presented a linear second order system to represent an isometric muscle (Bobet, et al., 2005). The model's parameters had to be adjusted to provide good fitting, where the coefficients stayed as constants only in impulse intervals.

It is also suggested by Happee that the traditional activation dynamics can be divided into two states: excitation dynamics and activation dynamics, which is shown in Figure 2.11 (Happee, 1994). Each dynamic process is described by a first order system. Compared with the second order system methods, such modification considerably reflects the dynamic relationships among neural input, neural excitation and muscle activation.

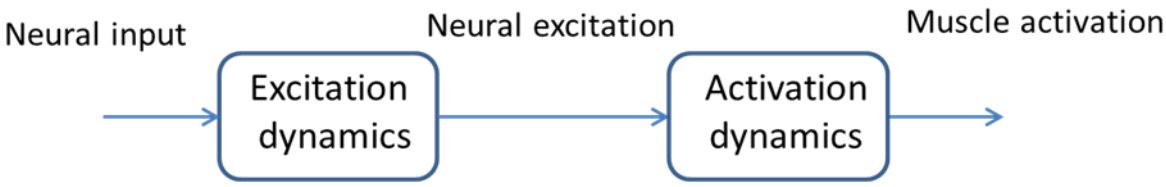

Fig. 2.11Happee's two first order model

Although second order system had been widely used in representing muscle activation dynamics, Bobet still found the non-linear model could provide a perfect fit to the data and predict muscle forces in most of the conditions (Bobet, et al., 2005). Due to the non-linear effect on the model, a Hammerstein structure has been adopted in muscle mechanics modelling (Bernotas et al., 1986; Durfee and Maclean, 1989; Bobet et al., 2005; Hunt et al., 1998; Chia et al., 1991). The model is a non-linearity followed by a linear dynamics, where the non-linear system is time invariant, and a second order system represents the linear dynamics. The block diagram of such a structure is shown in Figure 2.12. The static nonlinearity (time invariant) represents the activation dynamics more realistically, and the linear dynamics describes the muscle contraction dynamics.

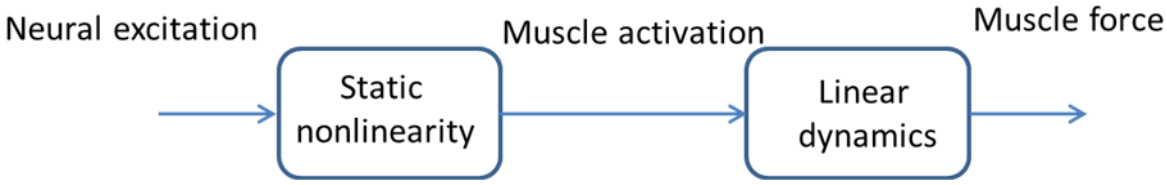

Fig. 2.12 The Hammerstein model structure

However, the static nonlinear system was commonly chosen by researchers who modelled the activation dynamics. Hunt still argued that it was not an accurate enough method for the muscle force description, due to the change of system strongly

depending on the level of electrical stimulus (Hunt et al., 1998).

Another popular approach that has a two serial second order systems followed by a nonlinearity activation dynamics has been developed (Ghigliazza and Holmes, 2005; Riener and Quintern, 1997; Hatze, 1977; van Zandwijk et al., 1998; Zakotnik et al., 2006). The system structure is based on Weiner system, which is similar to the Hammerstein structure but conversely changes the sequence of nonlinearity and linear system. It should be noticed that, in Hammerstein structure, the activation dynamics is a pure nonlinear system, and linear dynamics is the transition from the muscle activation to the muscle force; but in such a quasi-Weiner system, the muscle activation dynamics is expressed by two linear second order systems plus a non-linearity, which is more complicated than the Hammerstein structure. There is still no evidence to prove that the method's higher order characteristic is able to provide a better fit compared with the methods before, and the necessity of the higher order model remains to be discussed in future investigations.

Contemporary nonlinear models have been proposed in many ways, such as Bobet and Ding's models (Bobet et al., 2005; Ding et al., 2002). In Bobet's model, the activation dynamics is comprised of a linear first order filter coupled with a nonlinear time invariant system. The mathematical expressions consist of a first order differential equation and a nonlinear polynomial,

$$\dot{q}(t) + a_a q(t) = \sum_{i}^{n} \delta(t - t_i) \tag{2.1}$$

$$x(t) = \frac{q(t)^m}{q(t)^m + k^m} \tag{2.2}$$

where the model has three parameters a_a, m and k. The first differential equation is the filter that represents calcium release and re-uptake, and the second equation is to describe the chemical process of calcium binding to troponin. Similar to Bobet's model, Ding presented a combined linear and nonlinear system to modify the activation dynamics, where one more filter was considered to represent the normalised amount of the ${C_a}^{2+}$ complex as C_n. In addition, the term R_i is used to account for the non-linear summation when fibres are stimulated by two closely spaced pulses. Both Bobet and Ding's models are shown as block diagrams in Figure 2.13.

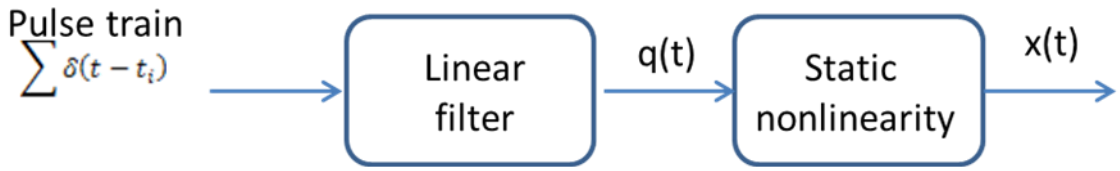

(a)

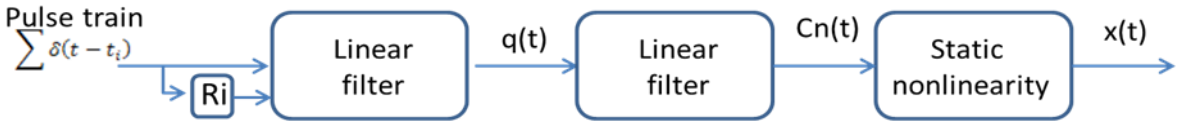

(b)

Fig. 2.13The Bobet's model structure (a) and Ding's model structure (b)

2.2.2 Contraction dynamics

Contraction dynamics of muscle tissue is the process that converts the stimulus signals to muscle forces. As introduced in the section of muscle anatomical structure, a muscle tissue is made up of amounts of serial and parallel muscle fibres, so the

properties of muscle tissues are assumed to be scale-up version of the muscle fibres, which are scale-up version of sarcomeres in turn. Given an individual muscle fibre is stimulated by the signal from the motor unit connected, it is defined that the input signal to the muscle tissue is the summation of the activation level in each muscle fibre, and the value is from 0 to 1(Winter, 2009).

2.2.2.1 The Hill model

As introduced before, a muscle consists of an active element, which could be induced by neural stimulus and contract actively. We define such an element as contractile element, and its contraction process represents the resultant action of each tiny sarcomere's contraction.

In 1935, Fenn and Marsh firstly proposed a mathematical relation between the muscle force and the muscle shortening velocity (Fenn and Marsh, 1935).

$$V = V_{0f} e^{\frac{P_f}{B}} - K P_f \tag{2.3}$$

where V is the shortening velocity at any force, V_{0f} is the shortening velocity of an unload muscle, P_f is the muscle force and B, K are constants. After three years, a famous equation on the relation of the muscle force, P, the muscle shortening velocity, V and the extra heat produced by muscle was proposed by Hill (Hill, 1938). The mathematical relation has been considered as one of the most influential contributions in biomechanics research, which is still used in muscle modelling and muscle measurement nowadays. The relation is expressed in the form of hyperbola,

$$(P + a_H)(V + b) = (P_0 + a_H)b \tag{2.4}$$

where P_0 : Maximum isometric force (N)

a_H: Coefficient of shortening heat (N)

b : $\frac{a_H \cdot V_0}{P_0}$ (m/s)

V_0 : Maximum velocity (when $P = 0$) (m/s)

Such relation can be re-written as,

$$P = \frac{P_0 b - a_H V}{V + b} \tag{2.5}$$

where the relation between the muscle force and the muscle shortening velocity is explicitly described.

Normally, the maximum shortening velocity is often expressed as a function of optimal muscle fibre length, l_o, which is the muscle fibre length in rest (Winter 2009). It was reported that for different muscles, V_0 varies between $4l_0/s$ to $10l_o/s$. In 1939, Hill enhanced the muscle model by linking contractile element in series with an elastic spring to represent an individual contractile element (see Figure 2.14). The improvement better represented the motion of a skeletal muscle after stimulations.

Fig. 2.14The improved Hill model structure

2.2.2.2 Hill-type model

The muscle's dynamic response is dominated by the mechanical behaviour of the contractile element. From Hill's model, the influence of muscle shortening velocity on muscle force generation could be seen clearly. However, at steady state, the contractile element still involves a unique property as its tension varies against the change of muscle fibre length. Such force-length relation can be studied when the muscle activation is at constant. As shown in Figure 2.15, the shape of the curve depicts the relation between the forces produced by a muscle contractile element and its length changes. The force symmetrically decreases to the optimal muscle fibre length, l_o, which could be explained by the interaction of cross bridge in contractile element. Under different muscle activations, the forces are scaled by the activations. At maximum activation, the maximum isometric force F_o is produced at l_o. Normally, muscle contractile element generates force in the region of '$0.5l_o<l<1.5l_o$', where l is muscle fibre length.

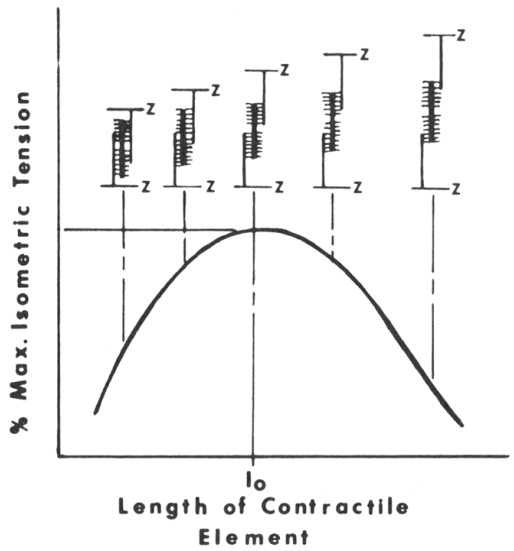

Fig. 2.15The tension produced by a muscle contractile element as it changes length (Winter, 2009)

Although Hill's model describes the relationship between the muscle shortening velocity and the tension it produces, the force generated by the muscle during lengthening is still unable to be expressed by Eq. (2.5). To describe the whole range of muscle contraction velocity versus the force it generates, a non continuous function is normally used, one part of which represents the force when muscle is shortening and the other part for lengthening (Thelen, 2003),

$$V^M = (0.25 + 0.75a)V_{max}^M \frac{\bar{F}^M - af_{lT}}{b_T} \tag{2.6}$$

where V^M is the muscle contraction velocity; a is muscle activation; V_{max}^M is the maximum contraction velocity; $\bar{F}^M$ is the normalized muscle force; f_{lT} is the muscle force at the current muscle length which is from force-length relation, and the parameter b_T is computed differently depending on whether the muscle fibre is shortening ($\bar{F}^M \leq af_{lT}$) or lengthening ($\bar{F}^M > af_{lT}$):

$$b_T = \begin{cases} af_{lT} + \dfrac{\bar{F}^M}{A_f}; & \bar{F}^M \leq af_{lT} \\ \dfrac{(2 + 2/A_f)(af_{lT}\bar{F}_{len}^M - \bar{F}^M)}{(\bar{F}_{len}^M - 1)}; & \bar{F}^M > af_{lT} \end{cases} \tag{2.7}$$

where $\bar{F}_{len}^M$ is the maximum normalized muscle force when the muscle is lengthening, and A_f is a force-velocity shape factor, which is set to 2.5.

The force-velocity relationship has been investigated by many researchers, and it is suggested that a continuous function could make the calculation easy in muscle

contraction simulation. Anderson used a continuous expression to fit empirical data (Anderson and Pandy, 2001),

$$\tilde{F}_V^M\left(\dot{L}^M\right) = 1.8 - \frac{1.8}{1.0 + exp\left(\frac{0.04 - \frac{\dot{L}^M}{\tilde{V}_{max} \cdot L_O^M}}{0.18}\right)} \tag{2.8}$$

where L_O^M and $\tilde{V}_{max}$ represent optimal muscle fibre length and maximum contraction velocity. The muscle force generated by muscle contraction and the muscle contraction velocity are expressed by variables $\tilde{F}_V^M$ and $\dot{L}^M$. Figure 2.16 shows these two variables' relationship. The words, 'eccentric' and 'concentric', are the terminologies for muscle lengthening and shortening in muscle mechanics.

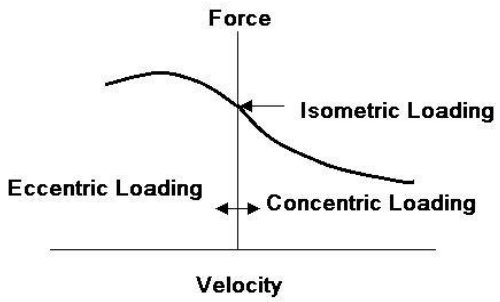

Fig. 2.16 The muscle force-velocity relationship

Digital image < http://www.springerimages.com/Images/RSS/1-10.1007_978-3-642-12883-7_2-13>

Based on these relations, a mathematical model of muscle contractile element can be developed. The tension produced by the contractile element F_{ce} is a function of three variables: the muscle activation, a, the tension from force-length relation, f_l, and the

tension from force-velocity relation, f_v.

$$F_{ce} = a \cdot f_l \cdot f_v \tag{2.9}$$

As introduced in section 2.1, perimysium, epimysium, endomysium and other soft tissue are the components that form the muscle tissue. In muscle mechanics, such connective tissue is named parallel element, being distinguished with series elastic element. Experimental data has indicated that hardly does parallel element act when muscle is at rest length or less. As muscle lengthening, the tension in parallel element increases quickly after a gradual increase at the beginning. If we sum the forces from both contractile and parallel elements, the overall force-length characteristics can be obtained (see Figure 2.17), where the percentage is the level of muscle activation.

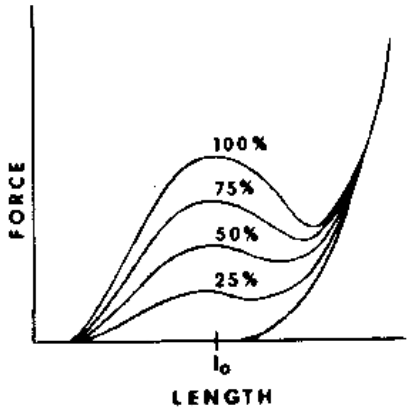

Fig. 2.17 The muscle tensions resulting from various levels of muscle activation (Winter 2009)

Based on the contractile element and the parallel element, the muscle structure could be simplified as a parallel structure in modelling. The contractile element actively generates contraction, and the parallel element responds passively. However, the arrangement on the series elastic element of muscle tissue is a question during

modelling. Fung has argued that both the structures in Figure 2.18 are mathematically equivalent, and it is meaningless to enforce to differentiate them (Fung, 1971). Zajac has further studied the influences of muscle tissue's series elastic element on the muscle dynamic response, and he concluded that the tendon compliance dominates muscle elasticity and the muscle series elastic element could be discarded (Zajac, 1989).

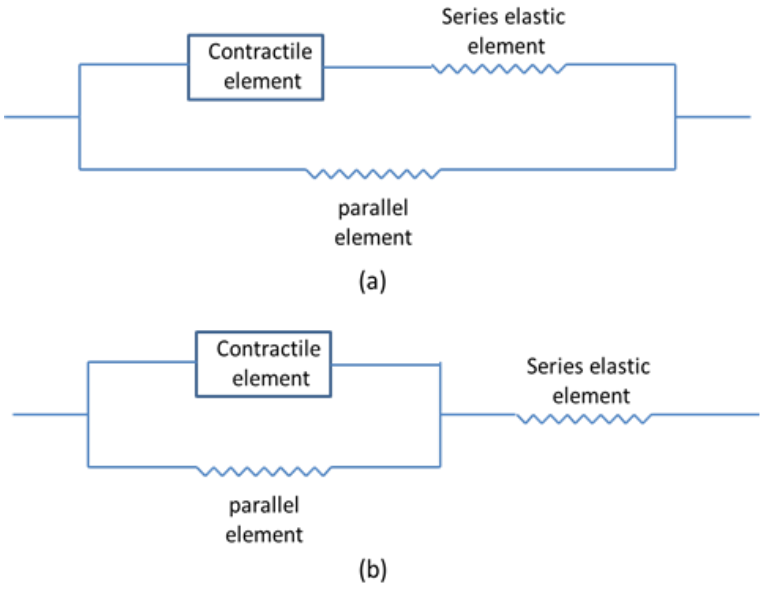

Fig. 2.18 The different structures of muscle fibre

Therefore, most of the muscle models proposed in biomechanics are clearly formulated as the parallel form, and the mathematical expression of muscle force could be derived as,

$$F_m = F_{ce} + F_{pe} \tag{2.10}$$

where F_m is the total muscle force; F_{ce} and F_{pe} represent the force generated by the contractile element and the parallel element.

2.2.2.3 Huxley muscle model

Huxley first proposed a biophysical muscle model, which defined a sliding filament theory from biochemical view (Huxley, 1957). He described the muscle behaviour based on the attachment rates of the cross bridges. The model was promoted by coupling with the excitation-contraction mechanisms (Winters and Woo, 1990). Huxley model is rarely used in dynamic musculoskeletal modelling and human motion analysis, for the model demands considerable computational cost.

2.3 Muscle preflex activities in postural control

Muscle preflex behaviour refers to the muscle coordination before active neural control when human confront with unexpected perturbations (Brown et al., 1995). Due to the fact that latencies in neural feedback loops are longer than the response time, it is difficult to produce stable posture solely depending on the neural control system when human face to unexpected perturbation. Therefore, muscle's self-adaptive characteristic is significant in offering a stable movement, which is named as self-stabilization movement. Previous research has demonstrated that muscles play an important self-stabilization role due to its force-velocity relationship (Chen and Ren, 2010). Furthermore, the viscoelastic property of series elastic tendon contributes to motion stability as well.

2.3.1 Contribution of muscle intrinsic properties to stability

The muscle intrinsic properties are defined as muscle force-length and force-velocity relationships (Brown et al., 1995). It is well known that the force produced by a muscle depends on the length of muscle fibre. Such dependent relation is easily understood when the muscle fibre length is at the ascending portion of its tension-length curve, and the muscle force will increase if the muscle stretches. Gordon has

proposed the force output from a muscle is relevant to its sarcomere length (Gordon et al., 1966). From the previous analysis, the length of sarcomere directly reflects the length of muscle fibre, which coincides with Gordon's conclusion.

It is found that the muscle contraction velocity has a big impact on the muscle force output (Harrison et al., 2004). For example, when a muscle is subjected to a large external load, the muscle force output gradually increases to resist the external load. If the muscle is suddenly unloaded, the rate of muscle shortening will rapidly rise and the force generated decreases correspondingly. Rassier and Herzog had concluded that the rapid change in muscle contraction rate occurred when the muscle experienced external load change, which resulted from the inverse force-velocity relationship. (Rassier and Herzog, 2004).

Several recent studies demonstrated that the muscle intrinsic force-length and force-velocity relationships could stabilize movements and simplify motor control. Brown and Loeb have built a specific model to explain that muscles intrinsic properties are of importance for the musculoskeletal system in keeping stable under perturbations (Brown et al., 1995). In their discussion, no nervous system was used and all the muscle activations were held as constant throughout various simulations. They summarized that the muscle force-velocity relationship provided a strong restoring force to the perturbation, whereas the force-length relationship offered little resistance. In addition, they addressed that the responses offered by the muscle intrinsic properties occurred with zero time delay, which could provide positive response before the neural active control was applied. Jindrich studied the contribution of intrinsic musculoskeletal properties to the stabilization of a rapid running insect by

using a novel apparatus to perturb the running cockroaches (Jindrich and Full, 2002). Almost at the same time, Richardson examined how the intrinsic muscle properties stabilize the wiping movement in the spinalized frog (Richardson et al., 2005). It is shown in Figure 2.19. In Richardson's study, a wiping limb was implanted with 12

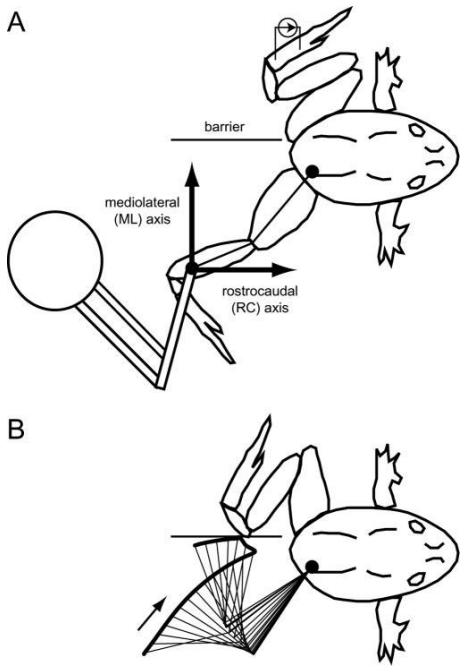

Fig. 2.19 The experiment of frog wiping movement (Richardson et al., 2005)

electromyography (EMG) electrodes and attached to a robot that recorded its trajectory and applied brief force perturbations. Cutaneous electrical stimulation was applied to the other hind limb, the target limb, to evoke the hindlimb-hindlimb wiping reflex. The experiment showed that no significant changes were seen in the EMGs after the perturbation, and it was also found that the intrinsic viscoelastic properties of the hind limb conferred robust stability properties to the hindlimb-hindlimb wiping behaviour.

Not only do the muscle force-length and force-velocity relationships improve the

stability of the musculoskeletal system when the system is suffering from an unexpected perturbation, but the series elastic tendon could provide self-stabilization to the system to produce successful movements in an unpredictable and varying environment as well. Lappin has modelled a mass-spring-damper system to represent the toad jaws which is shown in Figure 2.20 (Lappin et al, 2006). The muscle is thought to be a force generator in series with a spring which represents the series elastic component, such as the series elastic tendon and other connective tissues between the origin and insertion. Also, it is believed that the muscle itself relatively contributes less than other tissues in fast movement because lower tension is produced when muscle shorten rapidly. Lappin concluded that as the external load increased, the series elastic spring stretched and more forces were produced to resist the increase of external load. In other words, the resistant force kept the movement of jaw smooth and stabilized the whole musculoskeletal system.

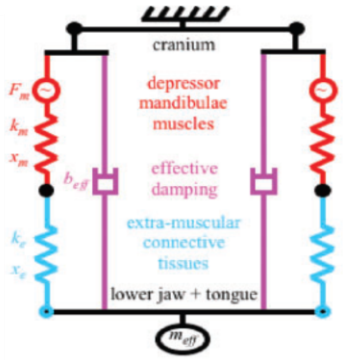

Fig. 2.20The toad jaw model (Lappin et al, 2006)

2.3.2 Energy cost and stability interplay in preflex behaviour during postural control

Due to the muscles' contraction and the chemical reactions in other organs, human consume energy to maintain daily living. Many investigations on energy consumption and stability during walking have been conducted, for example, elderly adults

consume about 15–20% more metabolic energy per kilogram of body mass for walking than young adults, but the reasons are not known (Martin et al., 1992; Waters et al., 1988). One possible cause of the greater metabolic cost of walking in elderly adults may be a greater cost of lateral stabilization. Regarding the energy of interest consumed in standing, Saha has analyzed force plate, kinematic, and metabolic energy data of 14 able-bodied subjects standing statically with upright and trunk-flexed postures. He concluded that changes in muscle activity associated with a trunk-flexed posture and the associated compensations likely contributed to the increased energy expenditure (Saha et al., 2007).

Stability is fundamentally critical in postural control and locomotion, which involves the ability of a system to return to its original state after a disturbance. In human locomotion, due to the stabilization action of central nervous system (CNS), a dynamically stable system, such as a walker, could move back to a certain trajectory after suffering from a disturbance. Ting also addressed that the acceptable time length that the system returned to its prescribed path was also important to such a dynamic stability (Ting, 1994). Considering the postural stability in human standing, Winter has presented a relatively simple control scheme for the control of upright posture in preflex period (Winter et al., 2001). It was like an invert pendulum which related the controlled variables (centre of mass (COM)) to the controlling variable (centre of pressure (COP)). The difference between the COM and the COP would be proportional to the acceleration of COM in the control scheme. A couple of estimated ankle joint stiffness and damping of invert pendulum was analytically evaluated in the model. Winter concluded that the quiet standing could be realized and controlled by a simple invert pendulum model. Although the model proposed by Winter is

mathematically feasible to be controlled, which means ankle stiffness could solely balance the system during standing in preflex stage, Morasso criticizes the inadequacy of the model and insists that it is not possible to keep stable when there is no anticipatory control input from central nervous system during standing (Morasso and Sanguineti, 2002).

In terms of the trade-off between energy cost and stability in postural control, previous studies range from animal to human being. Syme has pursued on the research of muscle function and energetic costs during steady swimming in Atlantic cod, in order to investigate whether energy cost may impact or dominate muscle function (Syme et al., 2008). The results implied that the production of powered forces for maneuverability/stability appeared to greatly impact the red muscle function during cruise swimming in the cod, particularly at slow speeds. It has been found that a trade-off between energy cost and stability happens in toddler gait compared to adults, toddlers will spend more energy to compensate stability (Hallemans et al., 2004). Houdijk made a study on the energy cost for balance control during upright standing and specially evaluated energy expenditure of the stroke patients during standing (Houdijk et al., 2009; Houdijk et al., 2010). It was concluded that the effort for balance control could elicit a meaningful metabolic energy demand.

There is rare research on the interplay between energy cost and stability during human standing in preflex stage. As the influence of muscle intrinsic properties on the stability of human musculoskeletal system is revealed gradually, an increasing number of studies on the trade off between energy expenditure and postural stability will be employed in the near future.

2.4 Muscle activities in human walking

Due to the biological and physiological characteristics, the human musculoskeletal system is more complicated than normal mechanical systems. It is far more difficult to quantify the relevant information on a skeletal muscle than to evaluate the result from a mechanical system. For example, it is possible to measure the displacement of the mass in a mass-spring system in Figure 2.21, and the work generated by the friction between ground and the mass can be estimated by a set of simple calculations. In terms of the energy that a single muscle consumes during human locomotion, hardly could any solution give an accurate estimation, especially the muscle length change is difficult to be measured directly. Such an example simply describes one of the difficulties existing in biomechanics - the estimation of individual muscle forces during human movement is a highly challenging topic nowadays.

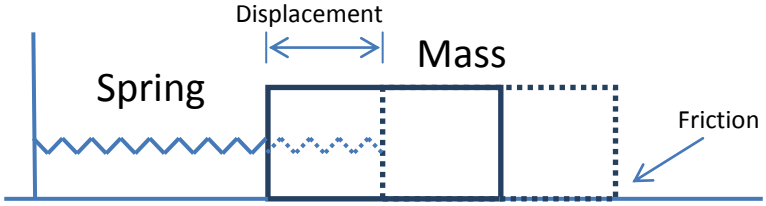

Fig. 2.21The mass-spring system

The estimation of individual muscle forces is also named ‘load sharing problem’ which could provide insight into neural control and the movement of the skeletal system. From the estimated muscle forces, the brief control strategy used by central nervous system could be identified and the kinematic data in the skeletal system is predicted as well. Clinically, both the diagnosis of neurological disease and the orthopaedic surgery could be improved by analysing the individual muscle forces. For

example, the muscles which are responsible for the abnormal gait in 'cerebral palsy' could be detected by clinicians, and the muscle could be targeted for surgery. The footballer who injures muscles could rehabilitate by figuring out the loads on joints and muscles. In this section, the methods currently used for evaluating the lower limb individual muscle forces during walking will be reviewed, and both the advantages and disadvantages will be discussed as well.

2.4.1 Direct measurement

Muscle forces could be measured in vivo by invasive method. Finni has measured the Achilles tendons with an optic fibre during human walking, and he concluded that the technique was well utilized in the study of loading of human musculotendon complex (Finni et al., 1998). In vivo, sensors were able to be implanted in surgery, e.g. Dennerlein's measurement of flexor tendon forces of fingers using a force transducer (Dennerlein et al., 1998; Dennerlein et al., 1999; Dennerlein, 2005). In addition, Fleming addressed that the in vivo measurements of ligament and tendon forces were more frequently used in laboratory than in clinics (Fleming and Beynnon, 2004). Clearly, direct measurement is not feasible to estimate the force from a single muscle (Zajac et al., 2003), thus the modelling method will be taken into account.

2.4.2 Non-invasive method using musculoskeletal models

Non-invasive method is the method based on musculoskeletal modelling, which takes advantage of the experimental data to evaluate the net muscle moments, the muscle moment arms and to optimize the individual muscle forces. It is widely used in current neuromuscular research and clinical practice. The methods are generally categorised into inverse dynamics method, forward dynamics based data tracking method and optimal control strategy (Pandy, 2001; Tsirakos et al.,1997), where the inverse dynamics analysis has become a routine in clinical gait analysis (Tsirakos et

al., 1997). Recent development in forward dynamics based data tracking method offers more insights in muscle physiological properties and neuromuscular coordination (Pandy, 2001). Muscle intrinsic properties and electromyography (EMG) signal play additional but essential roles in the modelling, and the forces at consecutive time steps are dynamically coupled during movement. The optimal control strategy is actually transformed from forward dynamics based data tracking method, which needs no experimental data in optimization process but in results validation (Pandy, 2001; Pandy et al., 1992). The major advantage of the method leads to a predictive simulations to assess the changes in the control of muscles and muscle forces as a result of therapeutic interventions, surgery and rehabilitation. Both the forward dynamics based data tracking method and the optimal control strategy are limited by their computational requirement, and the methods are difficult to be implemented in the clinical environment.

2.4.2.1 Modelling of the musculoskeletal system

The modelling of musculoskeletal system is essential for analyzing the human locomotion, and many review papers have been published (Pandy 2001; Fernandez and Pandy 2006; Viceconti, et al. 2006; Erdemir, McLean et al. 2007). Especially in human gait, one of the important behaviors of human movement, a few investigations have been conducted as well (Zajac, Neptune et al. 2002; 2003).

A query that could be of great interest is how complicated model that has to be used. Simple models can be helpful in identifying basic features of muscle function, and more complex models are implemented to study the functional roles of specific muscles in human movement (Pandy 2003). One of the simplest models ever used was a spring-mass model which was constructed by Bullimore (Bullimore and Burn,

2007). It was for analyzing human running (3-5 m/s). The spring-mass model is usually used to predict the external kinetic and kinematic variables of interest (Cheng and Hubbard 2004; Robilliard and Wilson 2005), or the joint torque (Cheng and Hubbard 2005).

Many models are built in two dimensions to make the study less complicated. However, when looking at the locations of the origin, insertion and via-points of most muscles, it is obvious that three-dimensional vectors instead of two-dimensional vectors better represent the line of action of the muscles (Nagano et al., 2005). Due to that reason and the improving computer capacity, many models are developed in three dimensions (Pandy 2003). The three-dimensional finite-element models are able to represent complex muscle geometry and the variation in moment arms across fibres within a muscle. This framework for representing muscle will enhance the accuracy of computer models of the musculoskeletal system (Blemker and Delp 2005).

2.4.2.2 Statement of the problem and preliminary knowledge

Before comparing the methods presented above, we have to briefly review the mathematical and mechanical difficulties in 'load sharing problem'. The well recognized difficulty in determining the individual muscle forces is the so-called redundancy problem in mechanics. For example, it is believed that the degree of freedom (DOF) at the ankle, knee, and hip joints are simplified to 6 DOF while the number of muscles rotating about those joints is more than 40. Therefore, if attempting to determine the individual muscle forces, we can find more unknown forces than the number of equations, and the muscle forces could not be determined directly from mechanical relationships alone. Mathematically, optimization schemes are adopted to solve the problem, which has been proved more effective and

reasonable than other solutions.

Additionally, equation of human motion is the basic knowledge to work out the individual muscle forces. We treat the human musculoskeletal system as an n DOF system, and the relationship between movement and muscle forces could be expressed by Eq. (2.11)

$$M(q)\ddot{q} + C(q,\dot{q}) + G(q) + R(q)F_{MT} + E = 0 \tag{2.11}$$

where $M(q)$ is the system mass matrix $(n \times n)$; $C(q,\dot{q})$ is the centrifugal and Coriolis loading $(n \times 1)$; $G(q)$ is the gravitational loading $(n \times 1)$; and E represents external forces. $R(q)F_{MT}$ represents net muscle moment $(n \times 1)$, where $R(q)$ is the matrix of muscle moment arms $(n \times m)$ and F_{MT} are the muscle forces $(m \times 1, m: number\ of\ muscles)$. From the equation, it is apparent that the system is redundant. $(m > n)$

2.4.2.3 Inverse dynamics method

The inverse dynamics method used to evaluate individual muscle forces is a technique based on the gait data combined with inverse dynamics and static optimization. It is easy to re-arrange Eq. (2.11) to the following form

$$-R(q)F_{MT} = M(q)\ddot{q} + C(q,\dot{q}) + G(q) + E \tag{2.12}$$

Due to the availability of the time history of the joint kinematic data q and the ground reaction forces E, the net muscle moment of each joint is possible to be calculated. Usually, the net muscle moment is worked out recursively from distal to proximal

instead of solving it with system dynamics. The ground reaction forces are used for calculating the most distal joint's net muscle moment.

After the net muscle moment obtained, the second step is to solve the load sharing problem, namely, to work out the individual muscle forces at each instant of time. Each step's muscle forces are optimized by minimizing an objective function J and subjecting to the net muscle moment constraints and other physiological value boundaries. Each joint's net muscle moment from inverse dynamics analysis represents the summation of the muscle moment due by each individual muscle force, and the boundaries are always derived from human anatomical and physiological theory. Such as the upper bound of the certain muscle force is the product of the muscle's maximum stress and its PCSA. Figure 2.22 shows the process of inverse dynamics method. In the illustration, the muscle force constraints could also be represented as dynamic constraints on muscle forces from lower and upper bounds of excitation levels. Van der Helm also supplemented the additional constraints g, h, which depend on the specifics of the joint contact force to prevent dislocation of the glenoid joint (van der Helm, 1994).

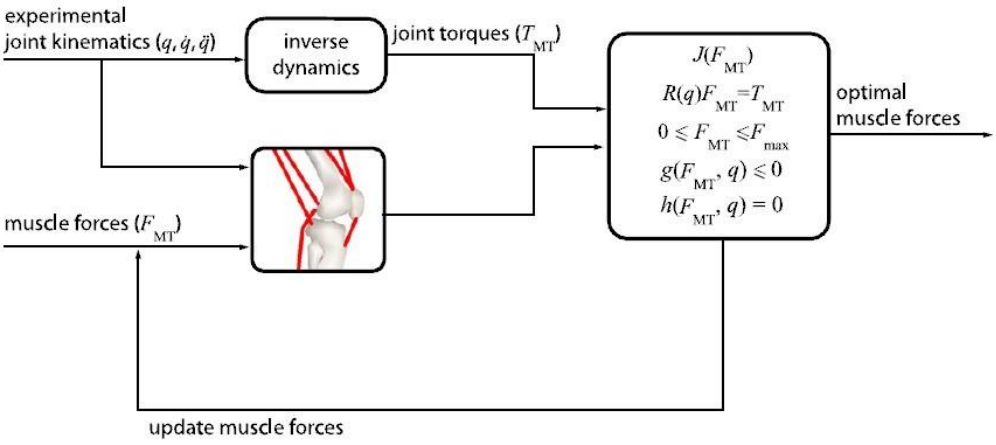

Fig. 2.22 The process of inverse dynamics method (Erdemir et al., 2007)

During human walking, most investigators have implemented inverse dynamics method to estimate the individual muscle forces in lower extremity (Crowninshield, 1978; Rohrle et al., 1984; Glitsch and Baumann, 1997; Lin et al., 2004), and the effects of objective functions and muscle parameters are also discussed (Glitsch and Baumann, 1997; Collins, 1995). Since no integration is required by inverse dynamics method, static optimization scheme is more computationally efficient than other optimization methods. Also, due to the linear equality and boundary constraints, if the objective function is selected as a linear function, the computational effort would be dramatically decreased by linear optimization (Rohrle et al., 1984; Pedersen et al., 1987). Although the method could be efficient in solving the individual muscle forces, it is not flawless due to the strong dependence on experimental data (Glitsch and Baumann, 1997). In addition, the lack of description on specific muscular dynamics and the excessive neglect of muscle physiological properties are what have been identified as weakness of the methodology.

The application of inverse dynamics ranges from lower extremity analysis to upper

limb studies. Both minimizing the sum of cubed muscle stress and maximizing the endurance have been widely used in predicting lower limb forces during human walking (Crowninshield and Brand, 1981) while minimizing the sum of squared muscle forces is commonly used in solving a load sharing problem in upper limb. Apart from this, various criterions have been attempted by investigators. How to compensate for the disadvantages of the inverse dynamics method without losing computational efficiency would be the direction of further research (Collins, 1995; Pandy et al., 2010).

2.4.2.4 Forward dynamics based data tracking method

When the muscle activations or net muscle moments are assumed to be known, the trajectory of each segment of the human musculoskeletal system could be calculated by solving equation (2.13) below,

$$\ddot{q} = \frac{C(q,\dot{q})+G(q)+R(q)F_{MT}+E}{M(q)} \tag{2.13}$$

Eq. (2.13) is another arrangement of Eq. (2.11), which predicts the movement pattern by the assumed inputs of muscle activation or net muscle moment. Such method is called forward dynamics, which is used to analyze the relationship between skeletal motions and muscle forces or net muscle moments.

Apparently, we could calculate the individual muscle force by using activation input. However, it is impossible to measure the exact muscle activations. Therefore, the forward dynamics in combination with optimization scheme is used to predict muscle forces. The approach needs an initial set of muscle activations to be fed into the musculoskeletal, and the gait data from the experiment is used as a reference. Such

process is iterated by searching for the muscle activations to best reproduce the kinematic data, where the individual muscle forces are verified during the searching process. In Figure 2.23, the forward dynamics based data tracking method is explicitly shown, and in some cases, the kinetics data, e.g. ground reaction forces are also treated as input to be compared in the optimization process.

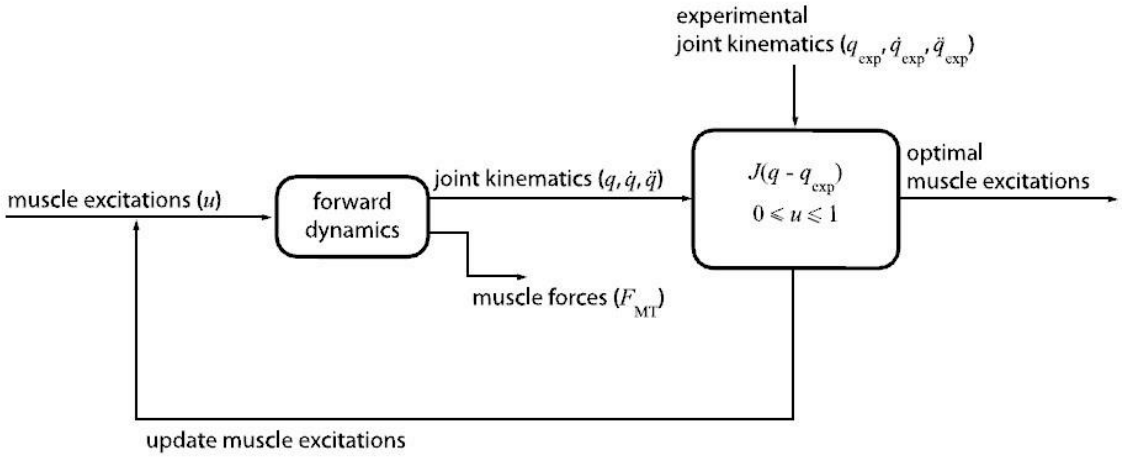

Fig. 2.23The process of forward dynamics based data tracking method (Erdemir et al., 2007)

Mclean has found the solution to explore injury mechanisms by using the forward dynamics approach, where a set of muscle activations is optimized to reproduce the movement pattern (McLean et al., 2004; McLean et al., 2003). In addition, the technique is particularly proven more reliable in a variety of high pace movement and might not be effective in low pace movement. Apart from evaluating the individual muscle forces, some additional estimation is obtained in the calculation. For example, Neptune and Hull has compared the untracked experimental data with model predictions (Neptune and Hull, 1999). Multiple objectives solution, such as minimizing the track errors in addition to the muscle stresses during movement, is possible to be conducted as well, but the weightings between different objectives are

still needed to be explored (Yamaguchi and Zajac, 1990).

Due to the forward nature of forward dynamics, Happee stated on that forward dynamics strategy had more advantageous over the inverse dynamics based static optimization method (Happee, 1994). Unlike the dependence of kinematics data in inverse dynamics, the forwards dynamics allows muscle forces estimations to be less sensitive to the gait data, which means the influence of measurement errors in kinematics input is reduced. Although the method has such advantages in theory, direct application is rarely adopted in clinical experiment. The difficulties include the computational burden and the parameter requirement. In the method, huge amount of integrations are used to obtain the joint kinematics, and more physiological details are requested in muscle mechanics. Recently, some effective solutions have been proposed, such as Thelen's method which results in muscle forces estimated are consistent with measured joint torques (Thelen et al., 2003).

2.4.2.5 Optimal control strategy

Optimal control strategy is a technique based on forward dynamics method as well. The significant difference between optimal control strategy and forward dynamics based data tracking method is the usage of kinematic data from experiments. As stated above, the experimental data is compared against predictive movement pattern as the objective function in forward dynamics based data tracking method. Whereas in optimal control strategy, an initial set of muscle activations is given as the input of solution, and the movement of the musculoskeletal system is first solved by forward dynamics. Unlike forward dynamics based data tracking method, the optimal control strategy uses muscle forces and kinematics related to task performance or physiological-based condition as objective functions, where the experimental data is

no longer used as the reference. The details of optimal control strategy are shown in Figure 2.24

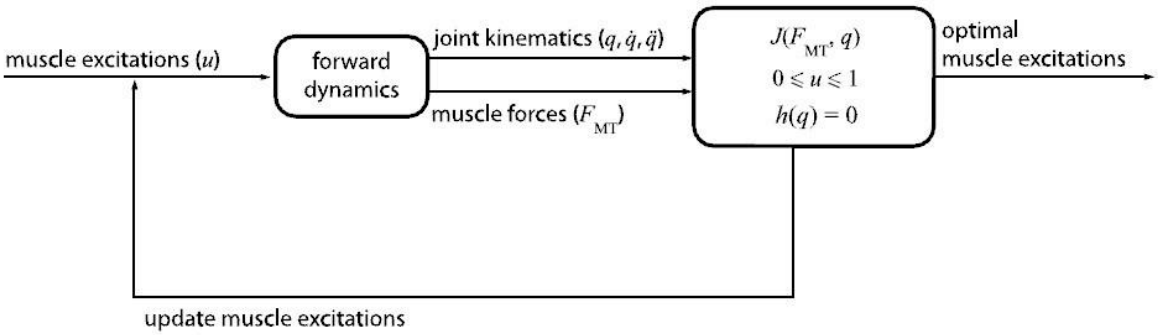

Fig. 2.24The process of optimal control strategy (Erdemir et al., 2007)

The approach has been used to investigate muscular functions in goal-directed movements of upper limb as well as the activities of daily living such as walking (Schouten et al., 2001; Ohta et al., 2004; Anderson and Pandy, 2001). It is helpful in assessing changes in control of muscles and muscle forces caused by surgery and other rehabilitations (e.g., plantar fasciotomy by Erdemir and Piazza, 2004). However, it is still under debate that how to select the objective function in optimization scheme. For movements that a have specific aim for performance, the selection of criterion is more reasonable and easier than other activities such as walking. Although similar movement patterns have been shown by different objective functions in walking, the selections still rely on the investigator's preference. Additionally, since the method is another form based on forward dynamics, the high computational cost is still an evitable problem in clinical application.

2.4.2.6 Other strategies

Recently, electromyography (EMG) data has been increasingly used in force calculation rather than validation only. EMG data could be directly incorporated into an EMG-driven forward dynamics model to predict muscle forces, and the method is

used in elbow motion and knee movement during swing phase (Koo and Mak, 2005; Piazza and Delp, 1996). The inaccuracies of the muscle parameters and EMG processing largely limit its further application. Also, EMG data combined with inverse dynamics approach provides a good result in force estimation, but the calibration of musculoskeletal models has to be implemented in the process (Amarantini and Martin, 2004). Referring to the utilization in the lower extremity including walking and running, Amarantini and Lloyd have employed the method requiring additional experimentation to obtain the relationship between isometric EMG and joint torque (Amarantini and Martin, 2004; Lloyd and Besier, 2003).

Forward dynamics combined with static optimization approach has been developed by Yamaguchi and Thelen (Yamaguchi et al., 1995; Thelen et al., 2003). In those studies, single forward dynamics at each time step was performed, which remarkably compensated the time-consuming disadvantage in standard forward dynamics based data tracking. Although such a method has been implemented in arm movement, cycling and other activities already, no evidence is shown that the strategy is effective in human walking behaviour.

2.5 Conclusions

A wide range of methods has been used to model the skeletal muscle. There exists truly little literature describing the skeletal muscle model with pronounced physiological characteristics. The studies of the influence of muscle intrinsic properties on the musculoskeletal system stability have been conducted on animal research, but most of them are based on experiment without model simulation. Most of the literature treat the standing behaviour as a control system and simplify the

musculoskeletal system. Such a simplification will bring the neglect of the muscle dynamic response without the adjustment of central neural system, and especially the function of muscular control system cannot be explicitly understood. The evaluation of the individual muscle forces during human walking has been a hot topic over the last decade. Many researchers have proposed a variety of strategies to solve it, and most of the methods are based on inverse dynamics and forward dynamics method. The forward dynamics method is disadvantageous in the high computational cost, which makes the method impossible to be implemented in clinical practice. Although the inverse dynamics method is more efficient, without muscle physiological characteristics and intrinsic properties, the dynamic response cannot be accurately described. A neuromusculotendon unit model with more physiological characteristics will be constructed in our study, and the model will be used in the evaluation of mechanical loading during standing and walking in the following chapters.

Chapter 3. Biomechanical Modelling of a Single Skeletal Muscle

3.1 Introduction

Mathematical modelling is an effective way to understand the underlying mechanism of a physical system, providing insights into the internal working principle of the system. Since the classic work was conducted by Hill in late 1930s, muscle models have been developed in three separate directions. Each of these modelling approaches has the advantages and the disadvantages, and the approach used is based on the role that muscle plays in the study of interest. As stated in the previous chapter, from a structural viewpoint, the types of models fall into three categories, which are simple Hill model, Hill-type model and Huxley muscle model. These models may result in preventing further understanding of muscle's physiological properties due to the simplicities, such as Hill model, or bringing extra computational cost caused by the complicated parameters and the mathematical expressions, such as Huxley model. The most efficient model for simulating a wide variety of human movement may be Hill type model. The model compensates for the disadvantages of both simple Hill model and Huxley muscle model with its certain structure and function. Compared with simple Hill model, the extra elements and characteristics of Hill type model could more accurately simulate various human movements and the corresponding dynamic responses. Although Hill type model has been used in the investigations on the single musculotendon unit or the musculoskeletal systems by many research

groups, the model is still lack of enough physiological characteristics. The goal of this chapter is to develop an improved Hill type muscle model based on the current state of muscle physiological knowledge.

3.2 Mechanical behaviour of skeletal muscles

A quantitative understanding of the mechanical behaviour of skeletal muscle is necessary in many fields of biomechanical research and applications. Electromyography (EMG) device has been used in measuring the muscle electrical signals to interpret the muscle dynamic response (Nigg and Herzog, 1999). It has been proved that EMG signals cannot directly relate to the muscle tension. This section is to develop a quantitative muscle mathematical model and analyze the relationships between the muscle force and each element in the musculotendon system.

3.2.1 Activation dynamics

As introduced in the preceding chapter, the activation dynamics refers to the transformation of the neural input to the activation of muscle contractile element, where the calcium pumped out of the sarcoplasmic reticulum to travel down to the T-tubule system and bind to troponin. Such a chemical procedure is treated as two first-order dynamic systems by most of the researchers, neural excitation and muscle activation. In our study, we still use two first order systems to represent the activation dynamics. Both the excitation time and the activation time are constants in the dynamic system, which correspond to the time constant in the first order systems. To sum up, the whole activation procedure is two coupled first order systems with in-series connection.

Mathematically, the first order system is expressed by a discrete model here, instead

of a first order differential equation, $E' = \frac{U-E}{T_{ne}}$ and $A' = \frac{E-A}{T_a}$, where U, E, A represent the neural input, the neural excitation and the muscle activation separately, and T_{ne}, T_a are the time constant of neural excitation and muscle activation (see Figure 3.1).

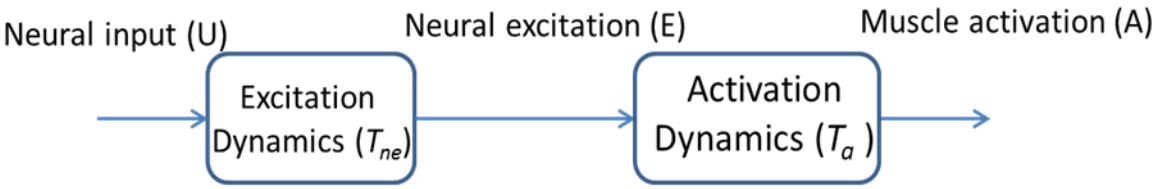

Fig. 3.1 The excitation and activation dynamics

For a linear first order system, assuming a constant input, the output could be analytically solved under an exponential function. We can express the neural excitation and muscle activation processes into two exponential functions,

$$E(t) = E(t-TI) + [U(t-TI) - E(t-TI)]\left[1 - \exp(-\frac{TI}{T_{ne}})\right] \quad (3.1)$$

$$A(t) = A(t-TI) + [E(t-TI) - A(t-TI)]\left[1 - \exp(-\frac{TI}{T_a})\right] \quad (3.2)$$

where TI is the time step in the discrete systems, and both TI in Eq. (3.1) and Eq. (3.2) are the same. Particularlly, what we need to pay attention to is the value of parameter T_a. Due to the physiological property, the increasing active state and the decreasing active state give different T_a value, the latter of which is larger than the former one. In neuroscience, the neural input is believed as an all-but-nothing event, and we normally treat it as a square wave which has ‘0 ’ and ‘1’ two levels (Winter 2009). Based on the description above, Figure 3.2 illustrates the signals in such a process.

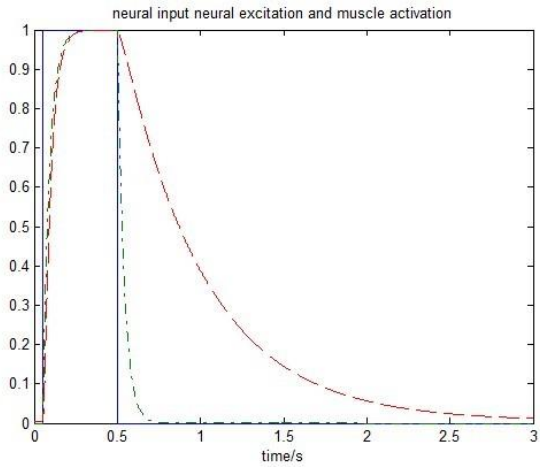

Fig. 3.2The neural input, the neural excitation and the muscle activation

The solid curve and the dash-dot curve are the neural input and the neural excitation while the time-history of muscle activation is demonstrated by dashed curve. From Figure 3.2, we can clearly see the response delay between neural input and neural excitation in the increasing active state, but the difference between neural excitation and the muscle activation is not obvious in the increasing active state. In contrast, the response delay between the neural input and the neural excitation is much smaller than that between the neural excitation and the muscle activation. The reason is that T_a in increasing active state is smaller than that in decreasing active state.

3.2.2 Contraction dynamics

The contraction dynamics converts the metabolic energy of the human body into muscular mechanical work. In contraction dynamics, the muscle force is the output which depends on the muscle activation level A. However, the muscle activation is not the only determinant that affects the magnitude of muscle force. The muscle fibre length, the muscle fibre contraction velocity and the tendon state all have influences on muscle force production. Also, due to the influence of muscle physiological

characteristics, more anatomical and biological details should be considered in the model.

3.2.2.1 Force-length property of contractile element

As shown in Figure 2.18 (b), the muscle tissue could be seen as a contractile element in parallel with an elastic element. The steady state of muscle tissue is defined by its force-length (f-l) curve, and the property is determined by the muscle activation A and the muscle fibre length L_m. In particular, the muscle fibre length here is the muscle tissue length along the direction of muscle force. As shown in Figure 2.17, the active force is the force generated when muscle is activated. Under different muscle activations, the active force follows the scaled version rule while the passive force developed by other interfibre tissues, such as the endomysium, the perimysium and the epimysium, have no relationship with the muscle activation. Normally, the region where the muscle active force is generated is $0.5L_{mo} < L_m < 1.5L_{mo}$, where L_{mo} is called optimal muscle fibre length, and at L_{mo}, the muscle active force can reach its peak force F_{mo} when the muscle is fully activated. F_{mo} is defined as the maximum isometric muscle force.

Although, the force-length curve provides the relationship between the length of muscle fibre and the muscle force, it is still limited by the spacial structure and geometry. The Muscle tissue is a three-dimensional entity, where the deformation is greatly influenced by the geometrical relations. Here, we propose our muscle tissue deformation assumption, and the details are shown in Figure 3.3. It is assumed that

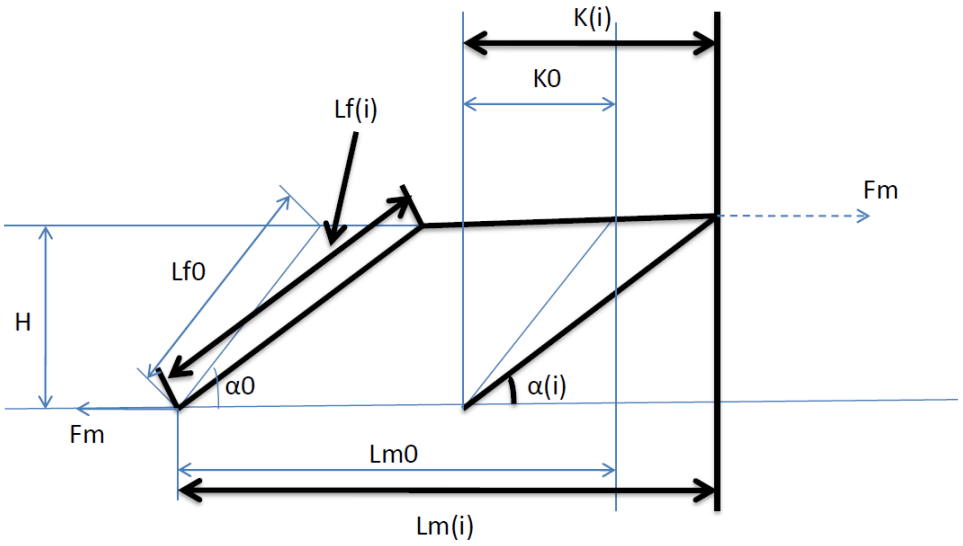

Fig. 3.3The deformation of muscle tissue in two-dimension

the depth (*H*) and the thickness of the muscle tissue keep constant value during deformation. And the variables are the muscle fibre length (L_m), the muscle fibre belly length (L_f) and the pennation angle (α).

Kaufman has presented a mathematical expression to describe the force-length relationship of the contractile element (Kaufman et al., 1991),

$$F_{f-l} = exp\left(-\left[\frac{\left(\frac{L_m - L_{mo}}{L_{mo}}+1\right)^{\left[0.963\times\left(1-\frac{1}{i_a}\right)\right]}-1.0}{0.353\times(1-i_a)}\right]^2\right) \text{ for } i_a < 1; \tag{3.3}$$

$$F_{f-l} = exp\left[-\left(2.727 \times ln\left(\left(\frac{L_m - L_{mo}}{L_{mo}}+1\right)\right)\right)^2\right] \text{ for } i_a = 1, \tag{3.4}$$

where a geometry value, $i_a = \frac{L_f}{L_m}$, was used and F_{f-l} is the normalized force which equals to $\frac{F_m}{F_{mo}}$. F_m is the real muscle force during contraction. Moreover, Benninghoff and Rollhauser proposed the equation below to express the relations among L_f, K and α (Benninghoff and Rollhauser, 1952),

$$L_f = \frac{K}{cos\alpha - \sqrt{(cos^2\alpha + n^2 - 1)}} \tag{3.5}$$

where $n = \frac{L_f}{L_{fo}}$, and L_{fo} is the muscle fibre belly length corresponding to the muscle fibre length L_{mo}.

Based on the Eq. (3.3), the Eq. (3.4), the Eq. (3.5) and our deformation assumption, we provided an improved way to calculate the muscle force. In Kaufman's statement, 'i_a' kept as a constant during the whole dynamic process and varied as diverse types of muscles. Apparently, the 'i_a' should have changed during shortening and lengthening, which gave us inspirations to consider it as a function of L_m and pennation angle α. Therefore, we used Eq. (3.5) to establish the relations among L_f, K and α, so as to get 'i_a' as a function of α and L_m.

By incorporating the relationship of i_a, α and L_m into Kaufman's method, we proposed a time-varying geometrical parameter "i_a", which gave the model more physiological and dynamic feature.

3.2.2.2 Force-velocity property of contractile element

In 1930s, Hill proposed an empirical relation between the muscle force, P, and the muscle shortening velocity, v (see Eq. (2.4)). In the equation, the muscle shortening velocity and the muscle force are explicitly expressed in concentric contraction, but there is no force-velocity relationship when the muscle lengthens. However, the lengthening occurs regularly during any movement, so it is important to see the effect of muscle lengthening velocity on the muscle force. In our study, we chose a continuous relationship as below (Hatze, 1981),

$$F_{f-v} = 0.1433 \times \{0.1704 + exp[-1.409 \times \sinh(3.2v + 1.6)]\}^{-1} \qquad (3.6)$$

Where F_{f-v} is the normalized muscle force, and v is the normalized muscle velocity. In the equation, $v = \frac{v_m}{v_{\max}}$, v_m is the muscle contraction velocity and $v_{\max}$ is the maximum muscle shortening velocity.

Hatze's force-velocity relationship offers an ideal way to make the function derivable at each point, and we prefer adopting such an equation to represent the relationship between muscle force and muscle contraction velocity which is shown in Figure 3.4.

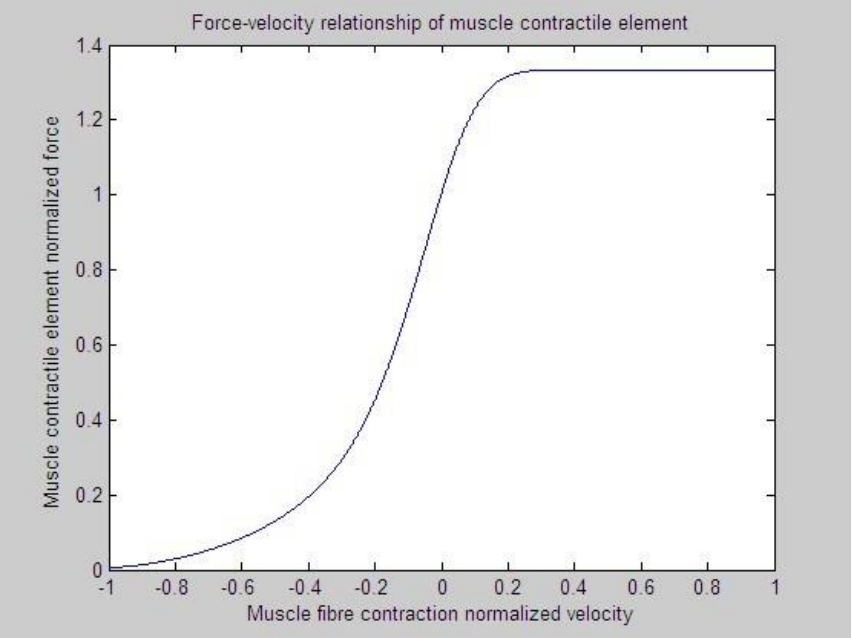

Fig. 3.4Muscle normalized force-velocity relationship

3.2.2.3 Combined force, length & velocity relationships

The muscle contractile element force is determined by the muscle activation level *A*, the maximum isometric muscle force F_{mo}, the muscle fibre length L_m and the muscle contraction velocity v_m. Therefore, the resultant force can be mathematically expressed as,

$$F_{ce} = F_{f-l} \times F_{f-v} \times A \times F_{mo} \tag{3.7}$$

Where, F_{ce} is the muscle contractile element force, F_{f-l} is the normalized force in force-length relationship, F_{f-v} is the normalized force in force-velocity relationship (Kaufman et al., 1991).

3.2.2.4 Parallel element and muscle tissue force

Referring to the force of parallel element, it can be expressed as a function of the muscle fibre length as below (Anderson and Pandy, 2001),

$$F_{pe} = F_{mo} \times 3 \times 10^4 \times exp\left[6 \times \left(\frac{L_m}{L_{mo}} - 3.2\right)\right] \tag{3.8}$$

where, F_{pe} represents the parallel element force of muscle tissue. Therefore, the muscle tissue force F can be derived by summating the contractile element force and parallel element force,

$$F = F_{ce} + F_{pe} \tag{3.9}$$

3.3 Series elastic element

Series elastic element is the component what connects the bone and the muscle tissue. Unlike muscle tissue, series elastic element is unable to contract itself and is completely analogous to a mechanical rope, because it offers no resistant force when it shortens. It has been proved that series elastic element and contractile element overlap each other anatomically, and it is hard to determine the length of series elastic element. In our study, we define the length of series elastic element is the difference value between the whole muscle group and the muscle tissue. One of the important parameters of series elastic element is the length at which it just begins to develop force. It is called slack tendon length, L_{st}.

During modelling, the elasticity of series elastic element is assumed to be linear or nonlinear, such as exponential style (Winters and Stark, 1985). In our study, we use this nonlinear function to express the tendon's force-length relationship,

$$F_t = \left[\frac{F_0}{exp(SE_{sh})-1}\right] \times \left\{exp\left[(L_t - L_{st}) \times \frac{SE_{sh}}{SE_{xm}}\right] - 1\right\} \quad (3.10)$$

Where F_t and L_t are series elastic element force and length, SE_{sh}, SE_{xm} are the subject-specific parameters.

It is noteworthy that due to the connection way of the muscle tissue and the series elastic element, the muscle tissue force is the same as the force of series elastic element all the time.

3.4 A computer simulation of isometric contraction

3.4.1 Mathematical modelling of the musculotendon unit

In biomechanics research, it is rarely to study the muscle tissue and the series elastic element (tendon) in isolation. Their integrated mechanical characteristics influence the performance of the musculoskeletal system during human movement. By combining the individual component stated before, we constructed a physiology-based musculotendon unit model in our study. The structure of the model is illustrated in Figure 3.5. It is clearly illustrated that under a certain neural input and

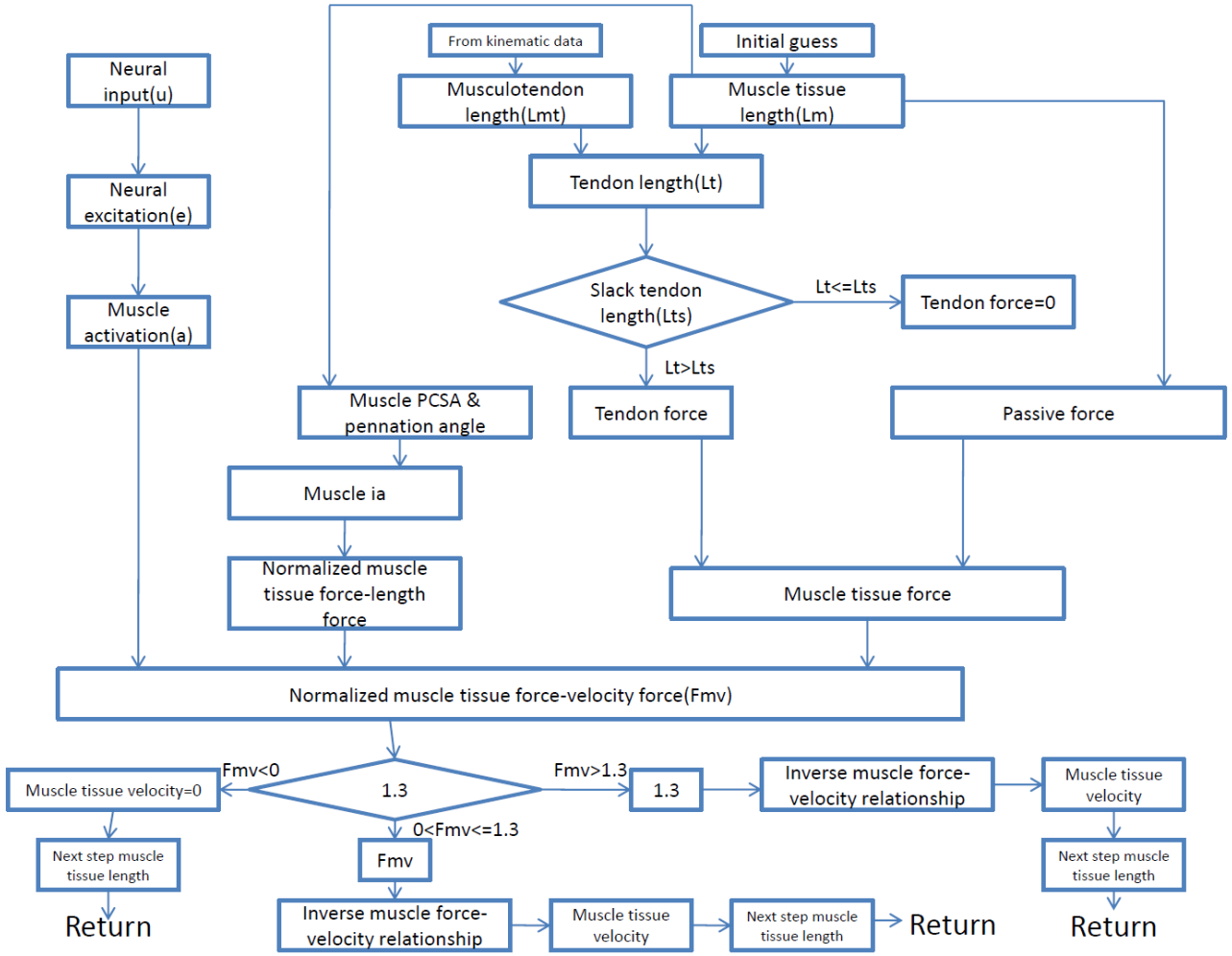

Fig. 3.5The structure of musculotendon unit model

musculotendon length, all the musculotendon variables can be obtained by our model. In our study, we successfully add PCSA and pennation angle into the musculotendon model. Moreover, due to the activation dynamics used in the model, it is feasible that the model can be implemented in forward dynamics of human motor control and locomotion.

3.4.2 Some simulation result of isometric contraction

Some simulations under isometric contraction were conducted, where the muscle anatomical parameters were obtained from the anthropometric data of a Tibialis Anterior muscle group (Friederich and Brand, 1990). The parameters are listed in Table 3.1.

Table 3.1 Anatomical parameters of a Tibialis Anterior muscle group

Optimal muscle fibre length, L_{mo} (m)	0.07
Maximum isometric muscle force, F_{mo} (N)	603
Slack tendon length, L_{st} (m)	0.27
Pennation angle at optimal muscle fibre length, α (^{o})	12
Muscle fibre volume, V_m (m^3)	1.3×10^{-4}

The muscle was stimulated using single square wave and periodic square wave neural inputs respectively. For the single square wave input, the time length of the neural input at level '1' was 0.01s. The parameters in Eq. (3.1) and Eq. (3.2) are as below,

$T_{ne} = 0.04s$,

$T_a = 0.01s\ (increasing\ active\ state)\ and\ 0.05s\ (decreasing\ active\ state)$,

$TI = 0.001s$.

In addition, since the muscle activation A is used as the denominator in the calculation, we enforced its normalized value in the range of 0.005 to 1 instead 0 to 1 to avoid numerical singularity. The total length of the musculotendon unit in isometric contraction was kept constant. In our simulation, the total length of the musculotendon unit equals to the summation of L_{mo} , L_{st} and ΔL_t (tendon stretch length) under 0.005 muscle activation ($A = 0.005$).

Figure 3.6 shows the muscle force and muscle tissue length changes under single square wave neural input. The muscle tissue here refers to the whole Tibialis Anterior muscle group. Since the muscle tissue initial length in our simulation was at its optimal muscle fibre length, the muscle force at the initial state was 36N rather than

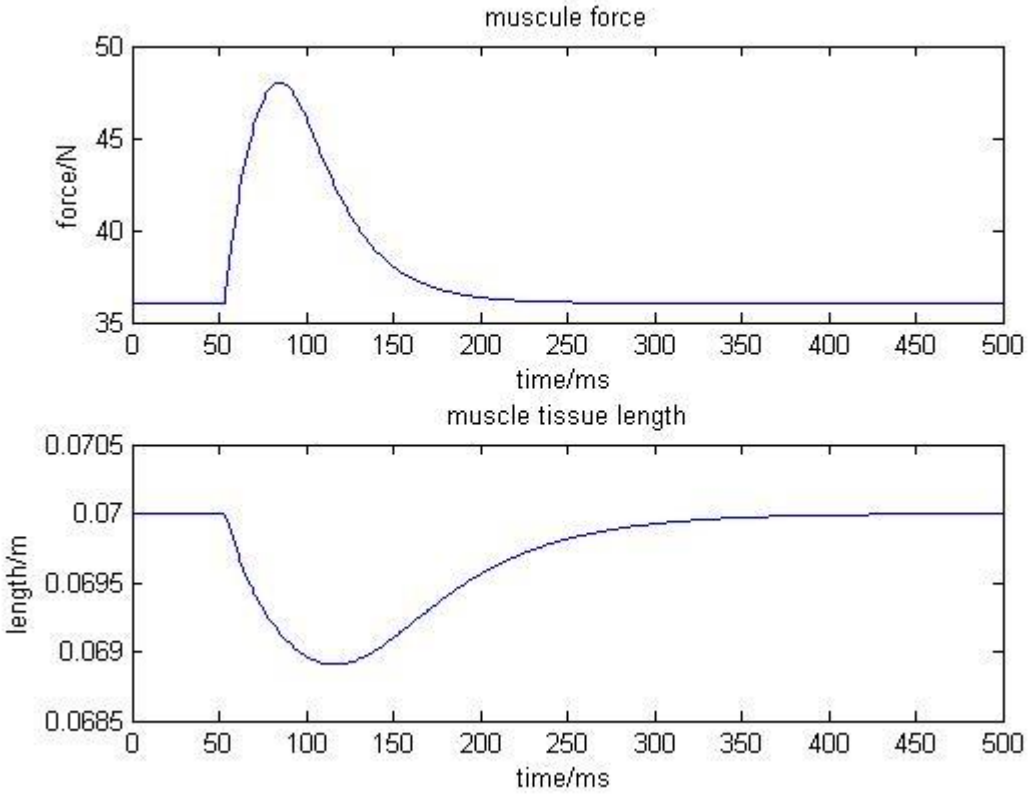

Fig. 3.6The isometric contraction simulation under a single square wave neural input

0N. In the muscle force history, there is a sharp increase followed by a gradual decline, because the increasing active state time constant is less than the time constant for decreasing active state. Such tendency in muscle force change has been demonstrated by other researchers using both experimental and modelling methods. Figure 3.7 shows the experimental and simulation results presented by Van Zandwijk (Van Zandwijk et al., 1996).

In Van Zandwijk's research, the muscle sample they used was a Gastrocnemius Medialis muscle from adult Wistar rat. Therefore, it is meaningless to compare the absolute muscle force value with our results. However, the percentage of increasing time (PIT) and the style of the pattern of the force increasing and decreasing processes can be analyzed. We define the percentage of increasing time (PIT) as the percentage of force increasing time with respect to the whole period of force change. We also consider that the muscle returns to its initial state when the muscle force reaches 1% of its peak value, and thus define the finishing time of muscle force change. In the experimental result of Figure 3.7, the muscle force starts increasing at about 0.003s and reaches its summit at 0.02s. The force returns to the initial state at around 0.08s. The PIT is $\frac{0.02-0.003}{0.08-0.003} \times 100\% = 22.08\%$. Similarly, the increasing time in our simulation result is 31 ms, and muscle force change last 146 ms in Figure 3.6. The PIT in our simulation result is $\frac{31}{146} \times 100\% = 21.13\%$. Moreover, when comparing the concave style of the muscle force decreasing, the muscle force increases more linearly in Figure 3.7. Our simulation result shows the highly similar tendency during both muscle force ascending and descending periods in Figure 3.6.

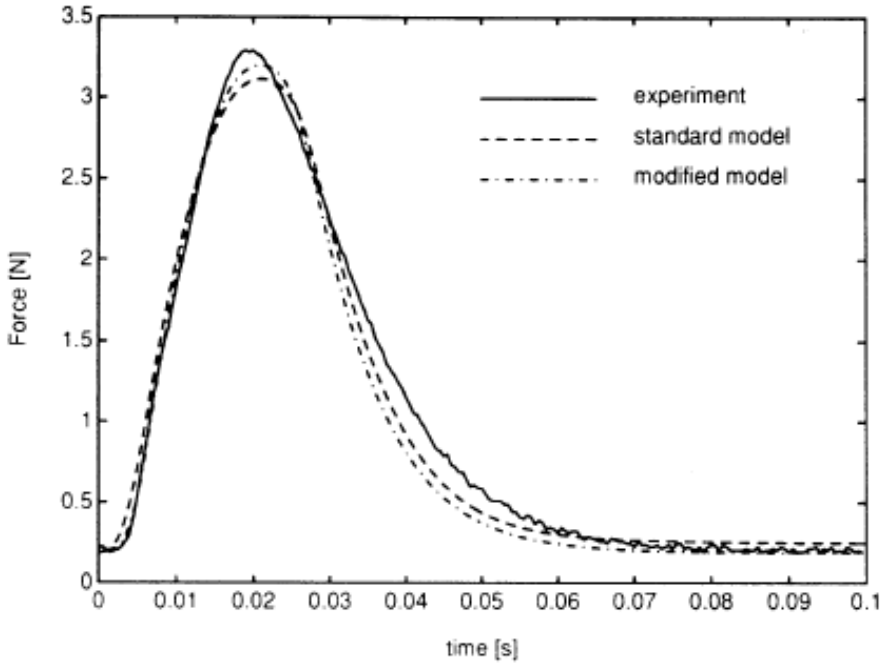

Fig. 3.7 The force histories of simulated and experimentally measured at Wistar rat Gastrocnemius Medialis (Van Zandwijk et al., 1996)

Zajac (Zajac, 1989) has explained that geometrical and mechanical characteristics of the muscle tissue are the same as that of the muscle sarcomere's, for the muscle tissues are the scale-up version of the muscle sarcomeres. Therefore, the force and length changes of sarcomere could directly reflect the changes in muscle tissue. Figure 3.8 shows the sarcomere tension and length changes during isometric contraction reported by Mutungi and Ranatunga (Mutungi and Ranatunga, 2000).

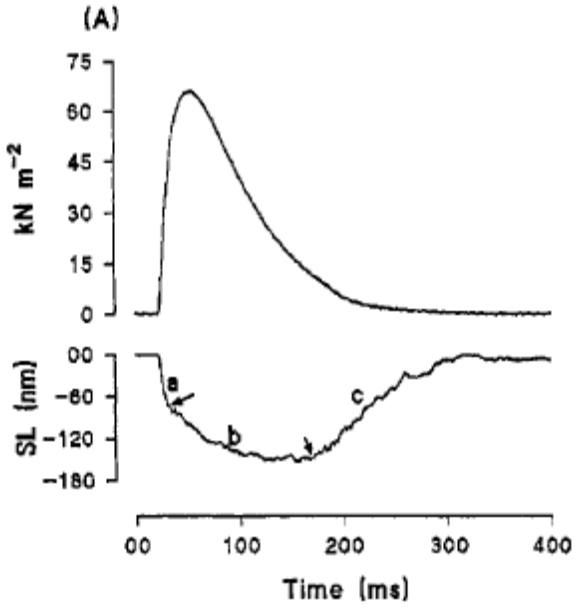

Fig. 3.8The sarcomere tension and length changes during isometric contraction (Mutungi and Ranatunga, 2000)

In Figure 3.8, the sarcomere shortening occurs in two phases: a period of rapid shortening (a) followed by a slow shortening (b). The slow sarcomere shortening is followed by sarcomere lengthening (c). The arrows indicate the end of phase (a) and (b). From our simulation result in Figure 3.6, we could easily see the (a), (b) and (c) phases in 'muscle tissue length' change. But within phase (c), our result shows a 'rapid lengthening – slow lengthening' trend, which is slightly different from the experiment result in Figure 3.8. However, the muscle force-velocity relationship in Figure 3.4 has explicitly showed that during muscle lengthening, muscle force decreases as the lengthening speed reduces, which could well explain the 'rapid lengthening – slow lengthening' tend during muscle force decreases in our simulation result. Because the magnitude of sarcomere length is in nanometre, and we believe some experimental error is unavoidable, which may affect the sarcomere length measurement. What we should pay attention to is the sarcomere lengthening begins

when twitch tension has relaxed to about 30% of its peak value in Figure 3.8. In our simulation result, the muscle tissue lengthening begins at 124ms, where the muscle force has relaxed to 39.04% of its peak value, which is very close to the measurement data.

Van Zandwijk (Van Zandwijk et al., 1996) has also reported the muscle force data under different stimulation frequencies in isometric contraction. In Figure 3.9, the continuous lines are experimentally measured forces and dashed curves are forces generated in their model simulations. For both the experimental and simulated force histories, the uppermost force trace corresponds to the stimulation at 80Hz and subsequent traces correspond to frequencies of 60Hz, 40Hz and 20 Hz respectively.

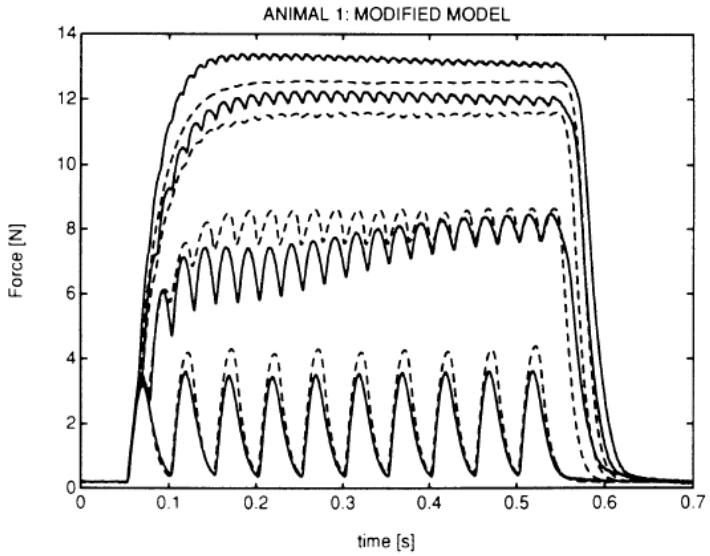

Fig. 3.9Force histories at different stimulation frequencies Van Zandwijk (Van Zandwijk et al., 1996)

In order to validate our model, we conducted similar simulations, where 20Hz, 40Hz, 60Hz and 80Hz stimulation frequencies were applied. Figure 3.10 shows our

simulated force histories at 20Hz, 40Hz, 60Hz and 80Hz stimulation frequencies in isometric contraction.

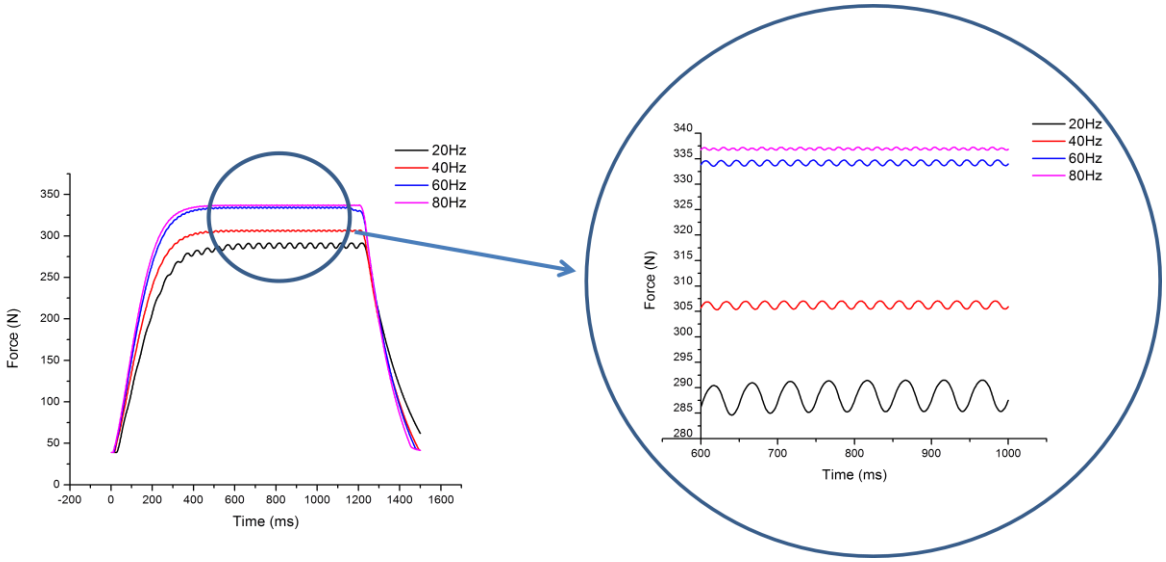

Fig. 3.10The force histories at different stimulation frequencies in our model

As different muscles were used in Van Zandwijk's work and our simulation, to compare the absolute force values, the force fluctuation amplitudes and the increasing time are not meaningful. Here, we proposed two new sets of values to validate our model.

1. The force amplitudes ratio between two consecutive stimulation frequencies (RA)
2. The ratio of the differences between steady state values for three consecutive stimulation frequencies (RDSSV)

The amplitudes and steady state values under different stimulation frequencies in both Van Zandwijk's experiment and our simulation are listed in Table 3.2

Table 3.2 The amplitudes and steady state values under different stimulation frequencies

	Van Zandwijk's experiment		Our simulation result	
	Amplitude (N)	Steady state value (N)	Amplitude (N)	Steady state value (N)
20Hz	3.6	2	6.25	286
40Hz	1.0	6.6	1.8	306
60Hz	0.6	12	1.23	333
80Hz	0.25	12.9	0.55	337

The RA value for 20Hz and 40Hz in the result of the experiment is $\frac{Amplitude\ at\ 20Hz}{Amplitude\ at\ 40Hz} = \frac{3.6}{1} = 3.6$, and the RA for 20Hz and 40Hz in our simulation result is $\frac{6.25}{1.8} = 3.47$. The percentage error is $\frac{|3.6-3.472|}{3.6} \times 100\% = 3.6\%$. The RAs in the results of experiment and our simulation are listed in Table 3.3

Table 3.3 The comparison of RAs in the experiment and our simulation results

	Van Zandwijk's experiment	Our simulation result	Percentage error
20Hz/40Hz	3.6	3.47	3.6%
40Hz/60Hz	1.67	1.46	12.6%
60Hz/80Hz	2.4	2.24	6.67%

The RDSSV for 20Hz, 40Hz and 60Hz in the result of the experiment is

$\frac{Steady\ state\ value\ at\ 40Hz - Steady\ state\ value\ at\ 20Hz}{Steady\ state\ value\ at\ 60Hz - Steady\ state\ value\ at\ 40Hz} = \frac{6.6-2}{12-6.6} = 0.852$, and the RDSSC for 20Hz, 40Hz and 60Hz in the result of our simulation is $\frac{306-286}{333-306} = 0.741$. The percentage error is 13.03%. The RDSSVs in Van Zandwijk's experiment and our simulation are listed in Table 3.4.

Table 3.4 The comparison of RDSSVs in the experiment and our simulation

	Van Zandwijk's experiment	Our simulation result	Percentage error
20Hz, 40Hz and 60Hz	0.852	0.714	13.03%
40Hz, 60Hz and 80Hz	6.0	6.75	12.5%

Not only has Van Zandwijk done the experiment to explore the muscle dynamic response under different stimulation frequency, but he also developed muscle models to simulate such dynamic process as well. From Figure 3.9, we could see the simulation result from his model. Hereby, we work out his model's RAs and RDSSVs compared to our simulation result, and the comparison results are listed in Table 3.5. From Table 3.5, we can conclude that,

1. The simulation results from our muscle model match the experiment results very well in terms of general trends and patterns

Table 3.5 Percentage errors of RAs and RDSSVs in Van Zandwijk and our simulations

		Percentage errors in Van Zandwijk's simulation result	Percentage errors in our simulation result
RA	20Hz/40Hz	11.11%	3.6%
	40Hz/60Hz	139.52%	12.6%
	60Hz/80Hz	108.33%	6.67%
RDSSV	20Hz, 40Hz and 60Hz	101.17%	13.03%
	40Hz, 60Hz and 80Hz	27.08%	12.5%

2. Compared to Van Zandwijk model simulation results, our model shows a better representation of the muscle dynamic response under different high-frequency neural inputs.

3.5 Conclusions

In this chapter, a phenomenological neuromusculotendon model including three basic elements has been presented, and more physiological characteristics are considered in the model. A set of isometric contraction simulations was conducted to validate the feasibility of the muscle model, which has proved that the model reflect the dynamic responses very well.

The muscle activation dynamics was divided into two first order system, which has been modelled into discretization model expressed by exponential functions. In the transformation from the neural excitation to the muscle activation, the time constants

in the first order system were different at increasing active state and decreasing active state.

An assumption of muscle deformation during contraction was proposed as well, where the intrinsic muscle force-length relationship is directly linked to the time dependent pennation angle. This assumption not only reasonably introduces the physiological characteristic, pennation angle, into the model, but also reflects the pennation angle as a dynamic variable.

As one of the most important intrinsic properties, the muscle fibre's force-velocity relationship was expressed by a continuous function in this chapter. The force of the contractile element can be continuous when muscle fibre contraction velocity changes its direction.

The tendon mechanics was represented by a nonlinear exponential function instead of linear expression. The exponential form can better reflect the realistic force -length relationship of tendon.

Based on the representation of each component, a neuromusculotendon model with contractile element, parallel element and series elastic element was adopted in muscle twitch simulations. Compared to previous experimental and simulation studies, our isometric contraction simulations suggest that the model proposed here produces very reasonable result.

Chapter 4. The Muscle Activities in Standing Postural Balance

4.1 Introduction

The skeletal system, connected together through ligaments, muscles and tendons, provides the vital structural support for the human body. With the aid of muscular actions, our body can perform a plethora of coordinated movements through the numerous articulating joints. In performing such movements, the muscles generate concerted forces to maintain joint and body stabilities. In recent years, the motion stability of neuromusculoskeletal systems has attracted increasing attentions. It has been shown that, during dynamic locomotion, a concert synergy of the muscle intrinsic properties and the geometric architectures of the musculoskeletal systems can guarantee the self-stabilization without the active Central Neural System (CNS) controls (Wagner and Blickhan, 2003; Wagner and Blickhan, 1999).

The objective of this study is to investigate how the intrinsic muscle mechanical properties would affect the musculoskeletal system self-stabilizing ability during standing posture and to understand the contribution of individual muscle component to the system stability. The investigation on the interplay between stability and energy expenditure of the musculoskeletal system responding to an external perturbation during standing posture will also be conducted.

In order to verify the stabilizing characteristics of muscles as a constituent component

of the musculoskeletal system and also to quantify the individual contribution of each muscle element, it is necessary to select a sufficiently simple and transparent example. Therefore, we restrict our simulations to a simple model with all the essentials of a dynamic musculoskeletal system: a single-joint inverted pendulum system with a rigid linkage driven by an antagonistic muscle pair. Also, a human standing neuromusculoskeletal model with six extensors and flexors around the ankle joint is constructed to evaluate each muscle's preflex dynamic response under four different criteria, and a set of multiple-objective optimization simulation is used for assessing the interplay between stability and energy expenditure during human standing.

It has been reported that a simple musculoskeletal model is useful for analyzing the muscle dynamics during human standing (Winter et al., 2001; Morasso and Sanguineti, 2002). In our research, the simplifications are justified by the idea that the reduced case is contained as a specific solution of more general case. Taking the inverted pendulum model we constructed for example, our specific purpose is to analyze the influence of muscle intrinsic properties on the musculoskeletal system stability. A simple inverted pendulum model will be more straightforward to investigate the problem without any other uncertain effect which may be brought by more complicated models. If the individual intrinsic properties are removed or changed, most of the system dynamic responses will vary observably, which makes the conclusion of the research more convictive. Six prime extensors and flexors around the ankle joint are constructed in our human standing model. Although the model tilts in the sagittal plane, the muscles' origins and insertions are not restricted in two-dimensional space, which means the muscles generate three-axis forces. The human standing model we constructed will be effective enough to analyze the certain muscles

dynamic responses and their control priority in preflex stage.

Our simulations support the general postulation that the muscle intrinsic properties provide the self-stabilizing ability for musculoskeletal systems. This has been proved not only for dynamic locomotor activities, but also for standing postural control. Our results show that the stabilizing behavior will not be realized if there is lack of the force-velocity relationship of the muscle contractile element and the force-length relationship of the series elastic element. In addition, the simulation results also indicate that the energy saving strategy will be more considered in human standing postural control during preflex stage.

4.2 Stability analysis of one DOF antagonistic system

4.2.1 Invert pendulum antagonistic system modelling

To investigate how the intrinsic mechanical properties of muscles will affect the postural stability of musculoskeletal systems, a typical musculoskeletal joint with one rigid linkage driven by a pair of antagonist muscles is constructed (see Figure 4.1). To simply, the joint motion is confined only in the sagittal plane with one degree of freedom. The dynamic responses of the flexor and extensor induced by the neural inputs are represented by three dynamic processes: neural excitation, muscle activation and muscle contraction dynamics. The mechanical parameters of the agonistic and antagonistic muscles are determined based on the anatomical data of a human tibialis anterior muscle (Friederich and Brand, 1990). The maximum isometric muscle force is 603N corresponding to the optimal muscle length of 0.07m. The muscle fibre pennation angle is 12^{o}, and the slack tendon length is 0.27m. The muscles are located to make a 45^{o} with respect to the linkage. The muscle insertions

are set at the same horizontal level as the joint centre, and the origins are fixed on the linkage without any relative motion. The rigid linkage was 1m length with uniformly distributed mass of 10 kg.

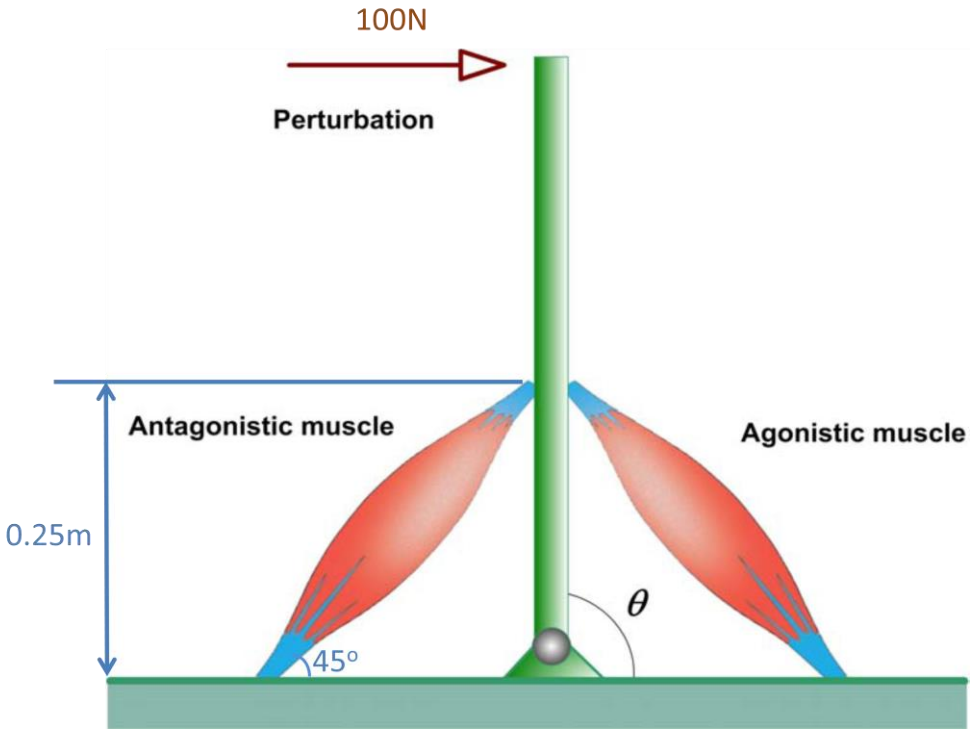

Fig. 4.1 The single-joint musculoskeletal system driven by an antagonistic muscle pair subjects to an external force perturbation.

4.2.2 Stability analysis under impulsive perturbation

To probe the system stability, a set of perturbation simulations, with an external impulsive force applied at the distal part of the linkage, is conducted. The initial position of the linkage is bolted upright with 90^{o} with respect to the horizontal direction. The initial muscle length of both flexor and extensor muscles are at their optimal muscle length. It is assumed that a coactivation occurs in the antagonistic muscle pair with equal muscle activation levels at both flexor and extensor muscles before the perturbation. Thus, the linkage is initially static. A 100N impulsive force along the horizontal direction is then applied at the distal end of the linkage lasting

0.01 second.

A set of sensitivity analyses has been conducted to investigate the effect of the muscle pennation angle, intrinsic muscle mechanical properties and muscle coactivation level on the dynamic stability characteristics of the system. To investigate the effect of pennation angle, initial angle values of 6^o, 12^o, 18^o are used by also considering muscle geometric deformation, with muscle coactivation level set to 0.5. As the muscle activation level is from 0 to 1, the value 0.5 we set represents that the antagonistic muscle pair both are activated moderately (Lloyd and Besier, 2003). The individual muscle mechanical properties, including the contractile element (CE)'s force-length relationship, the CE's force-velocity relationship, the parallel elastic element and the series elastic element, have been removed separately from the muscle model to investigate the individual contribution of each muscle component to system stability.

Finally, the effect of the muscle coactivation level has been simulated, including three different coactivation levels: low level (0.1), medium level (0.5) and high level (0.9). Two criteria are used to qualify the dynamic responsive characteristics of the musculoskeletal system, which include the angular displacement at 0.1 second, and the time duration for angular velocity to change to positive. The simulations and analysis are implemented in Matlab 2007a (Mathworks, Natick, USA).

4.2.3 Some simulation results

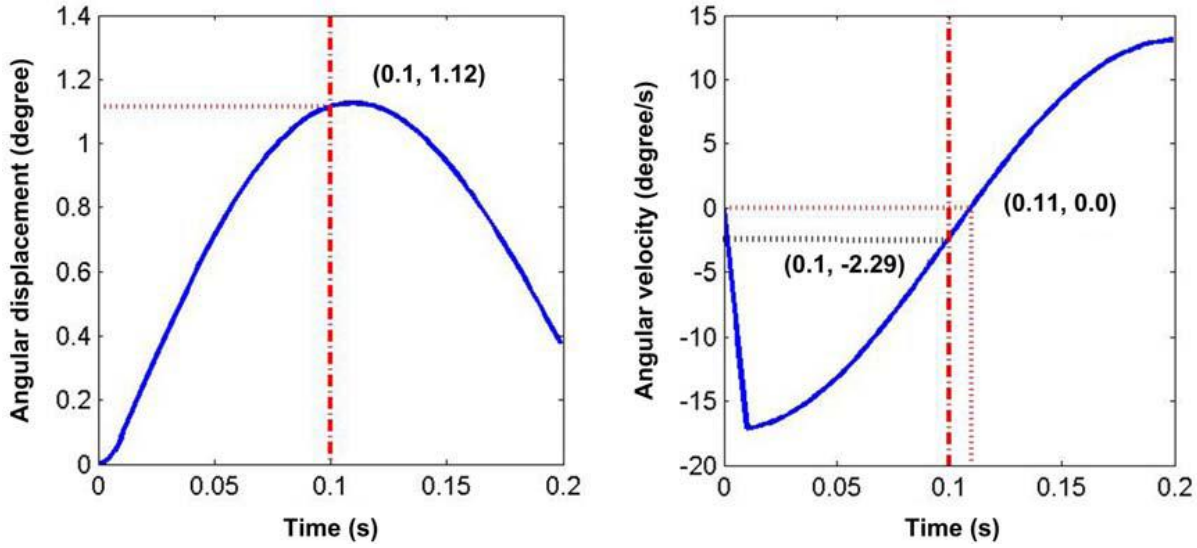

Fig. 4.2 The angular displacement and angular velocity time history in the first 0.2 second after the perturbation. The coactivation level is 0.5 with full muscle properties considered.

Figure 4.2 shows the angular displacement and angular velocity changes in the first 0.2 second after the impulsive perturbation. It can be seen that the linkage shows the strong tendency to move back to its initial position just after 0.1 second. The neuronal control system normally takes about 0.1 second to organize a reflective muscle coordination to stabilize musculoskeletal motion (Brown and Loeb, 2000). Especially for the tibialis anterior muscle, it has been experimentally proved that the preflex stage will last 0.1s (Nakazawa et al., 2009). Therefore, if the angular displacement is within the safe range at 0.1 second, the CNS will have a good chance to bring the system back to stable status after active feedback control is involved. In Figure 4.2, it is apparent that the system is pretty safe as the angular displacement at 0.1 second is only about 1.12^{o} if considering the system has a normal size of base of support. In addition, It can be seen from the angular velocity trajectory that the linkage will swing back to the neutral position just slightly after 0.1 second (at 0.11 second), which means that the system will return to its initial position even without the CNS control

after 0.1 second. The dynamic responses of the system in the first two seconds with different pennation angles and muscle geometric changes are shown in Figure 4.3.

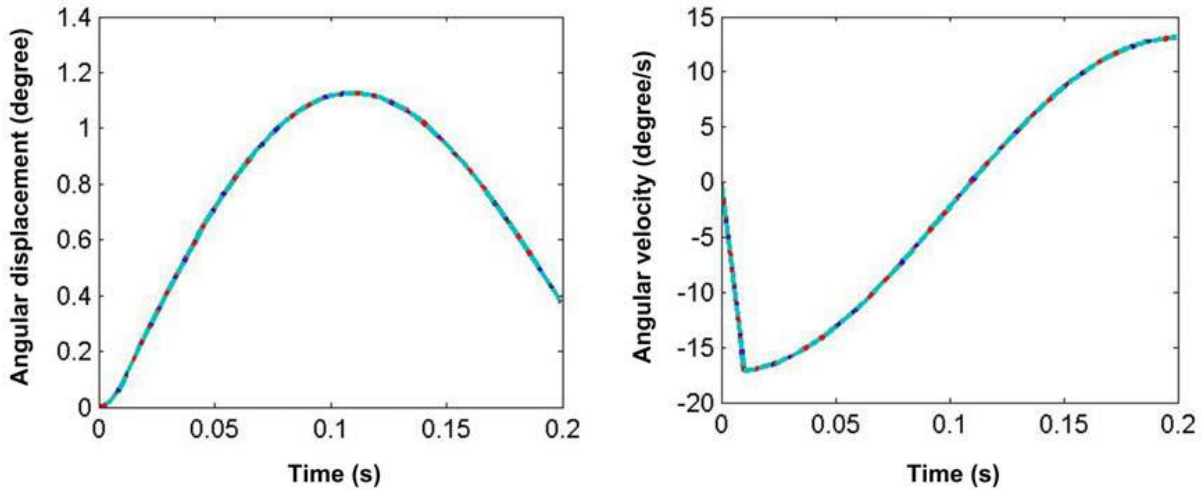

Fig. 4.3 The angular displacement and angular velocity time history in the first 0.2 second after the perturbation. The pennation angles are 6^o (dotted line), 12^o (solid line) and 18^o (dashed line) respectively with muscle geometric deformation. The pennation angle is 12^o (dash-dot line) without muscle geometric deformation.

Although ±50% changes of pennation angle about the baseline value have been simulated, there is no particular change on both angular displacement and angular velocity trajectories. Similarly, the integration of muscle geometric deformation into the muscle model made little effect on the system responses. Figure 4.4 shows the system responses after each individual muscle component is removed separately from the muscle model. Two instable states have been found if the antagonistic muscle pair does not have CE's force-velocity relationship or the series elastic elements (tendons) are absent. Without CE's force-velocity relationship, both angular displacement and angular velocity increases monotonically, which means the linkage will move away from its initial position. In the absence of series elastic elements, the linkage is pushed to a position slightly away from its neutral location and then creeps away from its initial state. The system show stable pattern after the CE's force-length relationship or

the parallel element is removed. It is apparent from Figure 4.4 that the CE's force-length relationship and the parallel element have little effect on the system stability in the cases simulated in this study.

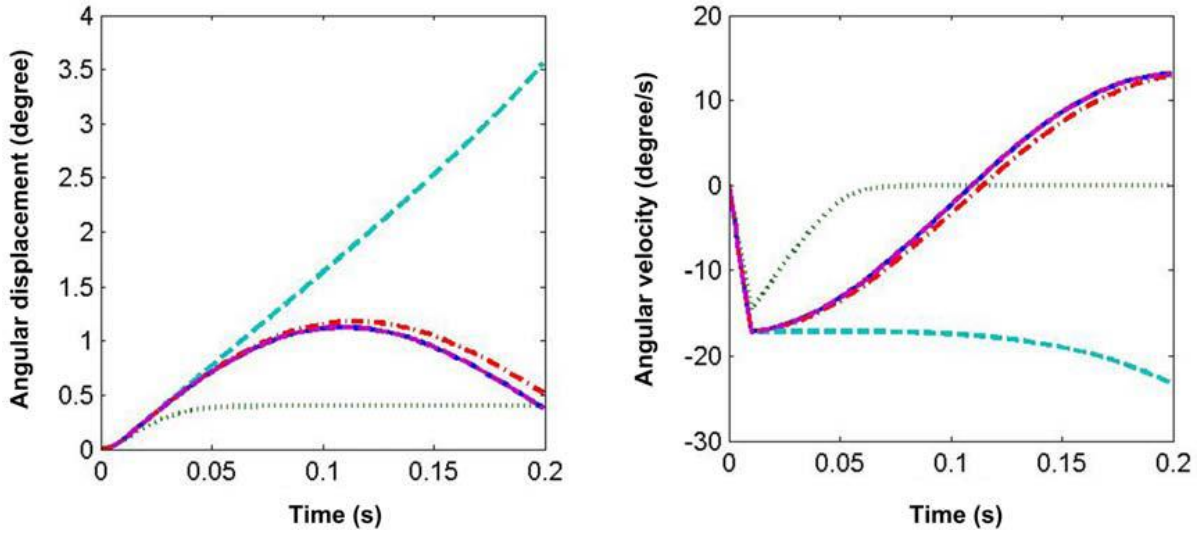

Fig. 4.4 The angular displacement and angular velocity time histories in the first 0.2 second after the perturbation. Each individual muscle component, CE force-velocity relationship (dashed line), parallel element (dash-dot line), CE force-length relationship (dash-dot-dot line) and series elastic element (dotted line) is removed separately from the full property (solid line)

In Figure 4.5, the angular displacement and angular velocity responses in the first 0.2 second at different muscle coactivation levels are compared. Apparently, the increase of muscle coactivation level enhances the system stability. The angular displacement at 0.1 second decreases rapidly with increasing coactivation level, and the time duration that angular velocity use to change sign decreases with the increase of coactivation level as well. A critical coactivation level 0.63 is identified, which can make the angular velocity change to negative at 0.1 second.

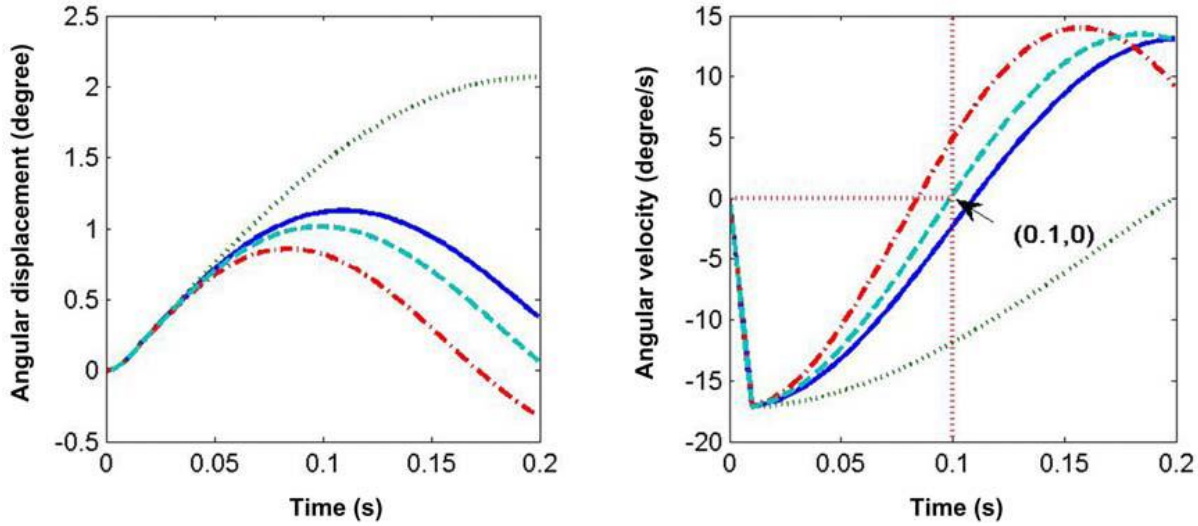

Fig. 4.5 The angular displacement and angular velocity time histories in the first 0.2 second after the perturbation. The coactivations of the antagonistic muscle pair are set at different levels: 0.1 (dotted line), 0.5 (solid line), 0.9 (dash-dot line), 0.63 (dashed curve)

It has been reported that increasing muscle coactivation level is able to enhance the stability of the musculoskeletal system. Runge had used Electromyography (EMG) technique to record the muscle activation levels in Tibialis Anterior and Gastrocnemius, a pair of antagonistic muscle pair, when subjects stood on a translated platform (Runge et al., 1999). Subjects stood on a flat support surface translating backward with a range of velocities from slow (15 cm/s, a in Figure 4.6) to fast (40 cm/s, e in Figure 4.6). The velocity tested for each subject was the velocity for which subject could reliably maintain balance without stepping. EMG activations pattern changes in Figure 4.6 show at higher velocity (c, d, e), both Tibialis Anterior and Gastrocnemius activities appear simultaneously, and the higher velocity the flat translates, the higher muscle activations and coactivations are recorded.

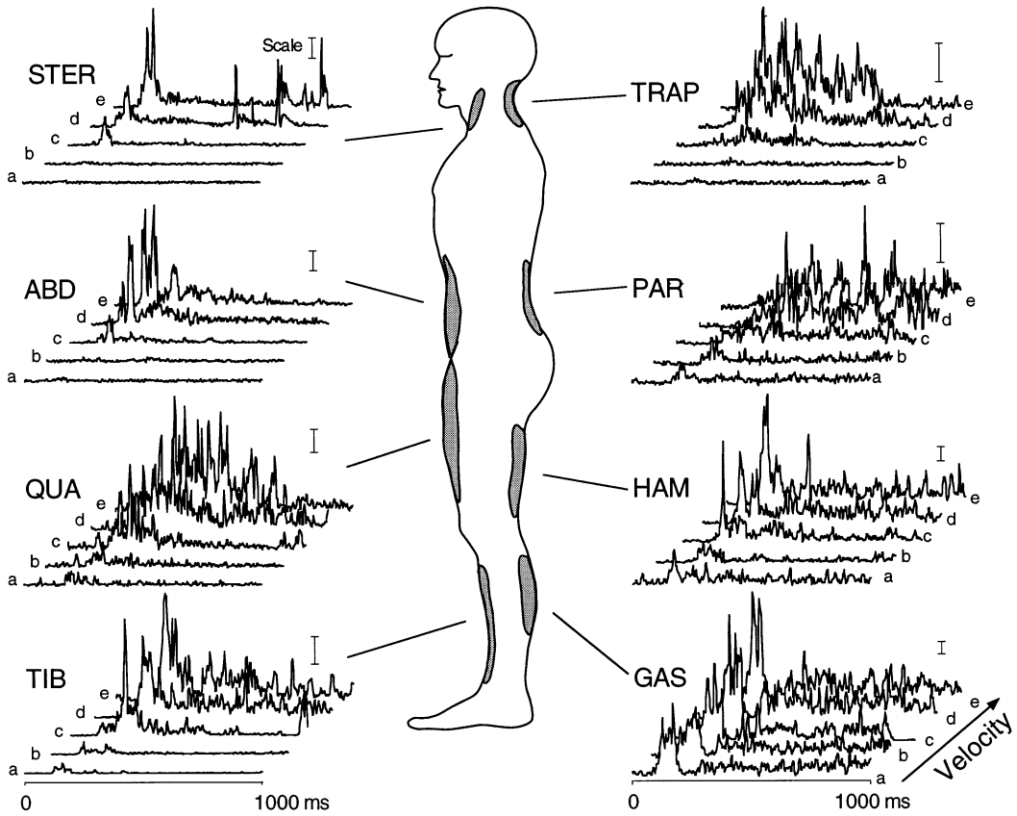

Fig. 4.6 Electromyography (EMG) record from the subject in response to backward platform translations at five different velocities (a, b, c, d, e) (Runge et al., 1999)

It is well known that the nervous system cannot change the resistance to stretch independent of the level of activation and thus a stiffness strategy requires coactivation to increase the level of muscle activity. By directly measuring the ankle stiffness during standing, Casadio has suggested that promoting stability during leaning forward may be produced by coactivation of muscles acting around the ankle joint, what may be called a ‘‘stiffness strategy’’ (Casadio et al., 2005). Apart from the measurement on the ankle joint, Holmes investigated the effects of arm posture and hand load on muscle activity during perturbations of the arm (Holmes and Keir, 2012). They concluded that the increase in forearm muscle coactivation indicated a forearm muscle contribution to elbow stability. The contribution of the forearm muscles to the elbow joint stability should be considered when evaluating sudden elbow loading

since an increase in forearm coactivation would influence elbow joint stiffness, which means increased muscle coactivation will influence elbow joint stiffness and thus, enhance elbow joint stability.

Table 4.1 and Table 4.2 list the simulation results of angular displacements at 0.1 second and the time duration for angular velocity to change sign at different combinations of coactivation level and muscle intrinsic properties. The percentages in Table 4.1 are the percentage variations with respect to the baseline value of including full muscle properties. It can be seen that the increase of coactivation level significantly enhances the system's capacity to maintain stability. These data further enforces the results obtained above and demonstrates the noticeable effects of the CE's force-velocity relationship, the parallel elements and the muscle coactivation level on system stability.

Table 4.1 The angular displacement (in degree) at 0.1 second at different muscle coactivation levels

Muscle Model	Muscle Activation Level		
	Low (0.1)	Moderate (0.5)	High (0.9)
Full Properties	1.447	1.112	0.822
Without CE F-L	1.447 (+0%)	1.112 (+0%)	0.822 (+0%)
Without CE F-V	1.616 (+11.72%)	1.613 (+44.97%)	1.614 (+96.34%)
Without PE	1.490 (+2.97%)	1.152 (+3.59%)	0.856 (+4.16%)
Without SE	1.289 (-10.89%)	0.402 (-63.89%)	0.202 (-75.42%)

Table 4.2 The time duration (in second) for angular velocity to change sign at different muscle activation levels

Muscle Model	Muscle Activation Level		
	Low (0.1)	Moderate (0.5)	High (0.9)
Full Properties	0.200	0.110	0.085
Without CE F-L	0.200	0.110	0.085
Without CE F-V	Instable	Instable	Instable
Without PE	0.231	0.115	0.087
Without SE	Instable	Instable	Instable

4.2.4 Discussions

Stability can be generally defined as the ability of a system to return to its initial situation after a disturbance. It is vital that the correct action takes place within the right time. In this study, two variables have been used to measure the system responsive performance to impulsive perturbation: the angular displacement at 0.1 second and the time duration for angular velocity to change the sign. Due to the intrinsic delay in neuronal control circuits, the organization of a complex reflexive control takes the nervous system about 50-100 ms (Brown and Loeb, 2000). Thereby, it is generally stable if the system position is in the safe range at 0.1 second when the CNS control starts to get involved. If the time duration for angular velocity to change sign is less than 0.1 second, it means that the system can return to its initial position even without the CNS control at 0.1 second. Our simulation results strongly suggest that the intrinsic mechanical properties of muscles have a great contribution to maintain postural stability. It seems to be possible to self-stabilize human posture using an antagonistic musculoskeletal system. With sufficient coactivation level, the

flexor and extensor muscles may generate self-stabilized postural sway that brings the human body back to its initial position.

The CE's force-velocity relationship showed large effect on the system stability. This corresponds with the results of previous researches on locomotor stability (Wagner and Blickhan, 2003; Wagner and Blickhan, 1999). The force-velocity relationship described by Hill's model has a negative slope with the muscle force decreasing monotonically with increasing contraction speed. This negative slope is one of the most significant features of muscle mechanics (Hill, 1938; Zajac, 1989). The force enhancement at eccentric contractions and the force reduction at concentric contractions would help to bring the system back to its initial position. Additionally, the damping effect of the contractile element at concentric contractions would support the stability of the system. Our results suggested that the series elastic element (tendon) appears to be compulsory to maintain system stability effectively. Although the action of a tendon is mainly considered as a non-linear passive spring, it plays a critical role to modulate the muscle contraction velocity by lengthening itself. The large angular momentum induced by the impulsive perturbation is absorbed by the stretch of the tendon at the initial stage, which allows for the force enhancement of the antagonistic muscle to build up gradually to counteract the agonistic muscle force and gravitational moment. The concerted action of the CE's force-velocity relationship and the series elastic element are critical muscle mechanical properties to stabilize the system motion. The simulation results also showed that the coactivation level of the antagonistic muscle pair can greatly improve the system stability. This is expected as humans tend to increase coactivation of antagonistic muscles in order to enhance joint stability (Hogan, 1984). However, two muscles in antagonistic geometric

configuration cannot guarantee that increase in coactivation level will necessarily lead to an increased joint stiffness.

An increase in joint stiffness by coactivation needs that the stiffness of each muscle increases with muscle force at isometric conditions (Wagner and Blickhan, 1999). Our results show that the muscle fibre PCSA and pennation angle have little effect on the dynamic characteristics of the system. This is probably because the effect of pennation angle changes on muscle force production is very small. Although the simulation results suggest that the CE's force-length relationship can improve the system stability, the effect is actually not significant. This is different from the results of previous researches on locomotor stability, as it is shown that the ascending limb of the force-length relationship improves the self-stabilizing ability during locomotion (Wagner and Blickhan, 2003). This may be explained by the fact that the actual muscle length change is small throughout the whole process, and the initial muscle length is set at its optimal muscle length.

The control of human motion is complex. The self-stabilizing effect of the musculoskeletal system would help to reduce the stress on the neuronal control system. This study would provide insight into the intrinsic design and function of the musculoskeletal system, and also give implications for the design of bionic actuators, biologically inspired robotics and prosthetic devices. Apparently, the musculoskeletal model used in this study is still far from adequate to account for the full range of musculoskeletal properties that will affect the stability of neuromusculoskeletal systems. Future work involves the modelling of both biarticular and uniarticular muscle groups and anatomically realistic musculoskeletal geometry. The

understanding of the complicated interplays between every single component of the musculoskeletal system and their contributions to the whole system performance is a great challenge for biomechanics, neuroscience and bionics science in the future.

4.3 The interplay between stability and energy expenditure in postural control

The objective of this section is to investigate the interplay between stability and energy expenditure of the musculoskeletal system in the response to the external perturbation during standing posture. A set of perturbation simulations was conducted based on a dynamic musculoskeletal model. The dynamic preflex responses without the active control of CNS were simulated. Four different performance criteria, which fall into two basic categories: energy criteria and stability criteria, were used to evaluate the muscles' dynamic responses. A set of multiple-objective optimization simulations was also conducted using the proposed performance criteria to explore the interplay between the energy strategies and stability strategies. The results suggest that the preflex postural control is a trade-off between energy cost and dynamic stability, and minimizing energy cost appears to be more important than maximizing postural stability.

4.3.1 Human standing posture musculoskeletal system modelling

A human musculoskeletal model is developed to simulate the standing posture (see Figure 4.7), which consists of two ankle extensor muscle groups and four ankle flexor muscle groups: tibialis anterior (TA), gastrocnemius medial (GM), gastrocnemius lateral (GL), soleus (SOL), flexor digitorum longus (FDL) and extensor digitorum longus (EDL). The human body is modelled as an inverted pendulum rotating around

the ankle joint in the sagittal plane. The muscle model used for constructing the musculoskeletal system is the musculotendon model we developed in Chapter 3. Additionally, all the muscle parameters including optimal muscle fibre lengths, maximum isometric muscle forces, slack tendon lengths and each muscle's origin and insertion as well as the anthropometric parameters for modelling are from SIMM software. The equation of motion is

$$I\ddot{\alpha} + R_G(\alpha)G + R(\alpha)F_{MT} + E = 0 \tag{4.1}$$

where α is the ankle angle; I is the moment of inertia of the human body with regard to the ankle joint; G is the gravitational loading; $R_G(\alpha)$ is the moment arm of gravitational loading; and E represents external loading. $R(\alpha)F_{MT}$ represents the net muscle moment, where $R(\alpha)$ is the matrix of muscle moment arms (1×6) and F_{MT} are the muscle forces $(6 \times 1{,}6{:}\, number\ of\ muscles)$.

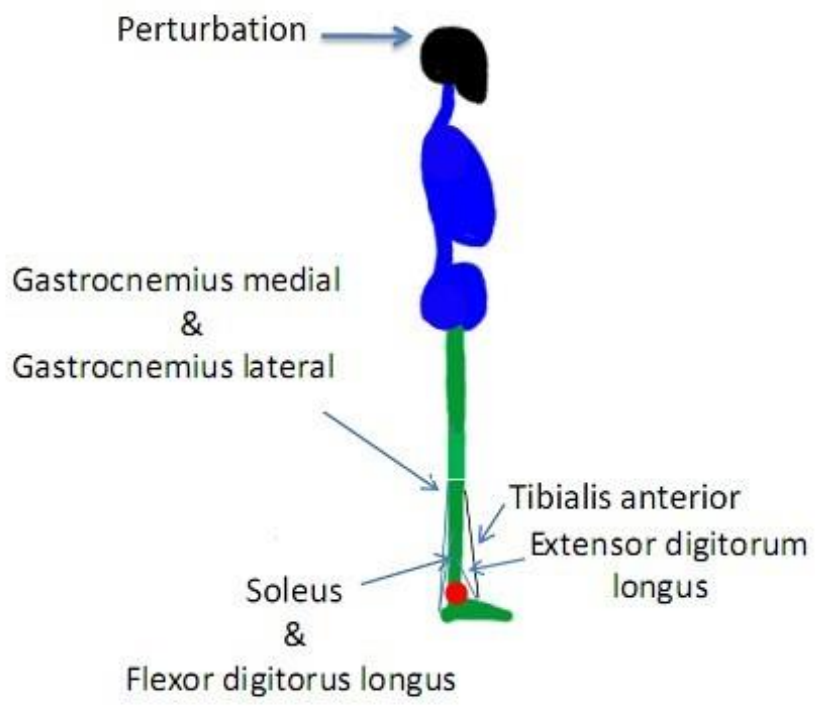

Fig. 4.7 The human musculoskeletal model with 6 muscle groups around the ankle joint subject to an external perturbation

4.3.2 Dynamic simulation with multi-objective optimization

To evaluate the preflex responses and the muscular control strategy in postural balance, a set of dynamic simulations subject to a horizontal perturbation was conducted. A 500N horizontal force was applied at the distal end of the model in the forward direction. Optimization schemes were used to assess the muscular control strategies. Two cost functions were used to represent the stability criteria, including,

Criterion 1 (C1) which is minimizing the sum of total potential energy changes (potential energy excursion).

Criterion 2 (C2): minimizing the sum of total angular displacement changes.

While two cost functions were employed to describe the energy criteria.

Criterion 3 (C3): minimizing the metabolic energy consumption.

Criterion 4 (C4): minimizing the muscular mechanical work.

The first two criteria were designed to represent the stability oriented strategy, which meant that the body would be more stable if less potential energy or angular excursion changed after external perturbation while the latter two were rough representations of the minimizing energy consumption strategy (Umberger et al., 2003). The forward dynamic simulations were conducted to obtain the preflex responses of the musculoskeletal system in the first 0.1 second after the perturbation, with all the initial muscle fibre lengths and muscle activations as the optimal variables.

A set of multiple-objective optimizations was also conducted to search the Pareto Front of the full feasible region by minimizing the potential energy excursion and metabolic energy consumption simultaneously, which meant to search the control solutions that to make the body most stable whilst with the lowest energy cost. In multi-objective optimization scheme, the weight ($0 \leq w \leq 1$) setting for both potential energy (w) and metabolic energy consumption ($1 - w$). w was set as a value from 0 to 1 with 0.01 increment, which meant in order to find out the the Pareto Front, the optimization ran 101 times.

4.3.3 Results and discussion

For each specific performance criterion, the simulation runs for 10000 times with random initial guess, and the one with the lowest cost is selected as the best solution. Our preliminary results (see Table 4.3) show that for the two stability criteria (C1 and C2), the obtained muscle activations are quite similar, with all the extensor muscle activation being small and most flexor muscle activations being close to 1.0. This

result is expected as the body will be more stable if the ankle muscles hold the ankle joint more firmly. While for the two energy criteria (C3 and C4), the results are dramatically different with most of the flexor and extensor muscle activations close to zero. This leads to a very economical solution as no muscle does much mechanical work during the first 0.1s. However, this also gives an unstable solution as a very small perturbation will push the system away from its original position quickly. This indicates that the optimal stability and optimal energy solutions cannot be achieved simultaneously.

Table 4.3 The muscle fibre length Lm and muscle activation level A for each muscle group obtained from the optimization simulations based on different performance criteria C1, C2, C3 and C4

	TA		**GM**		**GL**		**SOL**		**FDL**		**EDL**	
	L_m	A	L_m	A	L_m	A	L_m	A	L_m	A	L_m	A
C1	0.5	0.25	0.58	0.009	0.57	0.006	0.97	0.98	0.51	1	0.75	0.305
C2	0.56	0.605	1.28	1	1.02	0.99	0.86	0.6	1.16	1	0.89	0.288
C3	1.45	0.505	1.31	0.306	1.26	0.005	0.62	0.005	1.41	0.602	1.41	0.005
C4	0.7	0.065	1.2	0.005	1.15	0.009	0.59	0.005	1.34	0.206	1.39	0.005

The dynamic responses of Centre of Mass (COM) and ankle angle for criteria 1 and 2 are shown in Figure 4.8. It can be seen that both the moving directions of COM and ankle angle have changed during the first 0.1s. It means to prevent from falling down, the location of COM remains as close as its initial position; meanwhile the ankle

angles' maximum variances are only 0.3% and 1.3% under each criterion. The only difference is that both the maximum changes of the height of COM and the ankle angle using criterion 1 are smaller than those of using criterion 2.

Since for criterion 1, the aim is to minimize the sum of $\sin(90^{\circ} - \alpha_2) - \sin(90^{\circ} - \alpha_1)$, where $90^{\circ} - \alpha_2$ and $90^{\circ} - \alpha_1$ are the ankle angles at every two consecutive simulation points (see Figure 4.9). While minimizing the sum of $(90^{\circ} - \alpha_2) - (90^{\circ} - \alpha_1)$ is the objective that drives the optimizer to search for the best solution for criterion 2. Obviously, the certain regions for ankle angle changes in both simulations are roughly between $1.4rad$ to $\frac{\pi}{2}rad$ ($1.4rad$ is the ankle angle when human keep upstanding. The centre of mass is around 0.1m anterior to the ankle joint in longitudinal direction), where $\sin(90^{\circ} - \alpha_2) - \sin(90^{\circ} - \alpha_1)$ is always smaller than $(90^{\circ} - \alpha_2) - (90^{\circ} - \alpha_1)$. Therefore, the solution for criterion 1 is smaller than that for criterion 2, and that is why the changes of height of COM and ankle angles in criterion 1 is smaller than those for criterion 2. Furthermore, we could conclude that if the purpose is for keeping standing more stable in the simulation, the best way is to minimize the sum of total potential energy changes. Based on this reason, we will discuss the results in criterion 1, which could represent the stability strategy in the following paragraphs.

Criterion 1 Criterion 2

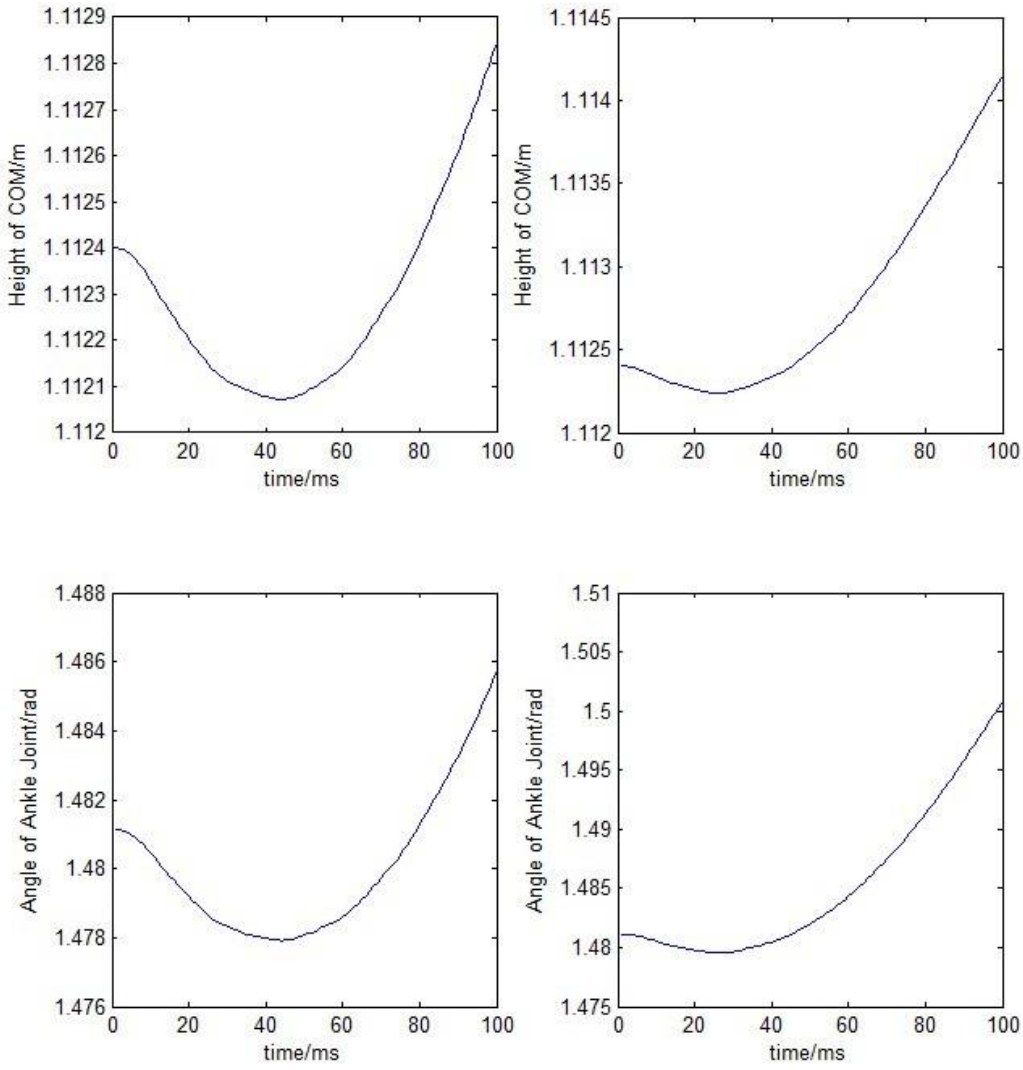

Fig. 4.8The height of COM and angle of the ankle joint changes in C1 and C2

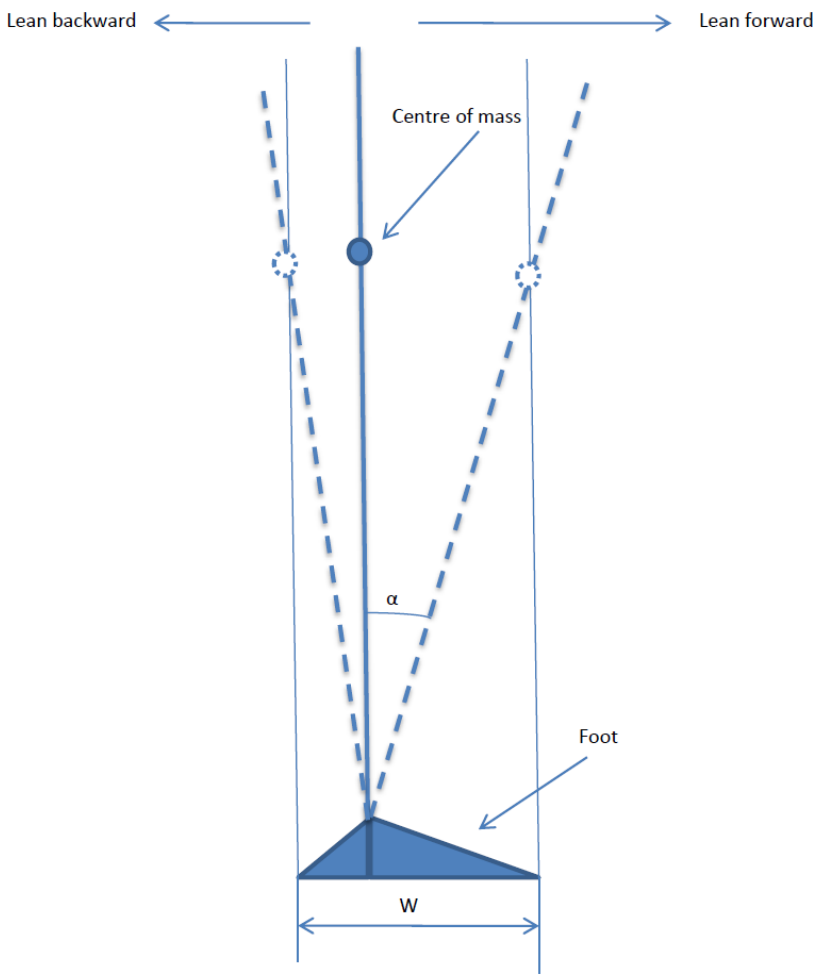

Fig. 4.9 The schematic diagram of the changes of the COM

Figure 4.10 shows the COM and ankle angle changes for criterion 1 and criterion 3. As we expected, to save energy, the optimal muscle forces will decrease in criterion 3. Therefore, the stiffnesses at both ankle joints will correspondingly reduce, and the musculoskeletal system will be easy to fall down. Within the first 0.1s, the height of COM and ankle angle both keep decreasing, and what could be predicted is without any adjustment from central neural system, the human body will lean forward onto the ground.

Criterion 1 Criterion 3

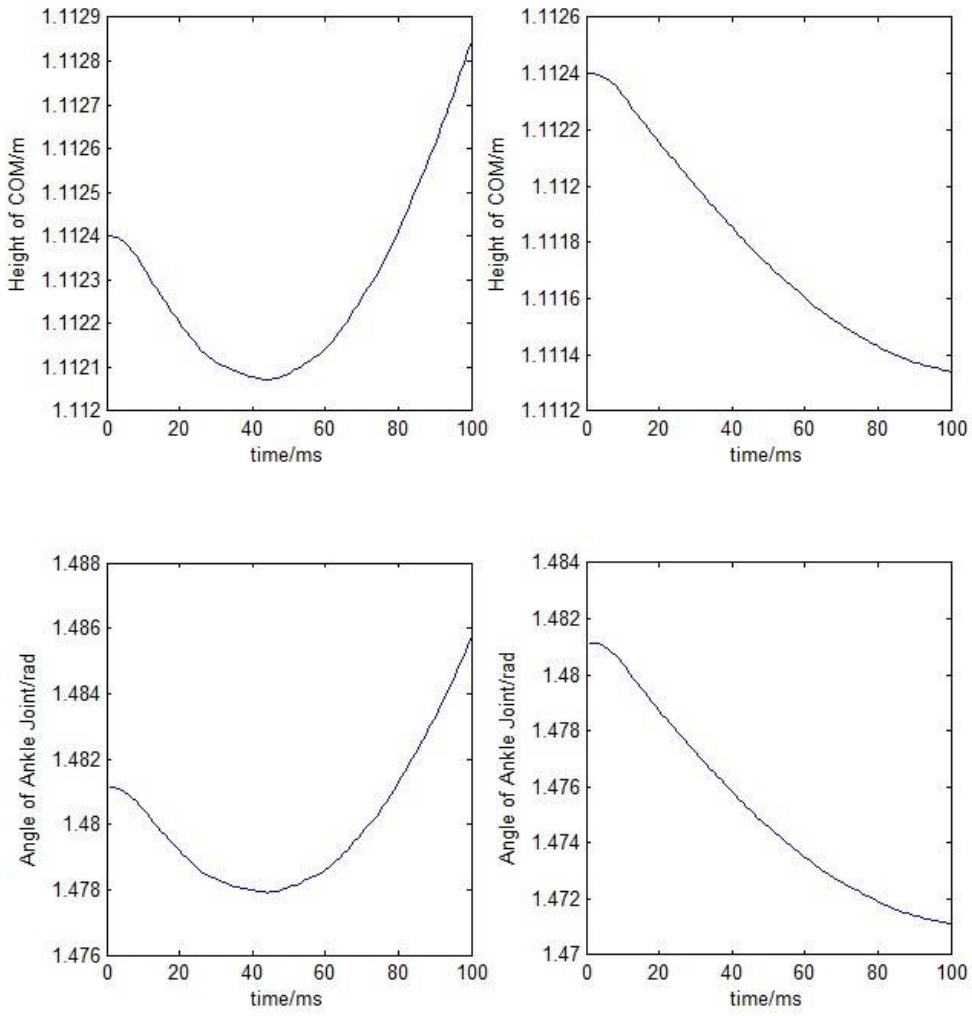

Fig. 4.10 The height of COM and the angle of ankle joint changes in C1 and C3

The individual muscle's performance is what we would like to make a further discussion. In Figure 4.11, the calculated time history of individual muscle fibre lengths using criterion 1 and criterion 3 have been compared, and the unit for muscle fibre length is metre. The first column of the Figure 4.11 is the muscle fibre length changes using Criterion 1, and the second column is for Criterion 3.

Criterion 1 Criterion 3

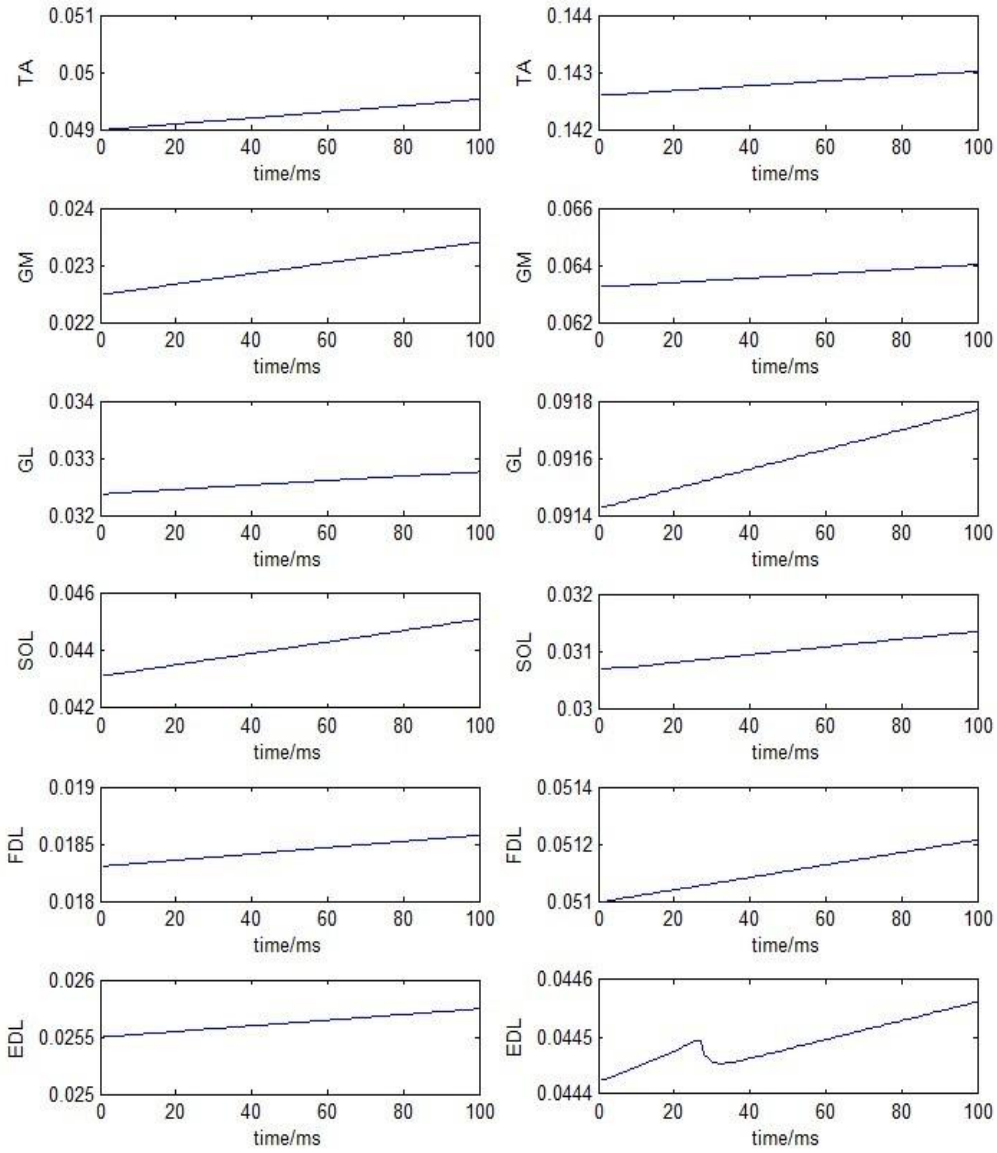

Fig. 4.11 The individual muscle fibre length changes under C1 and C3

For criterion 1, not only does the flexor fibre extend in the first 0.1s, but tibialis anterior and extensor digitorum longus contract eccentrically as well. Subject to the forward perturbation, the body correspondingly falls forward. In order to keep stable, all the flexors have to offer resistant forces to counteract angular momentum

generated by the impulsive perturbation and pull the body back to its initial position. As described in Chapter 3, during lengthening, muscles fibre can provide force bigger than maximum isometric force. Therefore, it is easy to understand the flexor muscle fibres lengthen during the simulation.

In the second column of Figure 4.11, although all the muscle fibres stretch during the first 100ms, all the muscle fibre forces will decrease rather than increase. Because the initial muscle fibre lengths are in the range of the descending part of the force-length relationship. In this part, the muscle fibre force decreases as the muscle fibre lengthens.

It is interesting that the muscle fibres vary linearly in most of the muscles. Under small ankle joint movement, the muscle fibre change of the ankle plantarflexors has been investigated by Loram (Loram et al., 2006). Ultrasound was used to measure the muscle fibre length change in gastrocnemius and soleus when the ankle rotated a small angle. Figure 4.12 shows the ankle rotation apparatus.

During the experiment, the subjects stood quietly while strapped securely around the hips to a vertical supporting board (Fig. 4.12). Subjects stood on two footplates, and their ankles were positioned to be coaxial with the axis of rotation of the footplates. The right footplate was locked in the horizontal position, and the left ankle was enforced to make dorsiflexion together with the left footplate. With the use of a pneumatic actuator, square pulse ankle

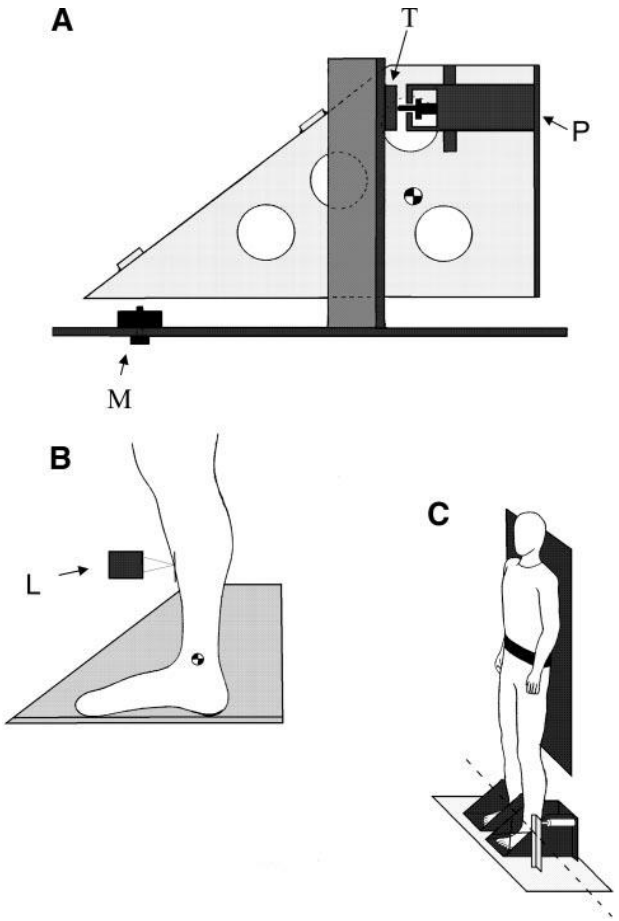

Fig. 4.12 Ankle rotation apparatus A: footplate is mounted on a rigid platform. Rotation of the footplate is caused by pneumatic actuator (P) acting in series with a load cell (T) and is measured using a contactless variable reluctance sensor (M). B: subjects stand, so their ankles are coaxial with the axis of rotation of the footplate. A laser range finder (L) measures the deflection of the shin relative to the platform. *C*: subjects are strapped to a vertical board and enabled to maintain minimal activity in the calf muscles. (Loram et al., 2006)

rotations of 0.2s duration were delivered approximately every second to the left ankle (Fig. 4.12). As the subjects' hips were strapped to a vertical supporting board, the muscles on the lower extremity would be fully relaxed. Such a scenario was similar to human quiet standing with low muscle activations, which was the initial status for Criterion 3. The following ankle dorsiflexion in Loram's experiment could be considered as the movement of ankle when the human model was subjected to the horizontal perturbation in our simulation. Therefore, the recorded gastrocnemius and

soleus' muscle fibre length changes in Loram's experiment were able to reflect the gastrocnemius and soleus' muscle fibre length changes under Criterion 3 in our simulation. Figure 4.13 is the gastrocnemius and soleus' muscle fibre length changes when the ankle rotates 0.15^{o} in Loram's experiment.

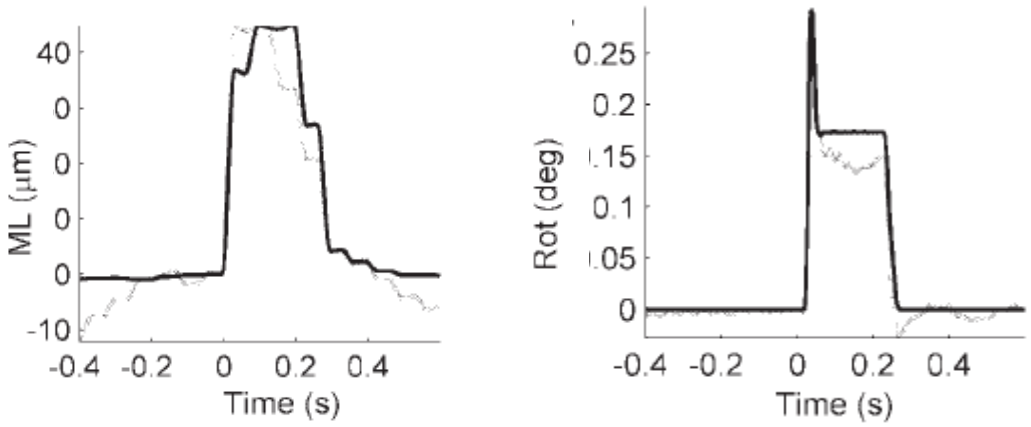

(a) (b)

Fig. 4.13Gastrocnemius (dark line) and soleus (light line) muscle fibre changes under ankle rotation of 0.15^{o} (b) footplate rotation (dark line) and true ankle rotation (light line) (Loram et al., 2006)

In Loram's experiment, the duration of square pulse was 0.2s. From Figure 4.13 (b), we could see the rising time for ankle dorsiflexion is about 0.02s. Correspondingly, the muscle fibre length changes during the first 0.02s in Figure 4.13 (a) is the exact muscle fibre changes for ankle dorsiflexion. The muscle fibre length change present apparent linear patterns for both gastrocnemius and soleus muscles. This is consistent with the linear patterns predicted by our model for both muscles and strongly supports the validity of our model. In addition, Loram and Lakie have discussed the situation that the ankle flexor's muscle fibre shortens while the musculotendon unit lengthens during the period that human lean forward (Loram et al., 2004; Loram et al., 2005;

Lakie et al, 2003). It may help explain the predicted patterns of the muscle fibre length changes in tibialis anterior and extensor digitorum longus by our model.

After comparing the muscle fibre length change of each muscle group, we would like to analyze the muscle force time history for criterion 1 and criterion 3. The muscle forces shown in Figure 4.14 are the musculotendon forces, which are different from the muscle fibre forces analysed in the previous paragraph. In the first column, the extensor muscle forces decrease within the whole period while most of the flexor muscle forces increase. It is interesting that the soleus' musculotendon force decrease compared with the other flexors. The reason may be the reduction of all extensor forces, whereas the forces of tibialis anterior and extensor digitorum longus dramatically decrease. The impulse only lasts for 0.01s, after which only 6 external forces are applied to the system (apart from gravitational force and ground reaction forces). If the trends of all extensor forces are fully against flexor forces, the human body's rotation acceleration could be changed immediately, which might bring unexpected injury, especially when we considering the force magnitude of the soleus and the tibialis anterior in Figure 4.13. The soleus initial muscle fibre length is at $0.97L_{mo}$, and it is obvious that the muscle fibre force decreases as its muscle fibre lengthens, because the fibre change in the range of $[L_{mo,}\ 1.5L_{mo}]$.

Although the flexor forces in the second column of Figure 4.14 show an increasing tendency, it is well accepted that due to the geometrical relation, the tendons elongation result in an increase of musculotendon force. Compared to the force change using criterion 1, soleus force grows a bit when using criterion 3. The magnitude of soleus force in criterion 3 is much smaller than that of criterion 1, which

makes it reasonable to be discussed.

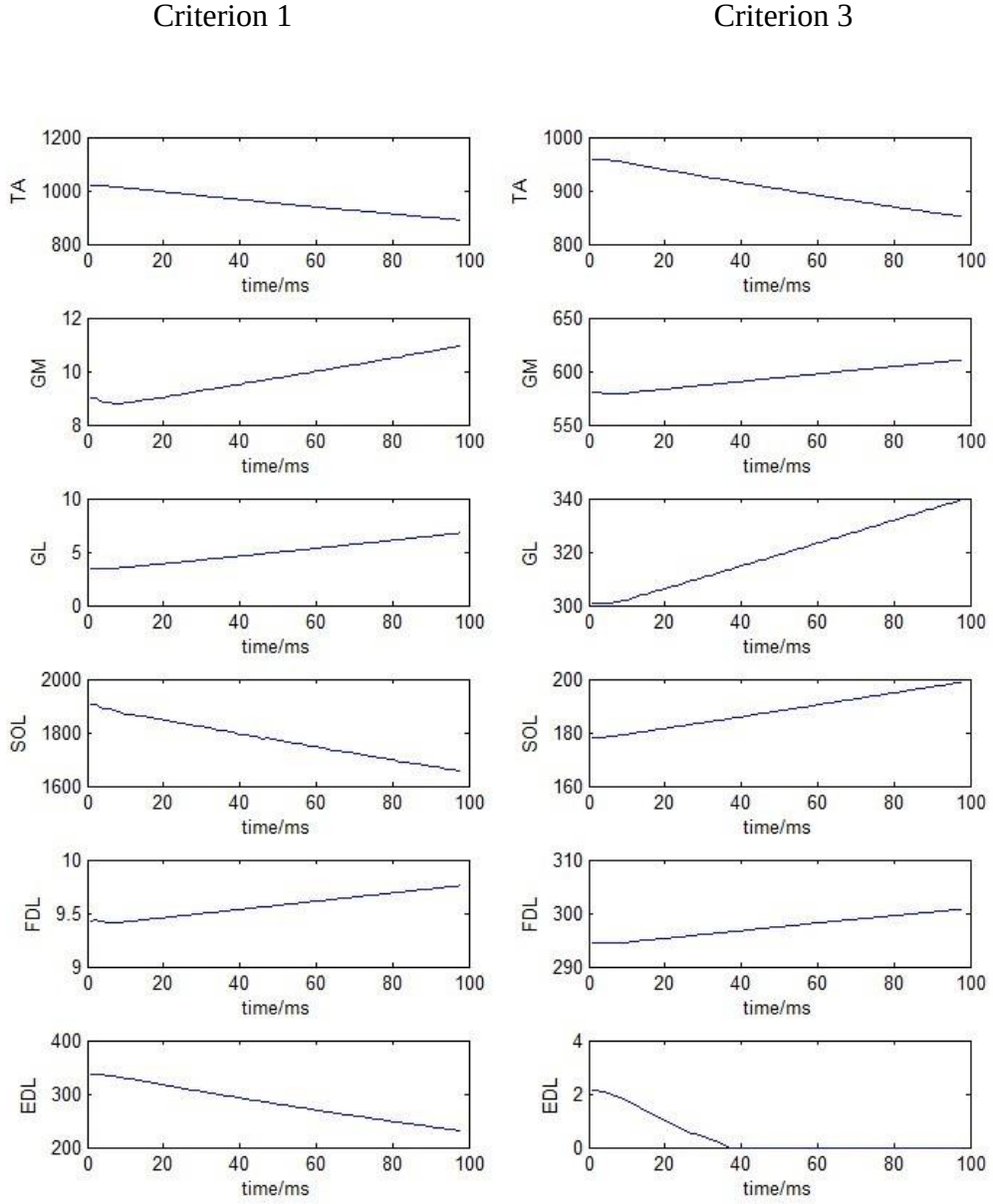

Fig. 4.14 The individual muscle force changes in C1 and C3

Criterion 1 Criterion 3

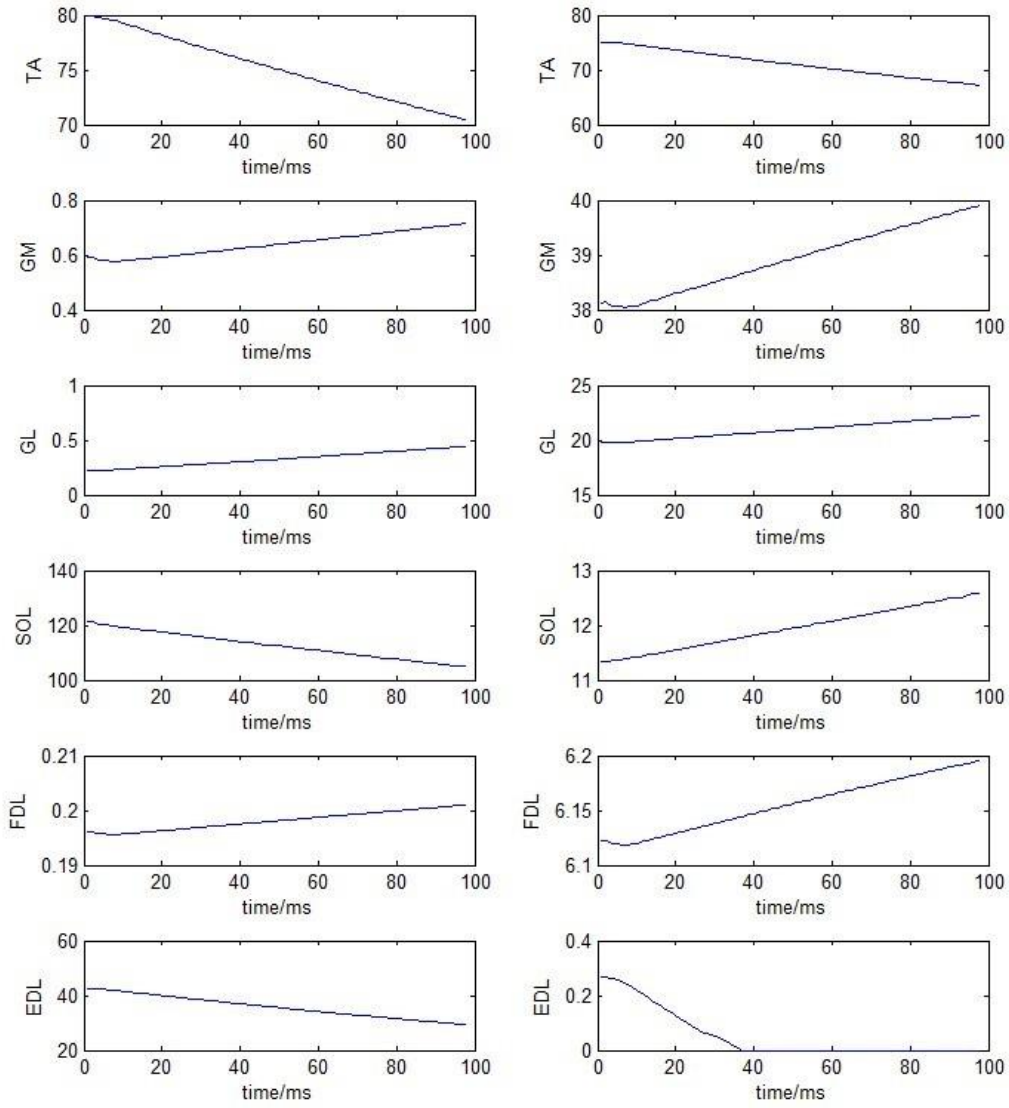

Fig. 4.15The changes of the moments generated by individual muscles in C1 and C3

The moments generated by the individual muscles in Figure 4.15 show the same trend as the musculotendon forces.

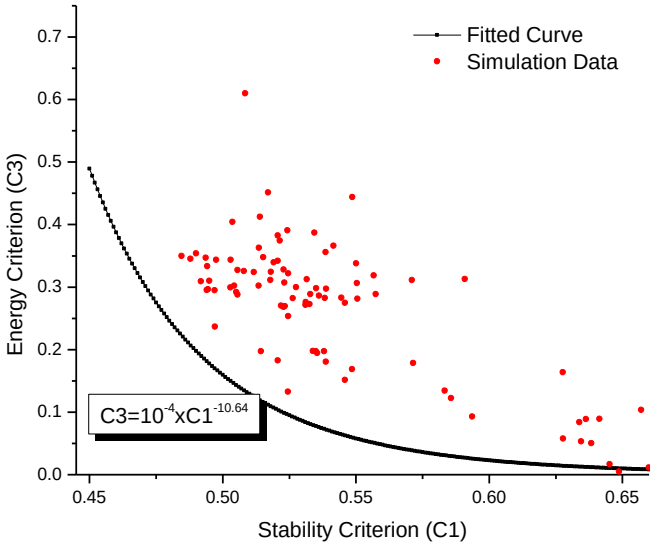

Fig. 4.16 The estimated Pareto front of the feasible region for multiple objective optimization

The interplay between the stability strategy and energy strategy was assessed by using a multiple-objective optimization simulation which uses criterion C1 and criterion C3 as the cost functions. Figure 4.15 shows the estimated Pareto front of the feasible region for the multiple objectives optimization. It is a collection of optimal solutions that the system may use to minimize both performance criteria. The values of C1 and C3 in Figure 4.16 are the scaled values, where the scaling factors are the potential energy changes when C3 is solely used, and the energy consumption when C1 is solely used. Apparently, both factors are the largest potential energy changes and energy consumption. All the optimal potential energy changes and energy consumption will be divided by the scaling factors.

It can be seen the value of criterion C1 is inversely proportional to the value of criterion C3. This means any control strategy attempting to increase the system stability will result in an increase in metabolic energy cost. Therefore, the human

body has to play a trade-off between the energy and stability to keep the body stable in an economic way. Moreover, from Figure 4.16, it can be seen that the region of energy consumption changes is larger than that of potential energy changes. Hence, the energy consumption may be more delicately regulated by the muscular control system, and more energy will be saved without sacrificing stability.

4.4 Conclusions

The influence of intrinsic muscle properties on the musculoskeletal system stability and energy cost in preflex response during standing have been investigated in this chapter. A one degree of freedom musculoskeletal model driven by an antagonistic muscle pair was constructed. To investigate the individual contribution of each muscle component to system stability, the initial values of the pennation angles were changed, and the individual muscle mechanical properties, including the CE's force-length relationship, the CE's force-velocity relationship, the parallel elastic element and the series elastic element were removed one by one. It is found that the muscle fibre pennation angle has little effect on the dynamic characteristics of the system, and compared with other components, the CE's force-velocity relationship has the most significant influence on the dynamic characteristic of the system.

A human musculoskeletal model during standing was used for investigating the interplays between stability control and energy consumption in this chapter as well. Optimizations with four different criteria were conducted to evaluate the musculoskeletal system performance and individual muscle's dynamic responses. The trade-off between energy and stability in human postural control strategy was revealed by the multiple optimization scheme, which is different from other people's analysis

that solely based on a single criterion optimization. The results show that during human standing, energy consumption is more concerned than stability in postural control strategy.

Apparently, the musculoskeletal models used in these two studies are still far from adequate to account for the full range of musculoskeletal properties that will affect the stability and metabolic energy consumption of musculoskeletal systems. Future work involves more realistic musculoskeletal modelling and experimental studies to verify the effect from intrinsic properties on stability and the trade-off strategy that human will adopt to adjust their standing posture.

Chapter 5. Construction of a Three-dimensional Musculoskeletal Model to Simulate Human Walking

5.1 Introduction

Walking is one of the most routine motor tasks in human daily life. Due to the importance of walking, such a challenging topic of interest has been investigated by numerous researchers over the past century. In this chapter, a three-dimensional multi-segment model capable of predicting the net muscle moments, the reaction forces, the individual muscle forces and the muscle activation levels during human walking are proposed. An inverse dynamics combined with inverse kinematics method is employed to estimate the dynamic responses of the human body over the stance phase of walking. Some simulation results during human level walking are obtained based on the gait measurement provided by the Grand Challenge Competition (GCC).

5.2 Grand Challenge Competition and database

Grand Challenge Competition is the competition held at the 2011 ASME Summer Bioengineering Conference in Farmington, Pennsylvania. The goal of the competition is to advance the entire field of musculoskeletal modelling by critically evaluating muscle and contact forces estimated at the knee during gait. The data collected from a new patient with a force-measuring knee implant was used to validate the estimated muscle and contact forces.

Since muscle forces are the primary determinants of joint contact forces, correctly predicted muscle forces should result in reasonable estimates of joint contact forces. Also, knowledge of muscle and joint contact forces during gait is necessary to characterize muscle coordination and function as well as joint and soft-tissue loading. Therefore, musculoskeletal modelling and simulation are required to estimate muscle and joint contact forces since direct measurement is not feasible under normal conditions. The Grand Challenge Competition provides the biomechanics community with a unique and comprehensive data set to validate muscle and contact force estimates in the knee. This data set includes motion capture, ground reaction, EMG, tibial contact force, and strength data collected from a subject implanted with an instrumented knee prosthesis.

5.2.1 Gait measurement

In order to provide the kinematic data for constructing the musculoskeletal model and evaluating the joint contact forces, a set of three-dimensional gait measurement including static trials, normal gait trials has been conducted to capture the whole body motions. The subject and equipment are as below,

Subject's name is DM. His height and weight are 172 cm and 67 kg. The instrumented knee is implanted in his right knee joint. During experiment, he was wearing New Balance 609 sneakers. The devices used in the measurement are 8-camera Motion Analysis system, Modified Cleveland Clinic marker set, three Bertec Force Plates and Delsys Bagnoli EMG system. As described previously, the competition collected data using a novel device, eKnee, with the force-measuring function, which was implanted at the knee joint. The eKnee is able to measure the tibial contact force at the knee joint.

(See details of the instrumented implant in the next section).

For each subject, the movements of 12 major body segments (torso, pelvis, right and left forearms, right and left humerus, and both legs (thighs, shanks and feet)) were recorded. In total, 43 reflective markers were used to capture the whole body motions during the static trials and walking trials (see Figure 5.1).

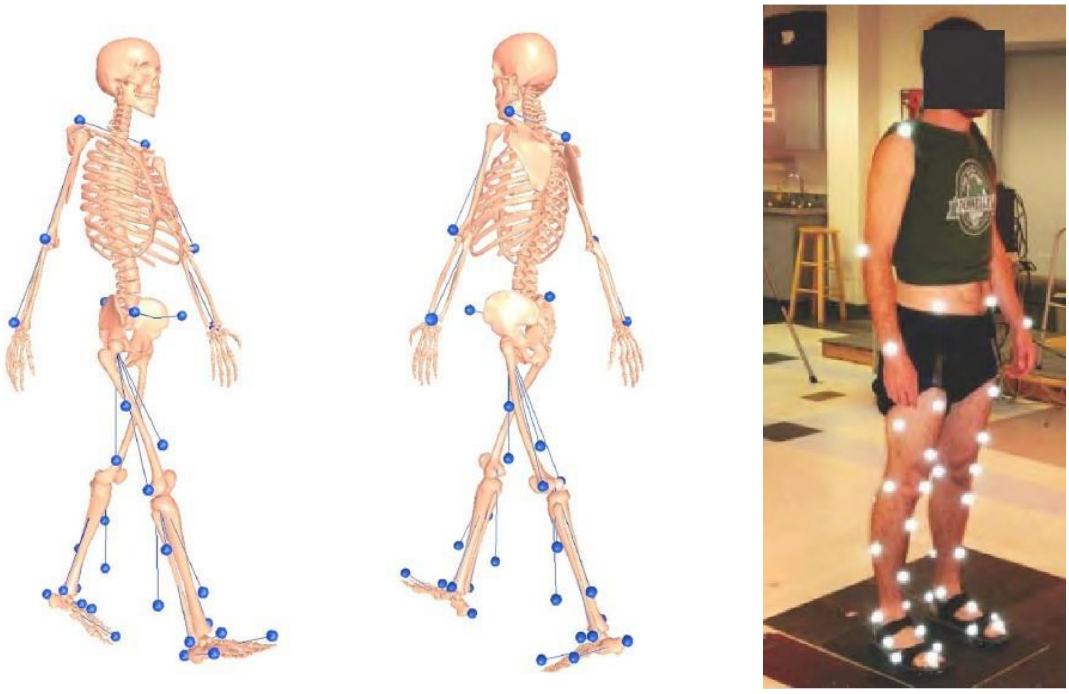

Fig. 5.1The movement of major body segments and a subject with a full set of markers

Totally 14 muscles EMG signals have been collected. The muscle names are: Semimembranosus, Biceps femoris, Vastus medialis, Vastus lateralis, Rectus femoris, Medial gastrocnemius, Lateral gastrocnemius, Tensor fascia latae, Tibialis anterior, Peroneus longus, Soleus, Adductor magnus, Gluteus maximus and Gluteus medius.

Three different types of trials were conducted. Static trials were for creating segment coordinate systems, and gait trials were to capture the kinematic data during walking. To normalize muscle EMG signals, the maximum EMG trials were employed as well. In static trials, the subject stood upright, facing to the $-y$ direction in global coordinate system, with toes forward, toes in and toes out postures separately. Figure 5.2 shows the global coordinate system and the subject in three static trials.

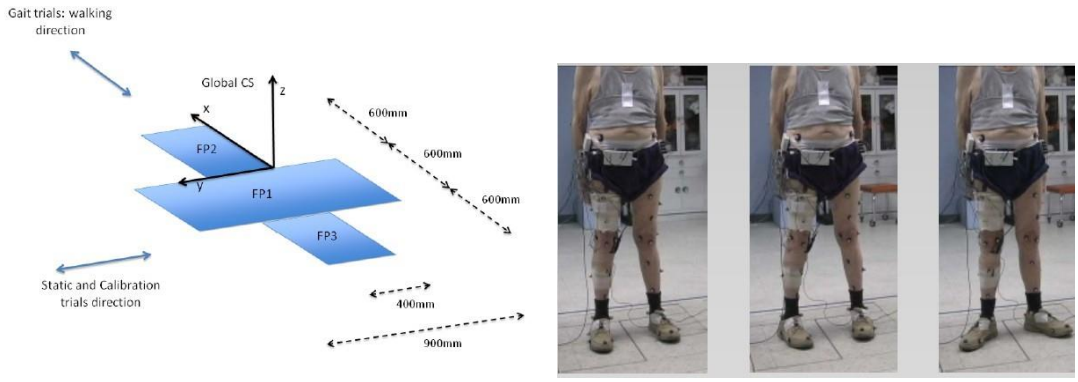

Fig. 5.2 The global coordinate system and the subject in static trials

After static trials, the subject walked along the x axis in global coordinate system to conduct the gait trials. In normal gait trials, the subject's motion data were completely captured by the cameras, and each experimental condition was measured six times to ensure that the repeatable data set for a complete walking cycle was obtained.

5.2.2 Contact forces measurement using implant joint

As introduced in the previous section, the joint contact forces at knee were measured by an implanted device called eKnee. The eKnee is instrumented at tibia, and its profile and structure are shown in Figure 5.3.

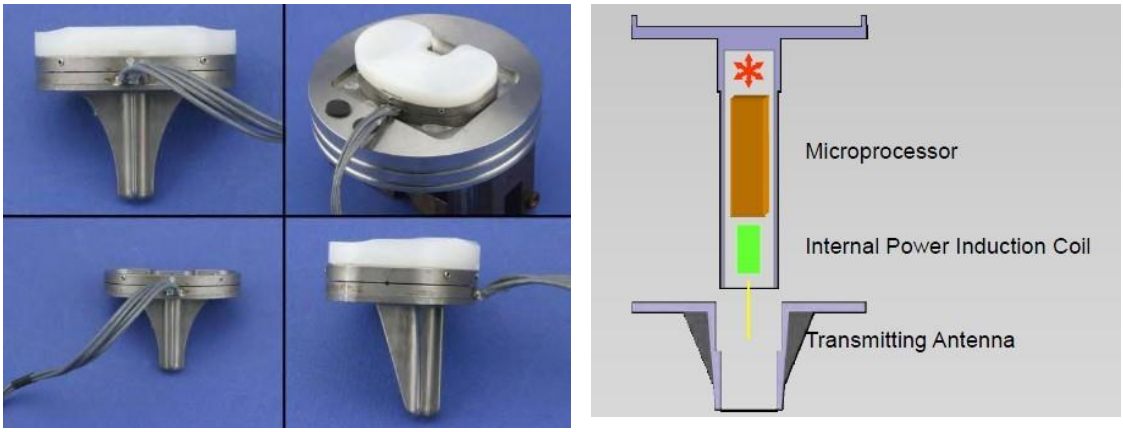

Fig. 5.3The profile and structure of the eKnee

The eKnee is implanted at the subject's right knee, and it can directly measure the three uniaxial forces on tibia tray by six sensors. The sampling frequency is $200Hz$, and the origin and axis directions of the coordinate system fixed in the tibia tray can be seen in Appendix C.

5.3 Construction of a three-dimensional musculoskeletal model

In this section, a three-dimensional musculoskeletal model using inverse dynamics combined with inverse kinematics method to predict dynamic response of human musculoskeletal system is constructed. The model is developed in OpenSim 2.2 environment. OpenSim is a software package for building the computer models of the musculoskeletal system and the dynamic simulations of movement (See Figure 5.4).

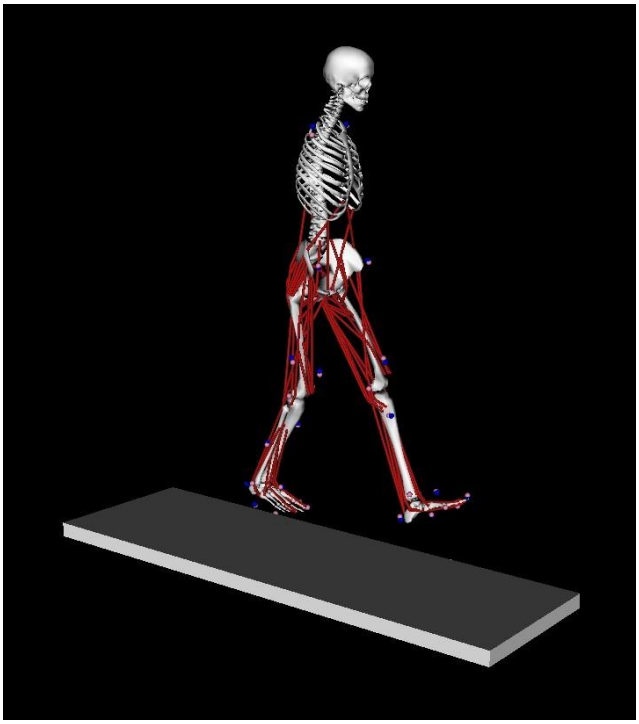

Fig. 5.4The graphical presentation of Opensim model

5.3.1 Model structure

The model constructed consists of 13 bodies which are, grand, torso, pelvis, right and left femur, right and left tibia, right and left talus, right and left calcaneus and right and left toes. The bodies spatially rotate about ground, pelvis, right and left hip, right and left knee, right and left ankle, right and left subtalar, right and left metatarsal phalangeal joints. Ground, pelvis, right and left hip joints are pivot joints, and right and left knee, right and left ankle, right and left subtalar, right and left metatarsal phalangeal joints are hinge joints. Also, 98 lower limb muscle groups have been attached on the bones. The path of a muscle is defined as a straight line between the muscle origin and insertion. The parameters, such as optimal fibre length, pennation angle, slack tendon length and the activation time constants, depend on the muscle type. There are two types of muscle in the model. One type was developed by Thelen (Thelen, 2003), and the other one was developed by Schutte (Schutte et al., 1993).

After the model construction, the GCC database can be used to drive the model walking and to conduct the dynamic simulations.

5.3.2 Data preparing

As introduced in section 5.2, the raw data used is from Grand Challenge Competition. The procedure of data processing is shown in Figure 5.5.

Fig. 5.5The procedure of data processing

As the data from the competition is collected by different equipment, it is inevitable that they are of difference in sample frequencies. Meanwhile, the raw data is quite spiky, which cannot be directly used for modelling. In addition, as the subject faced to different directions in static trials and normal gait trials, the filtered data should be transformed to the same global coordinate system. After resampling, all the data's sample frequencies are changed to 200Hz. The resampled data is filtered by Butterworth filter, and the low pass cut-off frequency is 6Hz. After the data processing, we can further refine the model in OpenSim environment.

5.3.3 Scaling

Due to the anthropometrical difference, we need to scale the existing model to match the anthropometric data of the subject as closely as possible. Scaling is typically performed based on a comparison of the experimental marker data with the virtual markers placed on the existing model, which is called measurement-based scaling.

In the measurement-based scaling, scale factors are determined by comparing

distances between markers on the existing model and experimental marker positions. A single scale factor for one segment is computed using one or more marker pairs. For example, suppose two marker pairs are used: p1=(R.ASIS, R.Knee.Lat) and p2=(L.ASIS, L.Knee.Lat) (See Figure 5.6). The distance (m1) for pair 1 on the model is computed by placing the model in its default configuration. The experimental distance (e1) between pair 1 is computed by looking at each frame of experimental marker data in the given processed experimental data, computing the distance between the pair for that frame, and taking the average across all frames in static trials time range. The scale factor due to pair 1 is then s1=e1/m1. The overall scale factor is then the average of the scale factors computed due to all of the pairs (e.g., s=(s1+s2)/2 in this case, where s2 is the scale factor due to pair 2). This overall scale factor s can then be used to scale the specific segments, femur. Figure 5.6 is the schematic diagram of the scaling process.

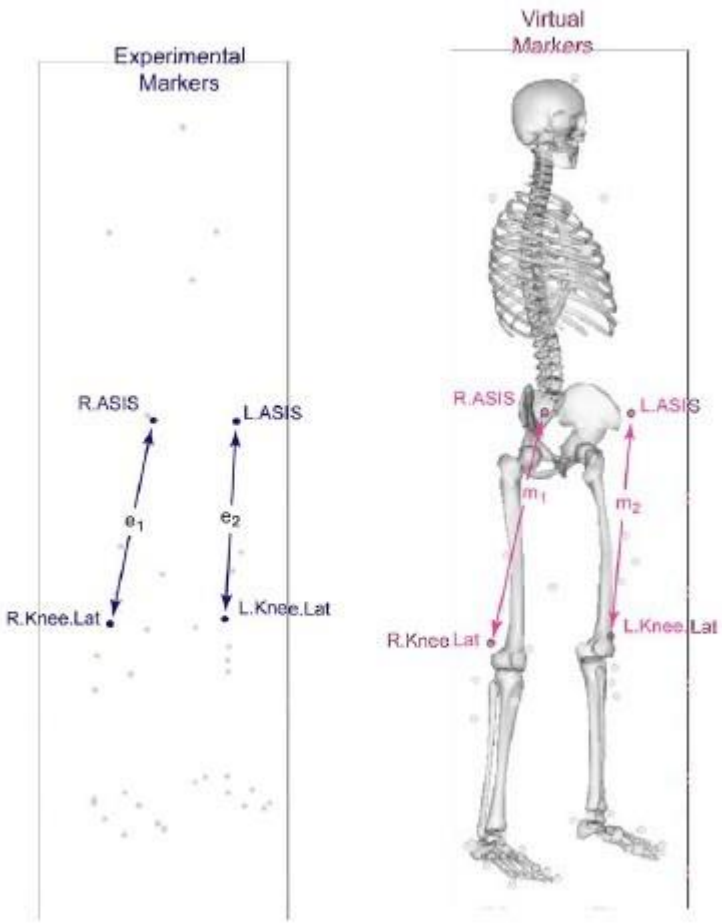

Fig. 5.6The principle of model scaling

The input and output files required for scaling are shown in Figure 5.7. All the '.xml' files are compiled by us in Java Applet environment, and the '.trc' file is the experimental data processed in section 5.3.2. The 'gait2354.osim' file is the model file in OpenSim. The 'subject01_simbody.osim' is the scaled model which will be used in the next step, inverse kinematics.

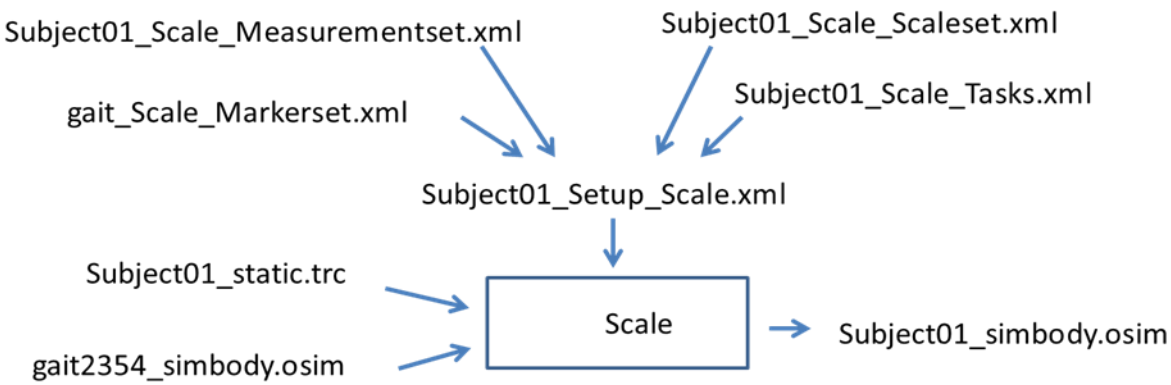

Fig. 5.7 The process of model scaling

5.3.4 Inverse kinematics (IK)

The purpose of the IK is to find the set of generalized coordinates (joint angles and positions) for the scaled model, which best match the experimental kinematics recorded.

The IK tool goes through each time step (frame) of the motion and computes generalized coordinate values, which positions the model in a pose 'best matches' experimental marker and coordinate values for that time step. Mathematically, the 'best matches' is expressed as a weighted least squares problem, whose solution aims to minimize both marker and coordinate errors. The weighted least squares problem solved by IK can be expressed as

$$\min_{q}\left[\sum_{i\in markers} w_i\left\|x_i^{exp}-x_i(q)\right\|^2+\sum_{j\in unprescribed\ coords}\omega_j\left(q_j^{exp}-q_j\right)^2\right] \tag{5.1}$$

$q_j^{exp}=q_j$ for all prescribed coordinates j.

where q is the vector of generalized coordinates being solved for, x_i^{exp} is the

experimental position of marker i, $x_i(q)$ is the position of the corresponding marker on the model (which depends on the coordinate values), q_j^{exp} is the experimental value for coordinate j. Prescribed coordinates are set to their experimental values. For instance, the subtalar and metatarsophalangeal (mtp) joints are locked and during IK they are assigned the prescribed value of 0˚. The marker weighting coefficient w_i and coordinate weighting coefficient ω_j vary with different markers and coordinates in our programme. Based on the trial-and-error process, w_i is always set as 0.5, 1 or 10 while ω_j is 1000 instead in our simulation.

The input and output files for IK are shown as below, in which the 'Subject01_simbody.osim' is the model output from scaling process. The 'Subject01_walk.trc' is the experimental kinematic data processed (See Figure 5.8).

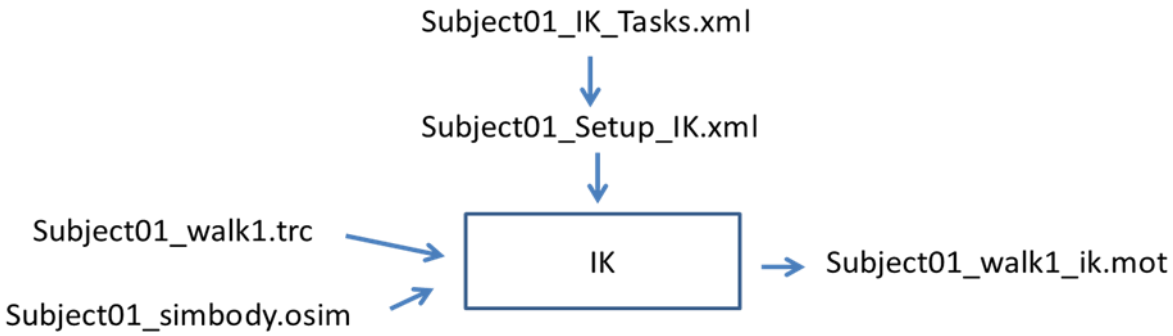

Fig. 5.8The process of inverse kinematics

5.3.5 Inverse dynamics (ID)

The inverse dynamics determines the generalized forces (e.g., net forces and torques) at each joint responsible for a given movement. Given the kinematics (e.g., states or motion) describing the movement of a model and perhaps a portion of the kinetics

(e.g., external loads) applied to the model, the ID uses these data to perform an inverse dynamics analysis. Classical mechanics mathematically expresses the mass-dependent relationship between force and acceleration, $F = ma$, with equations of motion. The inverse dynamics solves these equations, in the inverse dynamics sense, to yield the net forces and torques at each joint which produce the movement. The classical equations of motion could be written in the following form:

$$M(q)\ddot{q} + C(q, \dot{q}) + G(q) = \tau \tag{5.2}$$

where $q, \dot{q}, \ddot{q} \in R^N$ are the vectors of generalized positions, velocities, and accelerations, respectively; N is the number of degrees of freedom; $M(q) \in R^{N \times N}$ is the system mass matrix; $C(q, \dot{q}) \in R^N$is the vector of Coriolis and centrifugal forces; $G(q) \in R^N$ is the vector of gravitational forces; and $\tau \in R^N$ is the vector of generalized forces.

The motion of the model is fully defined by the generalized positions, velocities, and accelerations. Consequently, all of the terms on the left-hand side of the equation of motion are known. The remaining terms on the right-hand side of the equations of motion are unknown. The inverse dynamics tool uses the known motion of the model to solve the equations of motion for the unknown generalized forces. Figure 5.9 shows the input and output files for the inverse dynamics step in our study, where the 'subject01_walk1_ik.mot' and ''subject01_simbody.osim' are the motion files from IK and scaled model in the previous sections, and the 'subject01_walk1_grf.mot' is the ground reaction force from experimental data.

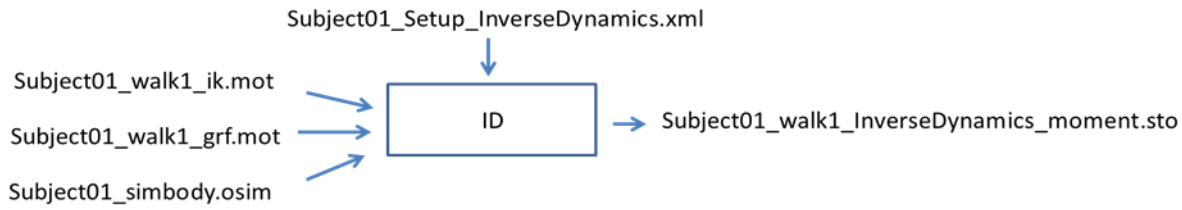

Fig. 5.9The process of inverse dynamics

The output data of ID calculation is the net muscle moments at each joint, which will be used in the next stage, static optimization.

5.3.6 Static optimization

Static optimization is an extension to the inverse dynamics calculation, which further resolves the net joint moments into individual muscle forces at each instant. As described in the section 5.3.4, the motion of the model is defined by the generalized positions, velocities, and accelerations. The static optimization uses the known motion of the model to solve the equations of motion for the unknown generalized forces (e.g., joint torques) subject to the following muscle activation-to-force conditions:

$$\sum_{m=1}^{nm} [a_m f(F_m^0, l_m, v_m)]\, r_{m,j} = \tau_j \tag{5.3}$$

while minimizing the objective function:

$$J = \sum_{m=1}^{nm} (a_m)^p \tag{5.4}$$

where *nm* is the number of muscles in the model; a_m is the activation level of muscle *m* at a discrete time step; F_m^0 is its maximum isometric force; l_m is its length; v_m is its shortening velocity; $f(F_m^0, l_m, v_m)$ is its force-length-velocity surface; $r_{m,j}$ is its muscle moment arm about the j^{th} joint axis; τ_j is the generalized force (net muscle

moment) acting about the j^{th} joint axis, and p is chosen as a constant 2. The input and output files of static optimization are as below,

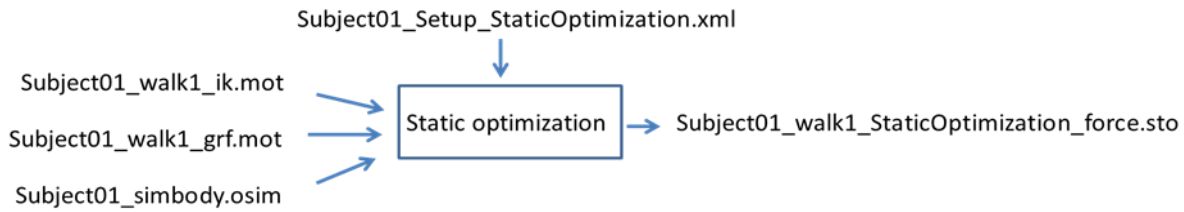

Fig. 5.10The process of static optimization

Compared with the inverse dynamics process, the static optimization has the setup '.xml' file, which is compiled in Java as well. The output file contains the time histories of the individual muscle forces (See Figure 5.10).

5.3.7 Some simulation results of human walking

We used the inverse kinematics method to re-describe the subject's walking in OpenSim, where the positions of all the subject's bodies were confirmed at each time step. The muscles' origins and insertions were attached to the bodies without any relative movement, so the positions of each muscle's origin and insertion were known. The muscle in our model was treated as a straight line between its origin and insertion, and the muscle force acted along the straight line. By using inverse kinematics method, the positions of model articulated joints would be known as well. Therefore, with the articulated joints positions and the directions of muscle forces, we could easily work out the individual muscle moment arms at each articulated joint. Taking the right leg for example, we chose 19 prime mover muscles to analyze their muscle moment arms. Those 19 muscles rotate about 3 different joints (hip, knee and ankle) with 5 motions (Hip adduction, hip flexion, hip rotation, knee flexion and ankle plantar/dorsiflexion). The changes of muscle moment arms for hip adduction in one

gait cycle have been shown in Figure 5.11. The 19 prime mover muscle groups and the abbreviations are listed in Table 5.1.

Table 5.1 The names and abbreviations of 19 prime mover muscles

Muscle Name	Abbreviation
ILIACUS	ILIACUS
RECTUS FEMORIS	RECTFEM
VASTUS MEDIALIS	VASMED
VASTUS LATERALIS	VASLAT
GLUTEUS MEDIUS_1	GLUTMED1
GLUTEUS MEDIUS_2	GLUTMED2
GLUTEUS MEDIUS_3	GLUTMED3
BICEPS FEMORIS LONG	BIFEMLH
BICEPS FEMORIS SHORT	BIFEMSH
SEMIMEMBRANOSUS	SEMIMEM
GLUTEUS MAXIMUS_1	GLUTMAX1
GLUTEUS MAXIMUS_2	GLUTMAX2
GLUTEUS MAXIMUS_3	GLUTMAX3
SEMITENDINOSUS	SEMITEN
GASTROCNEMIUS MEDIAL	MEDGAS
GASTROCNEMIUS LATERAL	LATGAS
SOLEUS	SOL
TIBIALIS ANTERIOR	TA
PSOAS MAJOR	PSOAS

Figure 5.11 is the changes of the muscle moment arms (MMA) at the hip joint for adduction and abduction in the frontal plane. The signs of moment arms are determined by the direction of moments, where moment arms are positive for hip adduction and negative for abduction respectively. The GLUTMAX2, GLUTMAX3, GLUTMED3 and RECTFEM share the similar tendency that the hip adduction moment arms increase from the right foot heel strike and get their peak values after the toe off. Then these muscle moment arms gradually decrease to the initial values. Although, BIFEMLH still gets its summit within the same period, it has no pronounced change at the early stage of stance phase. The GLUTMED1 and GLUTMED2's moment arms increase as well, but they are for hip abduction. Only

the muscle moment arms of the SEMIMEM and SEMITEN show decrease - increase trend during stance phase. The GLUTMAX1 muscle moment arm sees a fluctuation as time passes. GLUTMAX1 is the most superficial muscle for hip adduction, and in the interest of lateral stability during walking, the magnitude of hip adduction moment adjusts according to the body position, walking velocity and other parameters.

The muscle moment arms for hip flexion and rotation are shown in Figure 5.12 and Figure 5.13. It can be seen that most moment arms change trend at around 2.2s, which means they reach their extreme value at around 2.2s. In the simulation, the stance phase for right leg is from 1.57s to 2.2s and the rest period of the cycle is the swing phase. It is apparent that most of the moment arms reach their extreme value slightly before or after toe off. In addition, the moment arms of ILIACUS and PSOAS are quite small in hip rotation compared with the other muscles during hip flexion. Since the action lines of ILIACUS and PSOAS muscles almost pass through the hip rotation centre, and they contribute much less for hip rotation due to their small moment arms.

Knee muscle moment arms refer to the moment arms of the muscles during flexion and extension at the knee joint. Compared with the muscle moment arms at the hip joint, the time histories of knee muscle moment arms are more fluctuating and irregular, especially within the swing phase, and the changes are more evident (see Figure 5.14). The GASTROCNEMIUS MEDIAL, GASTROCNEMIUS LATERAL and SEMIMEMBRANOSUS' moment arms at the knee joint show a discontinuous change during the transition from stance phase to swing phase. Physiologically, the knee joint is comprised of two joints which are between the femur and the tibia, and between the femur and the patella. So it is more complicated than a simple hinge joint,

and it permits flexion and extension as well as slight medial and lateral rotation. Additionally, the instrumented implant was fixed at the knee joint, which would bring more unreasonable alteration. For instance, an obvious spike can be found during the transit period from stance phase to swing phase in MEDGAS, LATGAS and SEMIMEM.

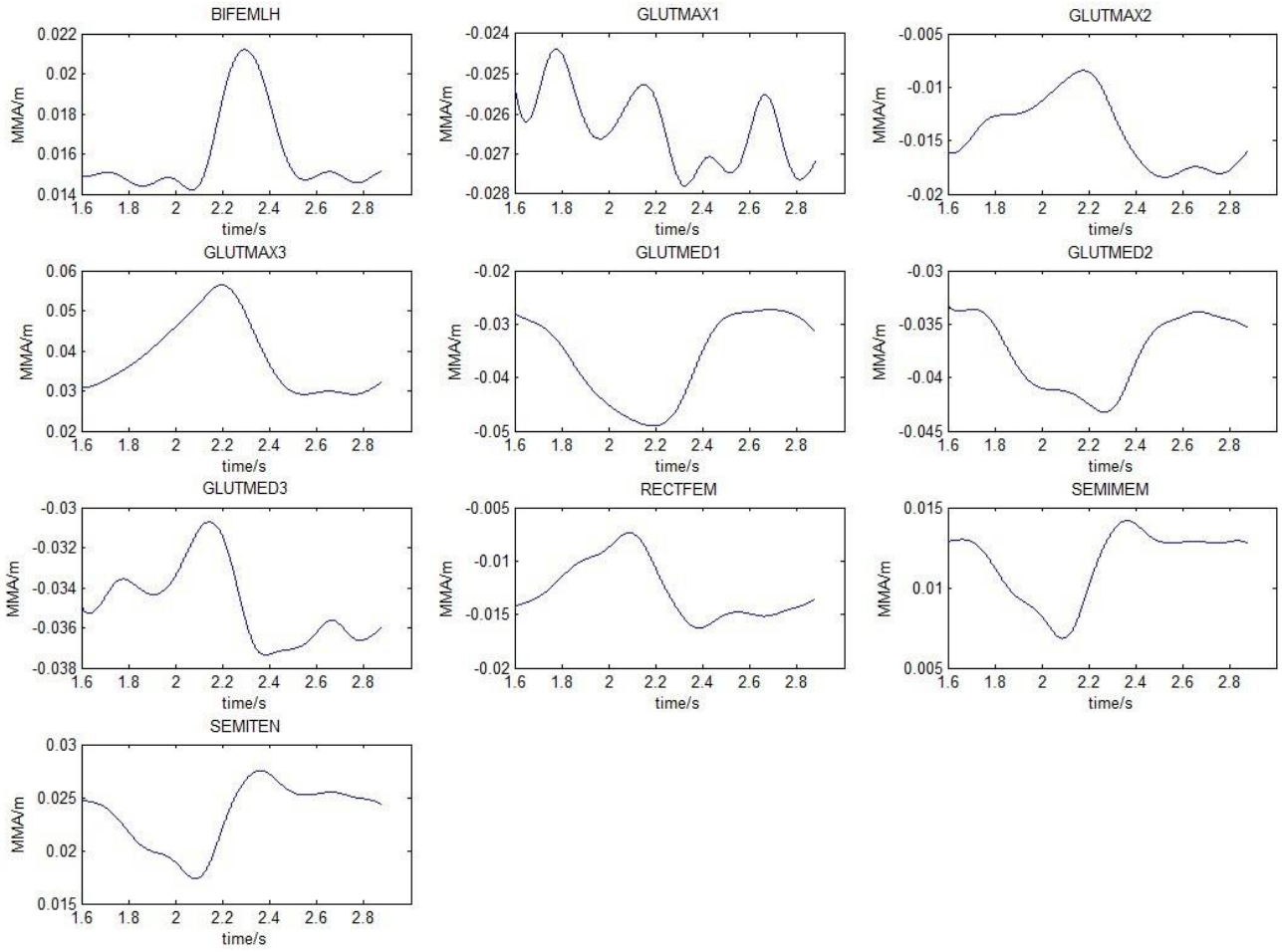

Fig. 5.11 The muscle moment arms for hip adduction

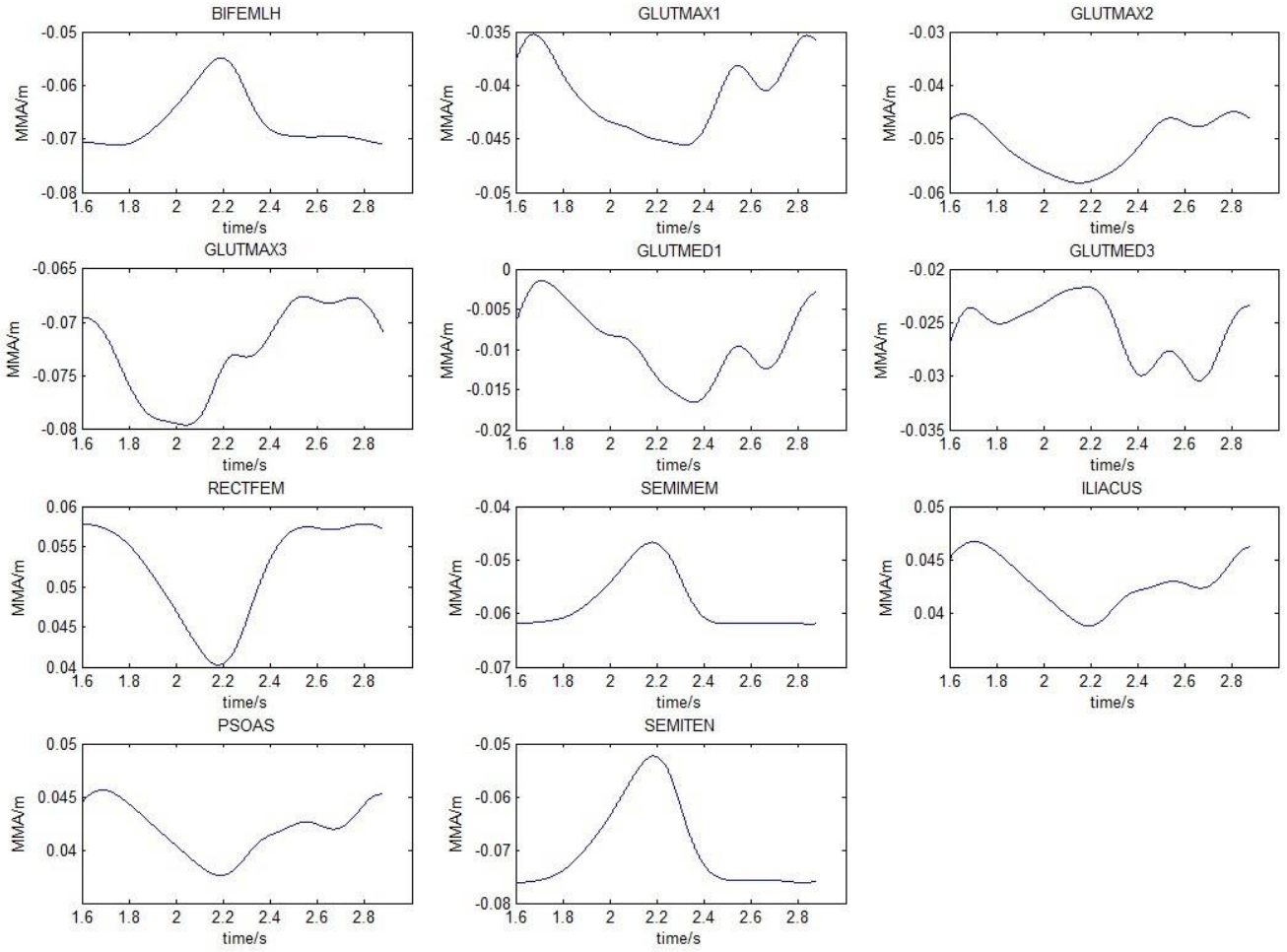

Fig. 5.12 The muscle moment arms for hip flexion

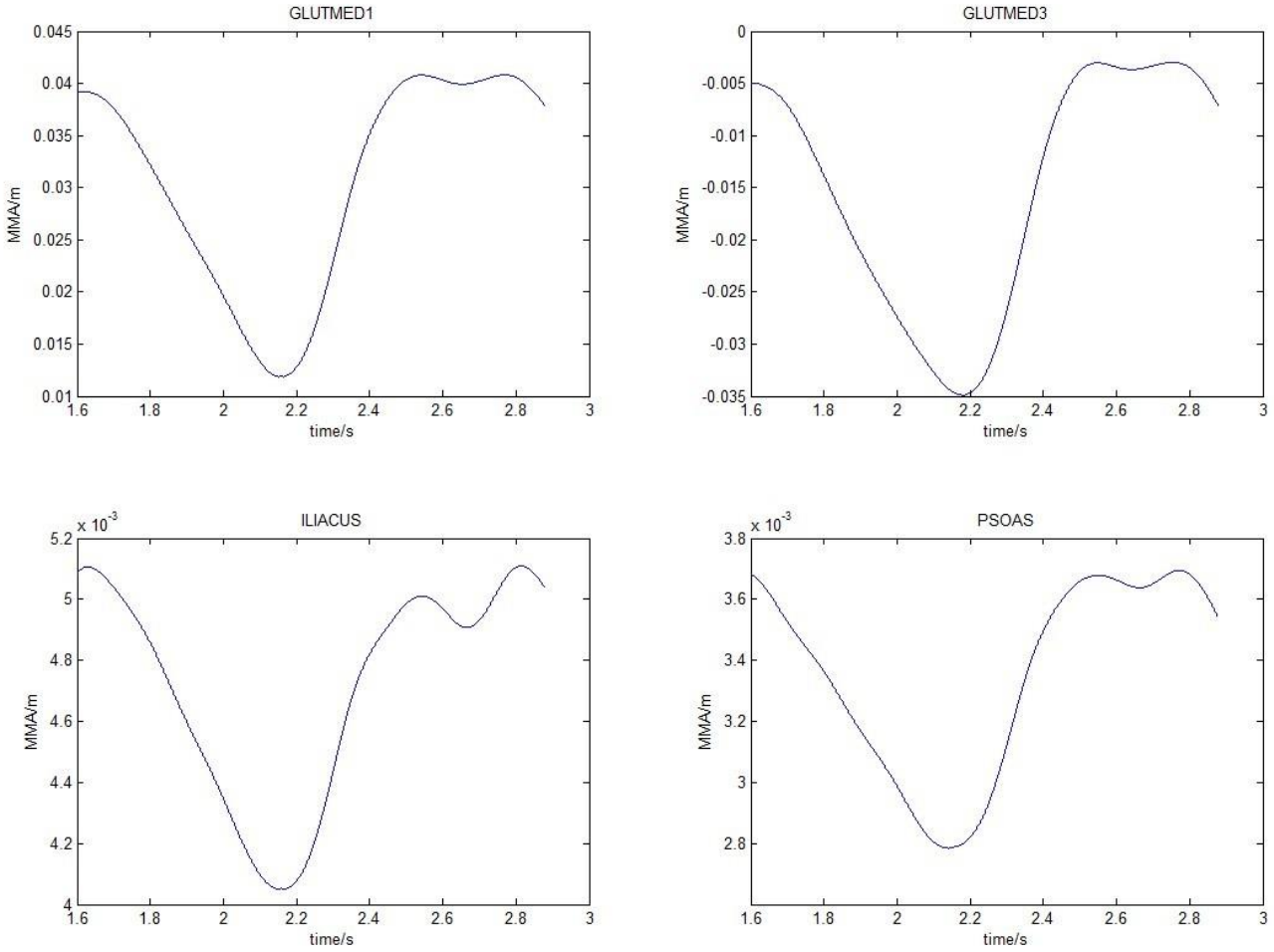

Fig. 5.13 The muscle moment arms for hip rotation

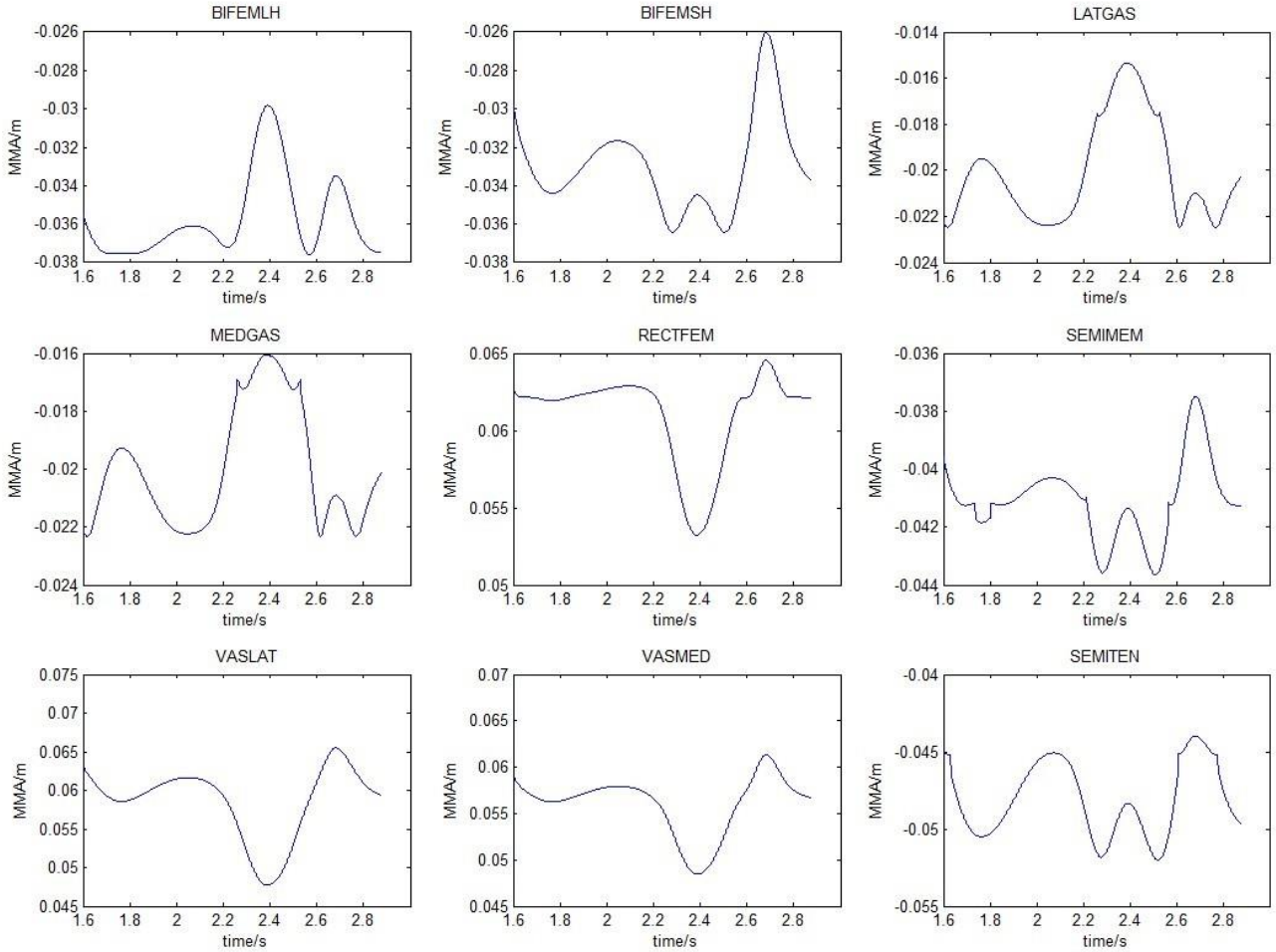

Fig. 5.14 The muscle moment arms for knee flexion

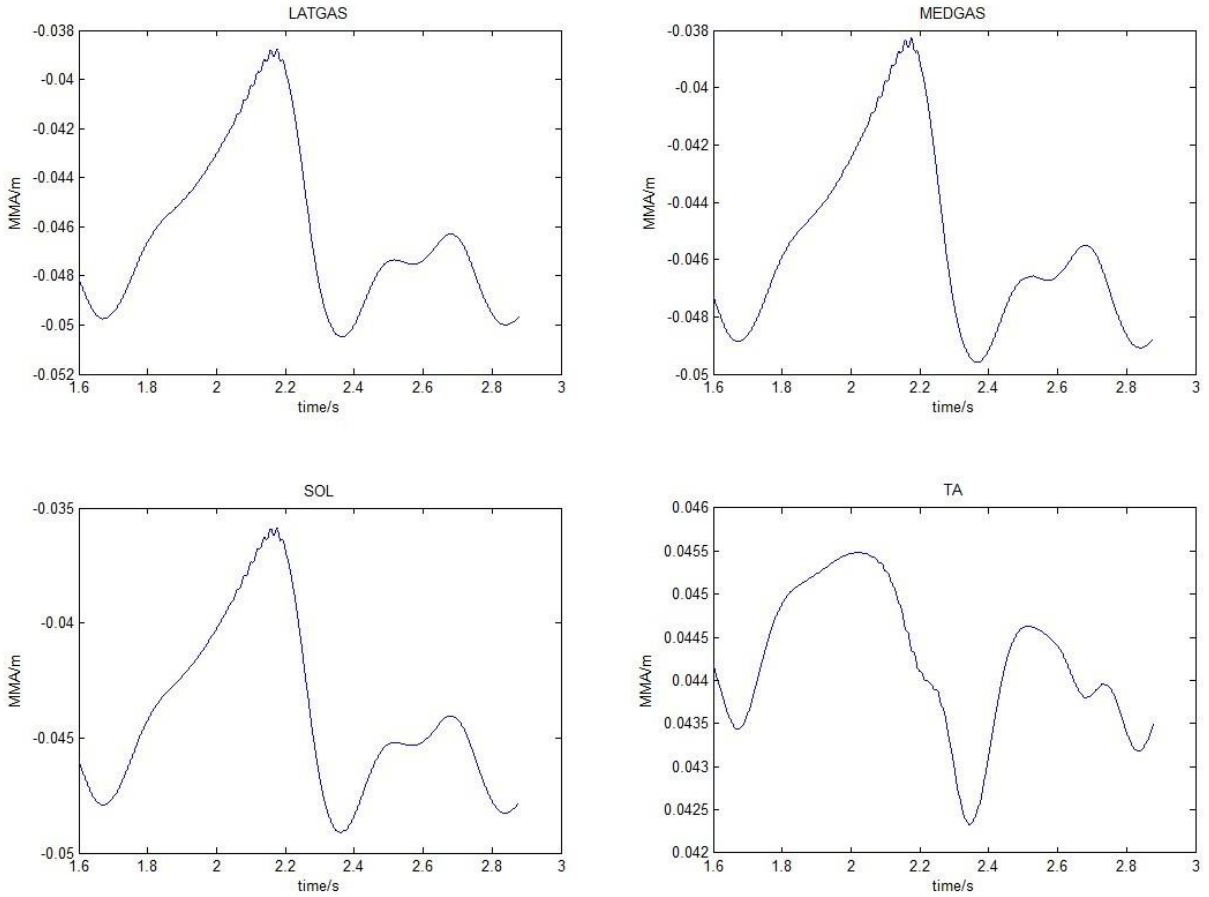

Fig. 5.15 The muscle moment arms for ankle plantar/dorsiflexion

The muscle moment arms of prime muscles at the ankle joint are shown in Figure 5.15. In the stance phase, the moment arm of dorsiflexor (TA) decreases a bit before gradual increase, and it reduces again after reaching the summit until the toe off point. In contrast to the TA, the lengths of all three plantarflexors' moment arms demonstrate an increase-decrease-increase tendency.

The net muscle moments (NMM) at each joint were calculated by the motion data and ground reaction forces. Figure 5.16 shows the calculated net muscle moments at hip, knee and ankle joints on the right leg of the subject in a gait cycle. Large differences in the magnitudes of the moments could be seen. In contrast to the other four moments, the average of hip rotation moment is of smaller value in the whole gait cycle. Additionally, all the moments change their directions within the gait cycle as well.

For hip joint, the moments reach the extreme values almost at the same time, which are -60Nm (hip abduction), -90Nm (hip flexion) and 16Nm (positive value for viewing from the head of the subject, hip clockwise rotation). Different from the hip adduction moment and the hip rotation moment, the hip flexion moment achieve its maximum value for hip extension at the toe off when the others return to 0.

The net muscle moment at the knee joint changes the direction three times in stance phase. Its peak value is around 30Nm for knee extension. It has been reported after getting the peak value, the moment should be positive (keep knee extension) till toe off (Ren et al., 2008). For this subject, the knee net muscle moment goes back to negative again before toe off. The reason should be the effect from the 'eKnee', which

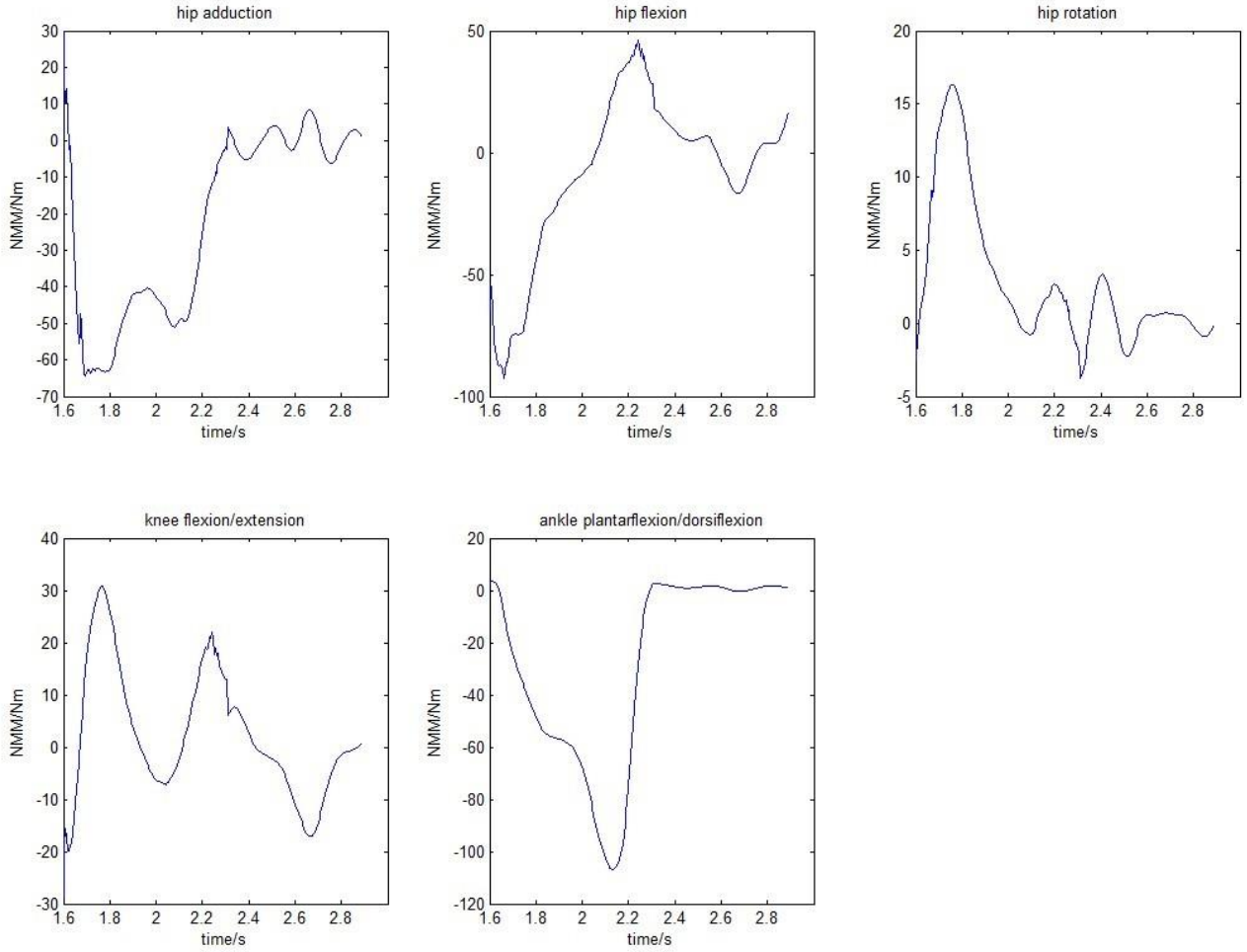

Fig. 5.16 The net muscle moments at three joints

enlarges the fluctuation of the moment. Apart from the net muscle moment at the knee joint, the others quite agree with the results shown in the literatures (Ren et al., 2008).

From the time history of the net muscle moment at the ankle joint, it can be seen that the ankle plantarflexors are active for the whole stance phase, and the net muscle moment reach -110 Nm which is the peak value for plantarflexion at toe off. After toe off, the moment sharply declines to zero.

It has been reported that the original models in Opensim are created based on three lower extremity cadaveric specimens and four subjects with cerebral palsy from MR images (Delp et al., 2007). The models characterize the geometry of the pelvis, femur, and proximal tibia, the kinematics of the hip and tibiofemoral joints, and the paths of the hamstrings, iliopsoas, and adductor muscles. The accuracy was quantified by comparing hip and knee flexion moment arms estimated from the models of the specimens to the moment arms determined experimentally on the same specimens. Errors in the hip and knee flexion moment arms of the muscles were less than 4 mm (within 10%) (Arnold et al., 2001; Arnold and Delp, 2001; Arnold et al., 2000). Based on these analyses, we believe that our model provide accurate estimates of muscle moment arms and net muscle moments in vivo. Meanwhile, the muscle moment arms and the net muscle moments estimated in our model will be the input of the algorithm we developed in the next chapter. The comparison between the bone-on-bone forces estimated by our algorithm and the contact forces measured by the ‘eKnee’ in the next chapter will be another indirect validation to verify the muscle moment arms and net muscle moments calculated here.

From the result of the net muscle moments, we can qualitatively figure out the resultant effect from muscles during walking. However, to specify the details of muscular dynamic response and its influence on human walking, we still need to understand the individual behaviour of each muscle. In the next chapter, the net muscle moments and muscle moment arms obtained above will be used as the input to the muscle force evaluation algorithm, analysing the muscle individual dynamic responses.

5.4 Conclusions

A three-dimensional musculoskeletal model was constructed using OpenSim software in this chapter. The dataset from Grand Challenge Competition was used to simulate human walking. The dataset included the subject's static standing and normal walking motion data. 14 muscles EMG signals during walking trials were provided as well.
Based on the experimental data, we scaled the generic musculoskeletal model to fit the shape of individual subject in OpenSim environment. The walking motion was optimized by inverse kinematics method to 'best match' the subject's motion in walking trials. Base on the ground reaction forces and the motion data provided by the competition, the net muscle moments at lower limb joints on subject's red leg were calculated by the inverse dynamics approach.

The results of muscle moment arms indicated that almost all the muscle moment arms of the muscles involved in hip flexion reached their peak value around toe off. Due to the small magnitude of moment arms for hip rotation, we concluded that both ILIACUS and PSOAS had little impact on the rotation of the hip.

Moreover, compared with literature data, the calculated results showed a good agreement with them. The calculated muscle moment arms, net muscle moments and the data in the 3D musculoskeletal model will be used as the input in the next chapter. Also, we will use the model and the calculated result to do the further investigation on human walking.

Chapter 6. Evaluation of Individual Muscle Forces during Human Walking

6.1 Introduction

As the biomechanical science advances in the last century, the medical treatment for curing disease and injury on human lower extremity has been improved. More and more quantitative methods have been implemented for analyzing the dynamic response of the musculoskeletal system during human locomotion, where the evaluation of the dynamic loading during human walking is one of the hot topics in biomechanics research over the past decade.

Theoretically, muscles are the most significant contributors to drive human locomotion. They contract by the stimulus from the neural system and develop the moments. Indirectly through their contributions to the ground reaction force via dynamic coupling, human realize various movement. Therefore, the individual muscle's action is the most essential factor to influence the resultant behaviour in human movement, and some prime movers' dynamic characteristics are even the determinant for a certain human movement. In this chapter, we are aiming to develop a novel strategy integrating the merits of both inverse dynamics and forward dynamics to calculate the individual muscle dynamic responses during human walking. A human lower limb neuromusculoskeletal model including 38 muscle groups (19 muscle groups on each leg) has been constructed for employing the new

strategy we proposed. A set of algorithm for model parameters calibration was designed. The experimental data from the Grand Challenge Competition were used for parameters calibration, model simulation and experimental validation.

6.2 Calibration of the model parameters

Many studies have indicated that in the model-based analysis, muscle's dynamic responses are quite sensitive to the selection of its parameters, such as the maximum isometric muscle force, the optimal muscle fibre length and the slack tendon length. Redl (Redl et al., 2007) has pointed out that muscle force estimation for walking are most sensitive to the changes in slack tendon length and least sensitive to the changes in muscle PCSA, particularly for those muscles that function as prime movers during walking. Slack tendon length was found to be the most critical parameter for both energetic and mechanical models, although the energetic model is always less sensitive to parameter changes than the mechanical model (Bisi et al., 2012). The fact that the sensitivity of a muscle's function is influenced by the magnitude of its maximum isometric muscle force as well as the operating region on its force-length curve has been presented (Ackland et al., 2012). Due to the subject-specific parameters required in model construction, the maximum isometric muscle force and the slack tendon length will be carefully calibrated in our study, and a set of novel calibration strategy is proposed here as well.

6.2.1 Calibration of the maximum isometric muscle forces (F_{mo})

Briefly speaking, the maximum isometric muscle forces are able to restrict the varying range for muscle forces as well as be an indicator of a certain muscle's maximum intension. It has been emphasized in Chapter 2 that the nature of the individual muscle forces evaluation is the process to solve an underdetermined question. In such a

circumstance, the optimization scheme will be used to search for the best solution for the question, where the individual muscle forces are considered as the optimal variables in the scheme. As we know, if loose constraint controls the optimal variables, the optimizer is definitely capable of finding out the best solution for the question, regardless of local or global solution. The optimizer highly likely fails to work out the solution if improper or intensive constraints are applied to the optimal variables. Being one of the constraints (upper bound) for the optimal variables, the maximum isometric muscle force should be adjusted to meet the request for solving the problem. In our study, the process of maximum isometric muscle forces calibration is illustrated in Figure 6.1.

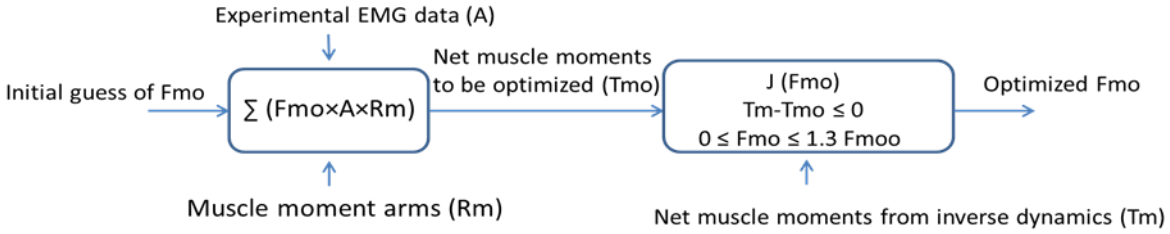

Fig. 6.1The process of F_{mo} calibration

In Figure 6.1, the measurement EMG data is from the Grand Challenge Competition, where EMG time histories for 16 muscle groups on each leg are needed. In chapter 5, 14 muscle groups' EMGs are provided, but we have three GLUTEUS MEDIUS branches, three GLUTEUS MAXIMUS branches and two BICEPS FEMORIS branches. In this study, we define three GLUTEUS MEDIUS are in the same EMG level as GLUTEUS MAXIMUS and BICEPS FEMORIS. The ILIACUS, SEMITENDINOSUS and PSOAS major's EMG data are unavailable in the experiment, and we assume they share the same EMG signals as the muscles in the identical muscle groups of the leg. For example, the EMG of SEMITENDINOSUS is

the same as that of the SEMIMEMBRANOSUS because they both locate in the posterior compartment of the thigh. The muscle moment arms (R_m) and net muscle moments (T_m) are the calculation results from inverse kinematics and inverse dynamics in Chapter 5. In this calibration process, we select the maximum and minimum T_ms of the hip adduction, the hip flexion, the hip rotation, the knee flexion and the ankle plantar/dorsiflexion in right leg's stance phase, where totally 10 T_ms are involved in the calculation. Therefore, the EMG data and muscle moment arms are the values of 19 muscle groups at these 10 frames. The optimization scheme could be expressed as

minimize

$$J = \sum_{i=1}^{19} \left(F_{mo,i} - F_{moo,i}\right)^2 \tag{6.1}$$

subject to

$$\left|T_{m,j}\right| - \left|T_{mo,j}\right| \leq 0 \qquad j = 1,2,\dots,5$$

$$0 \leq F_{mo} \leq 1.3 \times F_{moo}$$

where F_{moo} is the maximum isometric muscle fibre force from the scaled model in Chapter 5. j represents the jth motion, and in our study, they are hip adduction, hip flexion, hip rotation, knee flexion and ankle plantar/dorsiflexion. Therefore, two T_ms (Max and Min) are at each motion.

The optimization is implemented in Matlab2010a. The original F_{moo} and optimized F_{mo} are listed in Table 6.1.

Table 6.1 The original F_{moo} and optimized F_{mo}

Muscle name	F_{moo}/N	F_{mo}/N
ILIACUS	1073	757
RECTUS FEMORIS	1169	1207
VASTUS MEDIALIS	1294	1236
VASTUS LATERALIS	1871	1816
GLUTEUS MEDIUS_1	819	1009
GLUTEUS MEDIUS_2	573	679
GLUTEUS MEDIUS_3	653	813
BICEPS FEMORIS LONG	896	692
BICEPS FEMORIS SHORT	804	824
SEMIMEMBRANOSUS	1288	906
GLUTEUS MAXIMUS_1	573	739
GLUTEUS MAXIMUS_2	819	910
GLUTEUS MAXIMUS_3	552	484
SEMITENDINOSUS	410	344
GASTROCNEMIUS MEDIAL	1558	1562
GASTROCNEMIUS LATERAL	683	686
SOLEUS	3549	3566
TIBIALIS ANTERIOR	905	986
PSOAS MAJOR	1113	793

6.2.2 Calibration of the slack tendon lengths (L_{st})

Tendon is connected to muscle fibre in series, and it transmits the force produced by the muscle fibre to the skeleton. The mechanics of the tendon is similar to a nonlinear spring, where the tendon force exponentially increases as tendon lengthens. The most significant difference between a tendon and a nonlinear spring is the tendon provides nothing when it is compressed. In musculoskeletal modelling, it is believed that the muscle fibre force is equivalently transmitted by the tendon, which means tendon force equals to muscle fibre force at all times. Since tendon produces force only when it stretches, and muscle fibre always creates force, we have to keep the tendon stretching all the time during movement, which means the total tendon length should be longer than slack tendon length at any time.

We calculated the certain slack tendon length by scaling the model to the specific subject in Chapter 5, but it was conducted based on geometrical relationship only. In realistic, does the slack tendon length share the same ratio as what is used in bone scaling? Will each scaled slack tendon length make the equilibrium relationship between muscle fibre and tendon satisfied during the whole gait cycle? After some analysis in the study, we concluded that only depending on the geometry method, it is impossible to realize the equality between each muscle fibre force and tendon force during walking. Also, the slack tendon length scaled based on geometrical relationship only will bring unexpected divergence to the algorithm. The objective of this section is to present a novel optimization strategy to calibrate the slack tendon length. The optimization process is conducted frame by frame within the right leg's stance phase, which means the number of cycle that the optimization runs equal to the number of frames in stance phase we sampled. Figure 6.2 shows the process of such

calibration method.

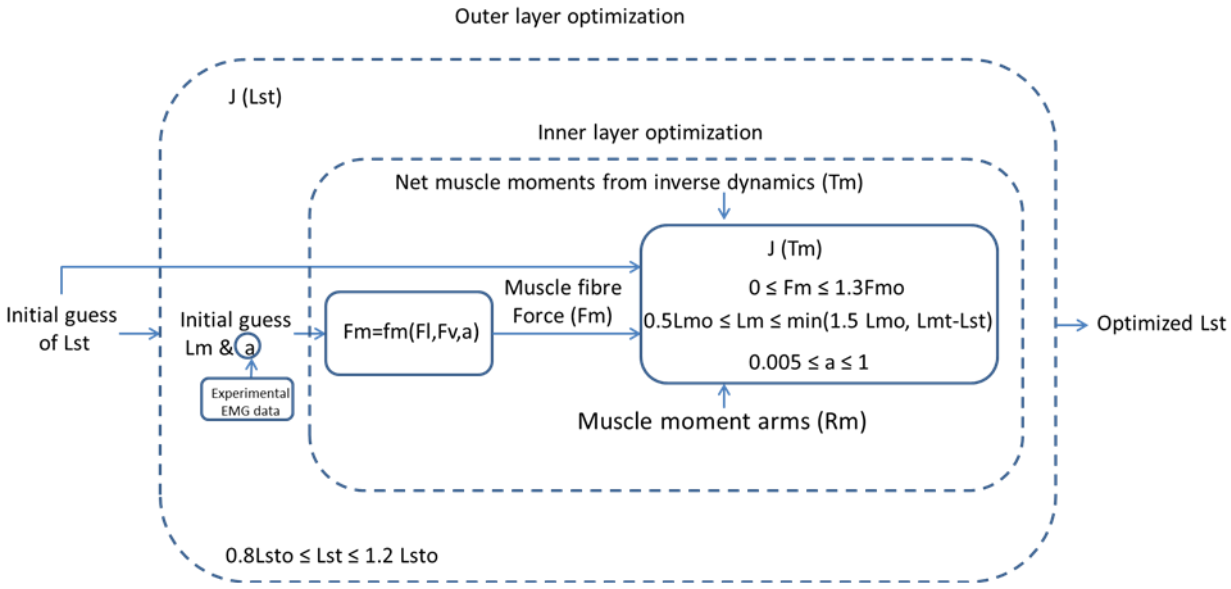

Fig. 6.2 The process of L_{st} calibration

In Figure 6.2, the initial guess of the outer layer optimization is the slack tendon length from the scaled model in Chapter 5. For the outer layer optimization, we minimize

$$J = \sum_{i=1}^{19} (L_{st,i} - L_{sto,i})^2 \tag{6.2}$$

subject to

$$0.8 \times L_{sto} \leq L_{st} \leq 1.2 \times L_{sto}$$

where L_{sto} is the slack tendon length scaled by geometrical method in Chapter 5. We set $\pm 20\%$ are the tolerances for the upper and lower boundaries in optimization scheme. For the 19 prime movers scaled model in Chapter 5, the minimum value of $, \frac{Optimal\ muscle\ fibre\ length}{Slack\ tendon\ length},$ ratio is about 20%, so 20% is chosen here as the tolerance

value.

Muscle fibre length L_m and muscle activation level a are selected as initial guesses for the inner layer optimization. At each optimization step, we use the EMG data from the Grand Challenge Competition as muscle activation level initial guess. The muscle moment arms from inverse kinematics and net muscle moments from inverse dynamics in Chapter 5 are used in the inner layer optimization as well. Mathematically, the inner layer optimization is

minimize

$$J = \sum_{i=1}^{5}(F_{m,i} \times R_{m,i} - T_{m,i})^2 \tag{6.3}$$

subject to

$$0 \leq F_m \leq 1.3 \times F_{mo}$$

$$0.5 \times L_{mo} \leq L_m \leq min(1.5 \times L_{mo}, L_{mt} - L_{st})$$

$$0.005 \leq a \leq 1$$

where T_m represents the net muscle moments at five joints, which has been described in the last section; therefore, F_m and R_m are the muscle forces and muscle moment arms involved in the ith corresponding joint's motion. F_{mo} is the maximum isometric muscle force calibrated in the last section. L_{mo} and L_{mt} are the optimal muscle fibre length and musculotendon length (time dependent) from the scaled model in Chapter 5. The calibration is conducted in Matlab 2010a. The original slack tendon lengths L_{sto} in the scaled model (from Chapter 5) and the optimized slack tendon lengths L_{st} are listed in Table 6.2.

Table 6.2 The original L_{sto} and optimized L_{st}

Muscle name	L_{sto}/m	L_{st}/m
ILIACUS	0.1039	0.0883
RECTUS FEMORIS	0.2964	0.2608
VASTUS MEDIALIS	0.1192	0.1311
VASTUS LATERALIS	0.1487	0.1338
GLUTEUS MEDIUS_1	0.0817	0.0784
GLUTEUS MEDIUS_2	0.0555	0.0450
GLUTEUS MEDIUS_3	0.0552	0.0607
BICEPS FEMORIS LONG	0.3111	0.3422
BICEPS FEMORIS SHORT	0.0868	0.0774
SEMIMEMBRANOSUS	0.3419	0.3282
GLUTEUS MAXIMUS_1	0.1292	0.1112
GLUTEUS MAXIMUS_2	0.1293	0.1164
GLUTEUS MAXIMUS_3	0.1477	0.1270
SEMITENDINOSUS	0.2457	0.2703
GASTROCNEMIUS MEDIAL	0.4075	0.3586
GASTROCNEMIUS LATERAL	0.3973	0.3655
SOLEUS	0.2618	0.3037
TIBIALIS ANTERIOR	0.2326	0.2001
PSOAS MAJOR	0.1678	0.1846

6.3 Optimization scheme based on muscle force only

As discussed before, many static optimization approaches based on inverse dynamics to solve the load sharing problem during human walking have been developed over the last 30 years, from the method based on two-dimensional human musculoskeletal model in the sagittal plane (Patriarco et al., 1981) to the method using three-dimensional large-scale model with more degree of freedoms (Rohrle et al., 1984). The advantage of static optimization method includes both reducing computational burden and being convenient to be applied into clinical practice. Here, we would like to start with a conventional optimization scheme using muscle forces as optimal variables to analyze the individual muscle behaviour, where the scheme is implemented on a three-dimensional human lower limb musculoskeletal model with 5 degrees of freedoms.

6.3.1 Information for modelling

The 19 muscle groups are the prime movers on each leg form the muscular system in the model. Five time dependent net muscle moment constraints correspond to the three degrees of freedom at the hip and one degree of freedom at both knee and ankle, which are hip adduction, hip flexion, hip rotation, knee flexion and ankle plantar/dorsiflexion. The muscle moment arms and net muscle moments are both from the output of inverse dynamics calculated in chapter 5. Each muscle's optimal muscle fibre length, L_{mo}, is from the scaled model in chapter 5 as well. The model is constructed in Matlab 2010a.

6.3.2 Estimation of individual muscle forces

The muscle forces multiplied by their corresponding time dependent muscle moment arms should equal to the net muscle moments, which can be expressed as:

$$R_m(t) \times F_m(t) = T_m(t) \tag{6.4}$$

where F_m is the vector of 19 muscle forces, T_m is the vector of the five net muscle moment at the joints stated above, and $\mathrm{R_m}$ is a 5×19 matrix of the time histories of muscle moment arms. The underdetermined solution associated with the muscle redundancy can be solved by minimizing the function below,

$$J = \sum_{i=1}^{19} \left(\frac{F_{m,i}}{PCSA_i} \right)^3 \tag{6.5}$$

where, $PCSA_i$ is the Physiological Cross-sectional Area of the ith muscle's at its optimal muscle fibre length. $PCSA = \frac{V_m}{L_{mo}}$, where V_m is the ith muscle's volume. Figure 6.3 shows the optimization process.

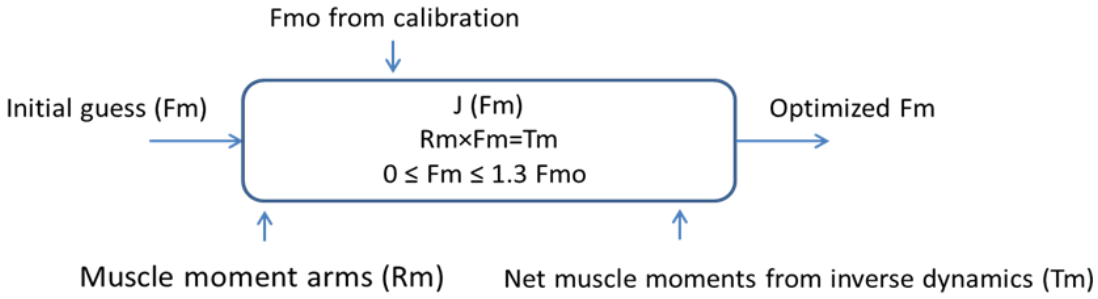

Fig. 6.3 The optimization scheme based on muscle forces

The calculated individual muscle forces based on this scheme are shown in Figure 6.5.

6.4 Optimization scheme based on muscle activation and contraction dynamics

Although the static optimization approach based on inverse dynamics has advantages of saving computational cost compared to the forward dynamics method, the static optimization approach which calculates at each time step separately leads to a non-physiological muscle force time history, where the dynamic characteristic is neglected. Most static optimization approaches do not involve muscle activation and muscle contraction dynamics.

The dynamic optimization solution based on forward dynamics only has been implemented in evaluating the individual muscle forces during human walking (Anderson and Pandy, 2001). However, the dynamic optimization of a large scale musculoskeletal model is extremely costly in terms of the computational effort since the differential equations that describe the musculoskeletal dynamics (See Figure 6.4) have to be integrated, and the number of optimal variables is much more than that in static optimization. This drawback prevents the method being used widely in evaluating the individual muscle behaviour during walking in clinical process.

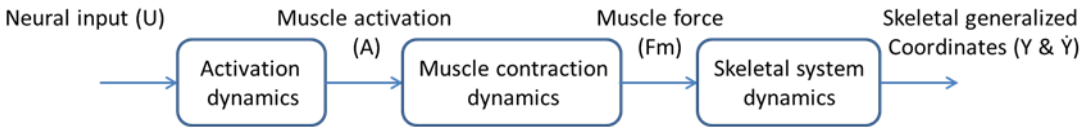

Fig. 6.4 The scheme of the musculoskeletal system dynamics

Here, we propose a novel method based on both inverse dynamics and forward dynamics, which conducts optimization at each time step. This method allows for the

calculation of the time history of muscle fibre lengths and other variables; also it is computationally more efficient than the conventional forward dynamic optimization method since the integrations are employed at each two consecutive time steps as well as the number of optimal variables is less than that used in purely forward dynamic optimization. The optimization scheme is shown in Figure 6.6. The simulations are conducted in Matlab 2010a.

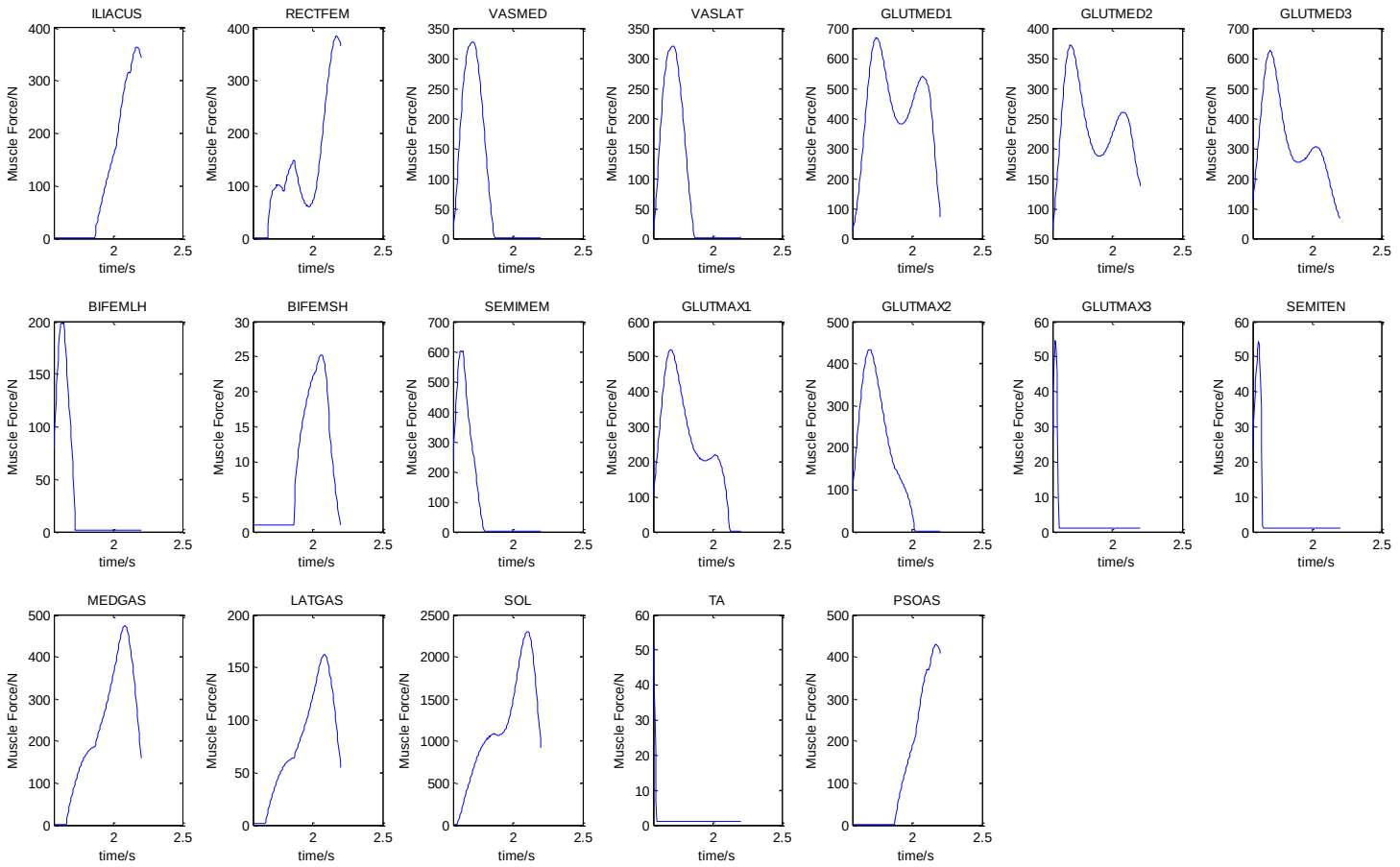

Fig. 6.5The calculated individual muscle forces by using the optimization scheme based on muscle force only

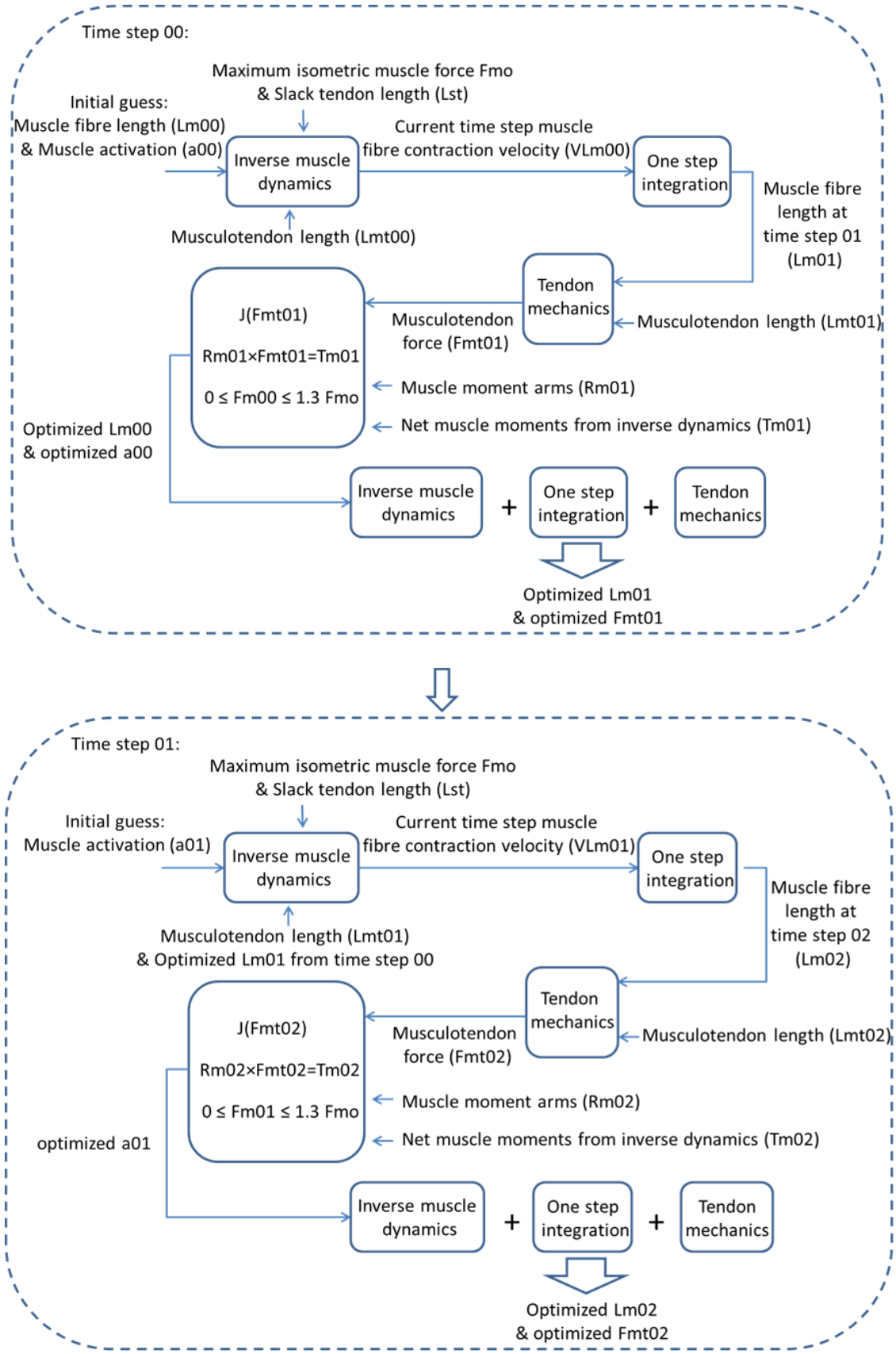

Fig. 6.6 The process of optimization scheme based on muscle activation and contraction dynamics

In Figure 6.6, the value of the maximum isometric muscle forces F_{mo} and slack tendon lengths L_{st} are from the calibration result. The musculotendon lengths L_{mt} are the output of inverse kinematics in Chapter 5. Same as the net muscle moments and muscle moment arms used in the optimization scheme based on muscle force only, we use the R_m and T_m in this optimization scheme to

minimize

$$J = \sum_{i=1}^{19} \left(\frac{F_{m,i}}{PCSA_i} \right)^3 \tag{6.6}$$

subject to

$$R_m \times F_m = T_m$$

$$0 \leq F_m \leq 1.3 \times F_{mo}$$

at each time step. The calculated individual muscle forces and the muscle fibre lengths based on this scheme are shown in Figure 6.7 and Figure 6.8.

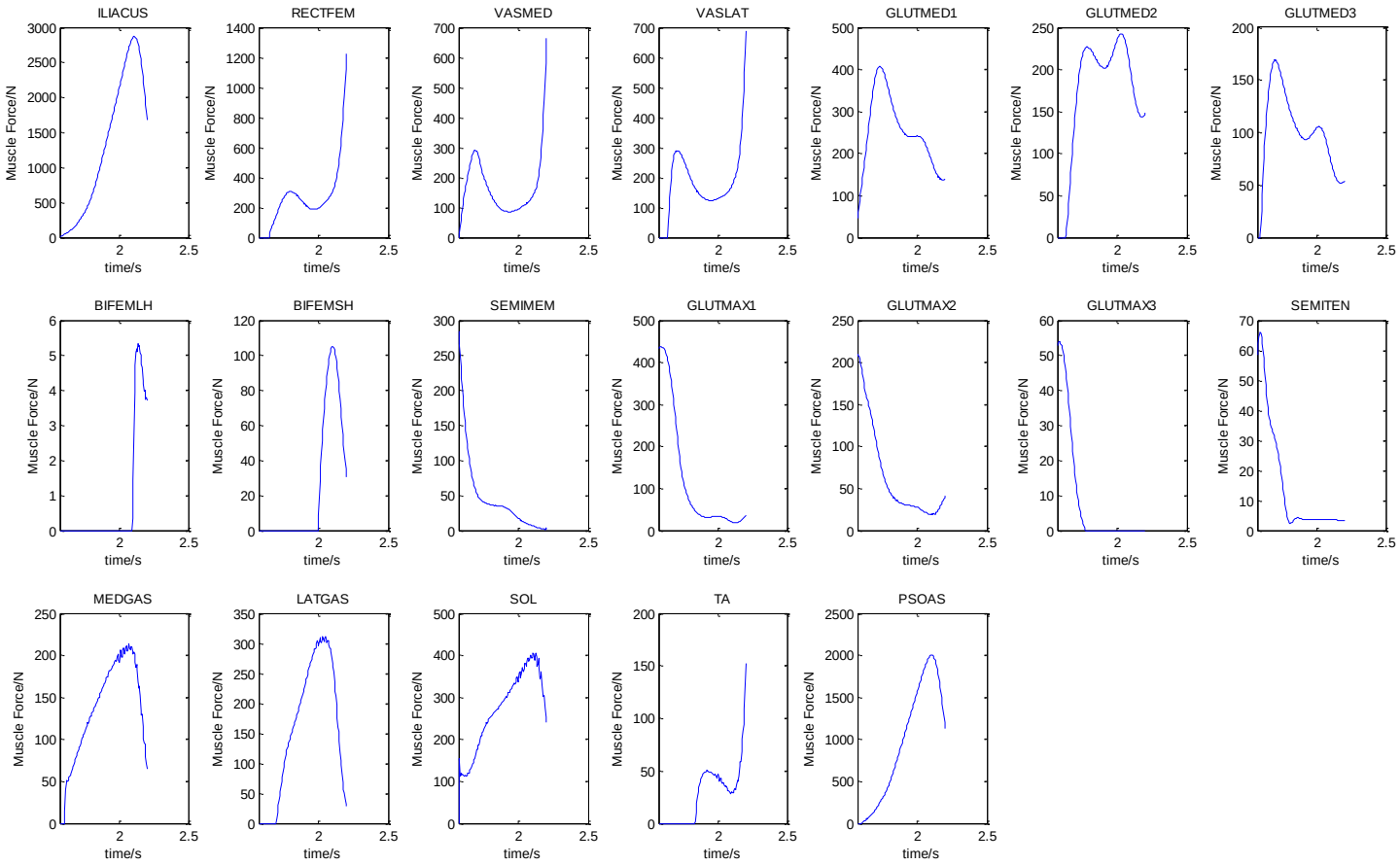

Fig. 6.7 The calculated individual muscle forces by using the optimization scheme based on muscle activation and contraction dynamics

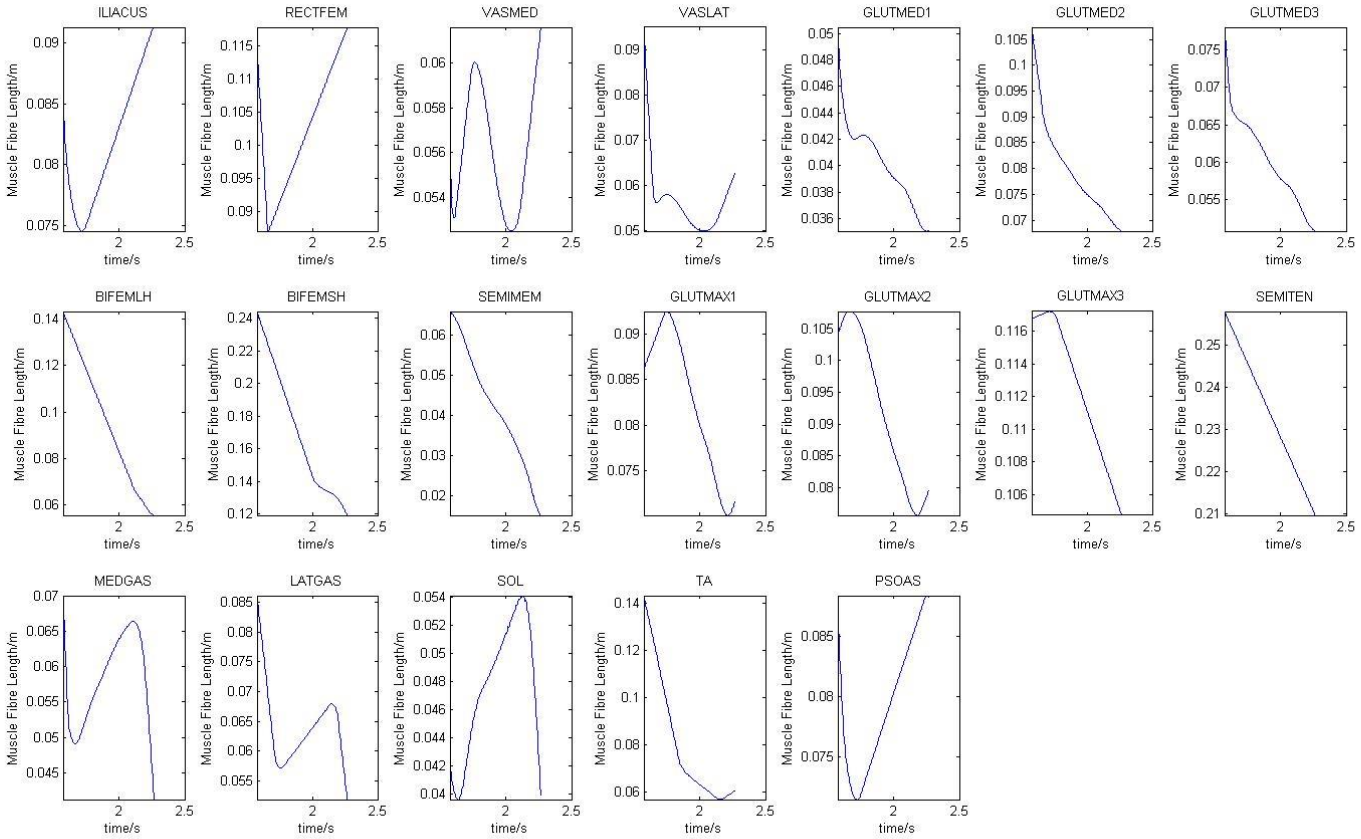

Fig. 6.8 The calculated individual muscle fibre lengths by using the optimization scheme based on muscle activation and contraction dynamics

6.5 Experimental validation

Two different optimization schemes are developed in this study, both of which are capable of estimating individual muscle forces during walking. In addition, the individual muscle forces were calculated in OpenSim software as well. In this section, we will compare the results of these three sets of individual muscle forces with the joint contact forces obtained from the eKnee in Chapter 5.

With the ground reaction forces provide by the Grand Challenge Competition and the anthropometric parameters from OpenSim, we can calculate the knee joint resultant force in three directions by using inverse dynamics method. Also, the muscle resultant force at the knee joint is the summation of the individual muscle forces of the muscles involved in knee flexion. Therefore, the knee joint contact force can be calculated by the relationship, knee joint resultant force = muscle resultant force + knee joint contact force, at each direction of the coordinate system.

6.5.1 Data processing

As stated in Chapter 5, the joint contact forces were measured by the eKnee implanted in the right knee joint. The eKnee force vector is the time history in the local frame. The origin of coordinate of the local frame locates at the plateau of eKnee. Meanwhile, the individual muscle forces we estimated are scalar but not vectors. In this section, we use a method to transform the ‘eKnee’ contact forces and the individual muscle forces to the same coordinate system first.

In our optimization schemes, we assume that each musculotendon unit length is the linear distance between muscle origin and insertion. Therefore, if the coordinates of

each muscle's origin and insertion are known, the corresponding muscle force can be represented as a vector. The direction of muscle force is defined as the vector direction.

6.5.1.1 Individual muscle forces transformation

In our method, all the muscles around right knee joint will be used to calculate the joint contact forces at the knee joint. The positions of these muscles' origins and insertions are from the scaled musculoskeletal model in Chapter 5. Their coordinates and parent body are listed in Table 6.3.

Table 6.3 The muscle's origin and insertion and the parent body

Muscle name	Origin				Insertion			
	X/m	Y/m	Z/m	Parent body	X/m	Y/m	Z/m	Parent body
BICEPS FEMORIS LONG	-0.1354	-0.1103	0.0747	Pelvis	-0.0245	-0.0589	0.0359	Tibia_r
BICEPS FEMORIS SHORT	0.0048	-0.2006	0.0222	Femur_r	-0.0245	-0.0589	0.0359	Tibia_r
GASTROCNEMIUS LATERAL	-0.0209	-0.3750	0.0259	Femur_r	0.0000	0.0319	-0.0055	Calcn_r
GASTROCNEMIUS MEDIAL	-0.0181	-0.3733	-0.0223	Femur_r	0.0000	0.0319	-0.0055	Calcn_r
RECTUS FEMORIS	-0.0317	-0.0334	0.1041	Pelvis	0.0559	0.0238	0.0015	Tibia_r
SEMIMEMBRANOSUS	-0.1281	-0.1048	0.0769	Pelvis	-0.0282	-0.0499	-0.0205	Tibia_r
VASTUS LATERALIS	0.0046	-0.1762	0.0331	Femur_r	0.0543	0.0221	0.0173	Tibia_r
VASTUS MEDIALIS	0.0133	-0.1995	0.0179	Femur_r	0.0498	0.0237	-0.0153	Tibia_r
SEMITENDINOSUS	-0.1358	-0.1181	0.0649	Pelvis	0.0028	-0.1000	-0.0202	Tibia_r

In Table 6.3, the Pelvis, Femur_r, Tibia_r and Calcn_r represent the pelvis, right femur, right tibia and right calcaneus of the subject who participated in the walking trials in Chapter 5, and each body segment has its own local coordinate. In our study, we define all the muscle origins and insertions are in the global coordinate system which is located on the ground. Figure 6.9 shows the position of the origins of the global and

the local frames. From top to bottom, they are the origins of pelvis, femur, tibia, talus, calcaneus and toes coordinate system in turn, and the global one sits on the ground. Red axis, yellow axis and green axis are the X, Y and Z axes for each frame in the figure.

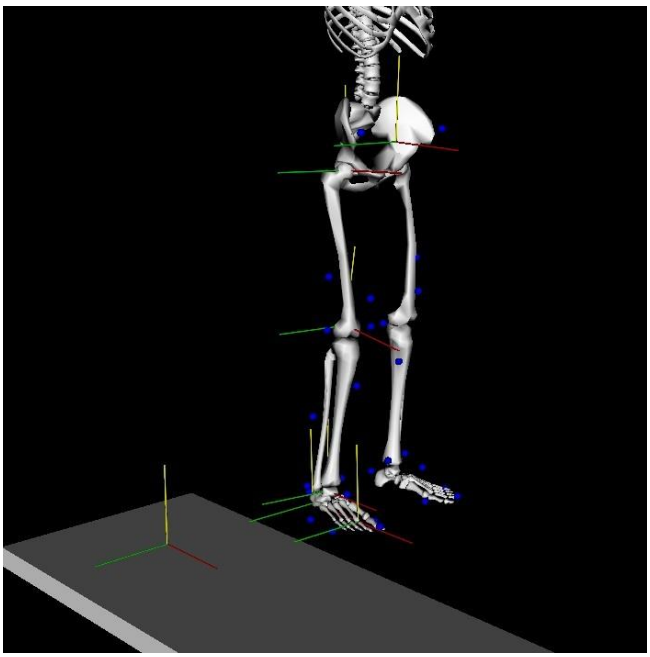

Fig. 6.9 The positions of the origins of global and local frames

Additionally, the local frames are in sequence as ground – pelvis – femur – tibia – talus – calcaneus – toes. Moreover, it is noteworthy that the talus and calcaneus frames rotate about a certain vector in the tibia and the talus systems. Also, not all the translations of the frames relative to their parents' frames are fixed. It is easily to be figured out that the translations of the pelvis relative to the ground are determined by the measurement data. The X and Y translations of tibia frame both are the functions of the knee flexion angles.

The transformation process is conducted in Matlab 2010a, where all the coordinates of

the origins and insertions are changed to the vectors in global frame ultimately. Based on the description above, the time histories of measured 'eKnee' forces have been transformed into global frame as well.

6.5.1.2 Joint contact forces calculation

The bone-on-bone force is the actual force seen across the articulating surface and includes the effect of muscle activity and the action of ligament. While the joint reaction force is defined as a force obtained from the free-body diagram of segment analysis (Winter, 2009). In a simple word, the joint reaction force is the resultant force acting on the segment while the bone-on-bone force is the contact force between two segments. The relationship between them could be expressed as 'joint reaction force = muscle forces + bone-on-bone force'.

In our study, we named joint contact force the same as the bone-on-bone force while the joint resultant force is the same as the joint reaction force. Based on the relationship between joint reaction force and bone-on-bone force, we have

$$\sum_{i=1}^{9} \vec{F}_{m,i} + \vec{F}_{con} = \vec{F}_{res} \tag{6.7}$$

where $\vec{F}_{m,i}$ is the summation of individual muscle forces at the knee joint, $\vec{F}_{con}$ is the knee joint contact force, and $\vec{F}_{res}$ is the knee joint resultant force obtained from inverse dynamics method. Based on the human motion data and the ground reaction forces provided by the Grand Challenge Competition, we conducted the inverse dynamics method to work out the $\vec{F}_{res}$. Based on the Newton's second law, the ground reaction forces and the foot motion data were used to calculate the joint resultant force

for foot segment at the ankle joint in three directions. For tibia segment, the joint resultant force at the ankle joint was opposite to the one for foot segment. By using the tibia's motion data and the joint resultant force for tibia at the ankle joint, the joint resultant force for tibia at the knee joint can be calculated.

6.5.2 Experimental validation

The simulations were conducted in the stance phase of the right leg (eKnee implanted). In order to avoid finding local minima, random check was conducted by repeating the minimization searching process with different initial guesses that were randomly set.

Longitudinal contact forces evaluated by three different strategies are compared with the eKnee contact force in Figure 6.10. 'ID & FD', 'Fm', 'OpenSim' and 'eKnee' represent the optimization scheme based on muscle activation and contraction dynamics, optimization scheme based on muscle force only, results from OpenSim software and the experimental data measured by 'eKnee' respectively. For most of the stance phase, the results from 'ID & FD' have the best agreement with the eKnee data. From 1.65s to 1.7s, the trend of 'ID & FD' is contrast to what in the eKnee. Within this period, the force in the positive X direction increase in 'ID &FD' method. Also, in the final stage of stance phase, 'ID & FD' method sees the contact force returning to zero, where 'eKnee' force sharply reduce to around 900N.

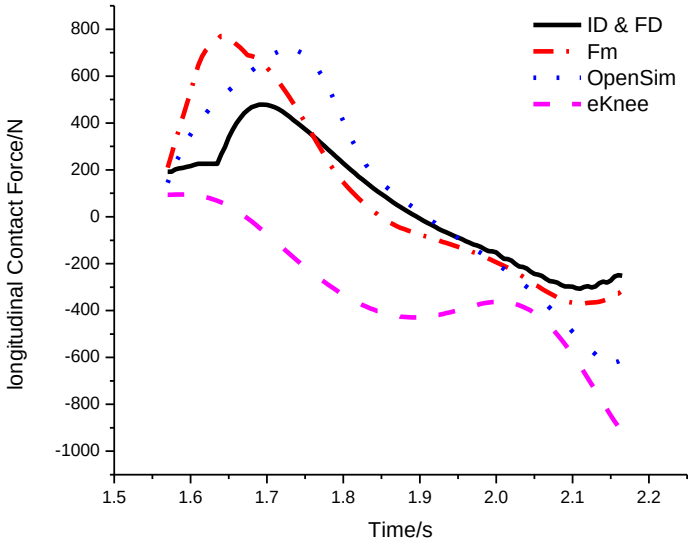

Fig. 6.10 The longitudinal contact forces comparison

Apart from those two periods, the majority of trend of the contact forces of 'ID & FD' are in good agreement with the measured data. The magnitude difference between them is obvious. Due to the lack of the number in muscles, our optimized result could have errors in magnitude. During 1.65s to 1.7s after heel strike, the right knee plays a role in decelerating the motion in X direction. It will offer a negative force to reduce the forward walking speed. Therefore, the contact force that the right femur gives to the right tibia should be a positive value. As the torso moves anterior to the right foot, the contact force in X direction will turn to below zero. In the final stage, although the X-direction contact force will function as accelerating the whole body's motion, the left foot has already been on the ground and started driving the body move forward (accelerating the whole body as well), so the X-direction force should have a trend to go back to zero (will toe off) instead of continuing to decline.

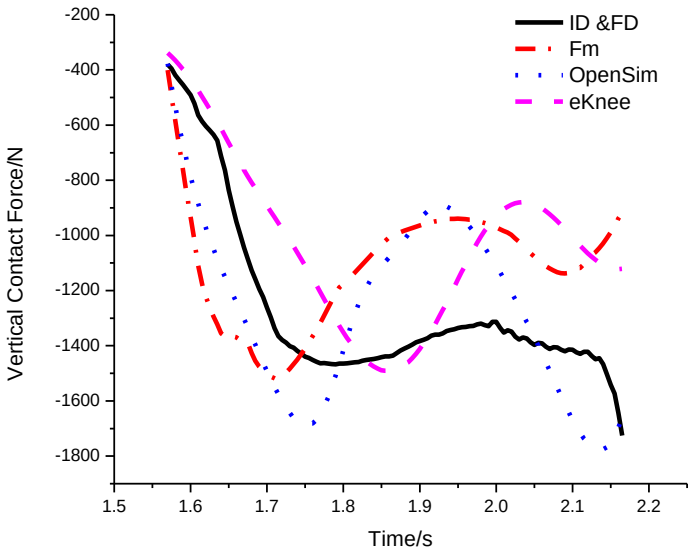

Fig. 6.11 The vertical contact forces comparison

In Figure 6.11, four time histories of vertical contact forces are depicted. The vertical contact forces estimated by 'ID & FD' are very close to the experimental data, either in magnitude or trend. A notable discrepancy in magnitude occurs before toe off from 1.95s to 2.15s. In our opinion, this is probably because the subject is implanted with an instrumental sensor at right knee joint, which could have enforced him to produce more intensive muscle forces to lift upward the body, even brought some tiny fluctuations in muscle forces. More strenuous muscle forces can increase the contact force in Y direction. It can be seen the difference between the contact forces based on 'Fm' method and the 'eKnee' data. It makes us surprising that the discrepancy in time phase hides the fact that they share even the same trend and magnitude in stance phase. The big difference in time phase may be caused by the flaw of optimization scheme itself. In 'Fm' method, there is no dynamic relation between every two consecutive time steps, which may bring the influence here.

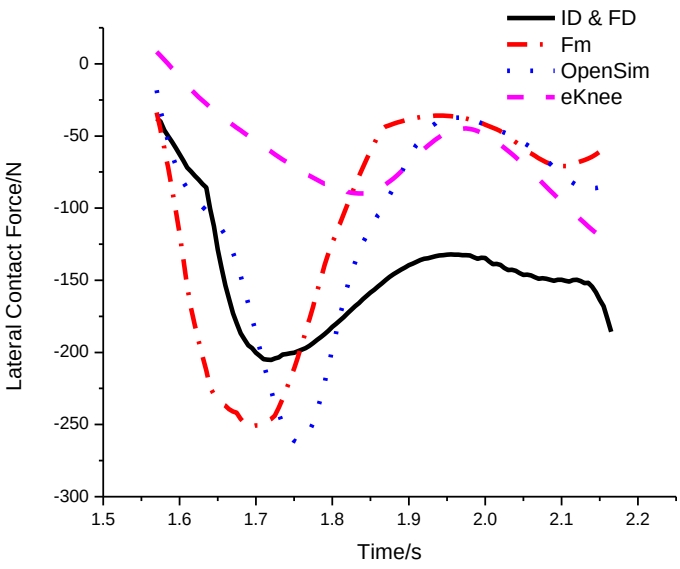

Fig. 6.12 The lateral contact forces comparison

Figure 6.12 shows the lateral contact forces comparison during stance phase. The 'eKnee' curve shows that compared with the other three curves, it changes in small amplitude in negative Z. There is a magnitude difference between the results based on 'ID & FD' and the measured data. The lateral contact forces are normal of small value during walking. However, the results calculated by the 'ID & FD' method are better than those of 'Fm' and 'OpenSim'. Because after around 1.7s, the peak value of 'ID & FD' is about 20% smaller than those of 'Fm' and 'OpenSim', which means the 'ID & FD' curve is closer to 'eKnee' than the other two. Although in the final stage of the stance phase, the 'ID & FD' results show exactly the same trend as the 'eKnee', the difference between the 'ID & FD' results and the 'eKnee' data may because some assumptions and simplicities in the model structure, and the muscle parameters for modelling are not the same as those of the subject. Also, the passive tissues, e.g. ligaments, have not been considered in the model, so the effects from them are neglected. Moreover, due to the eKnee implanted in the right knee, the cost function

using in the optimization scheme may not be the summation of cubed stress of the muscles.

6.5.3 Error Analysis

To evaluate model accuracy, the calculated contact forces from 'ID & FD', 'Fm' and 'Opensime' were compared with the measured 'eKnee' forces. The deviations of the calculated forces of the three different solutions from the measurement data were quantified using the root mean square error (RMSE) and the relative root mean square error (rRMSE) at all three directions,

$$RMSE = \sqrt{\frac{\sum_{i=1}^{n}(X_{eknee,i} - X_{model,i})^2}{n}} \tag{6.8}$$

$$rRMSE = \frac{RMSE}{X_{eknee,max} - X_{eknee,min}} \times 100\% \tag{6.9}$$

where $X_{eknee,i}$ is the 'eKnee' force at frame i; $X_{model,i}$ is the predicted forces from three different solutions at frame i; $X_{eknee,max}$ is the maximum 'eKnee' force within stance phase; $X_{eknee,min}$ is the minimum 'eKnee' force within stance phase; n=111. All the RMSEs and rRMSEs are listed in Table 6.4.

Table 6.4 The RMSEs and rRMSEs for three different solutions

Force component	Method	RMSE (N)	rRMSE (%)
Longitudinal	ID & FD	410.5571	40.44
	Opensim	493.3241	48.59
	Fm	454.4610	44.77

Vertical	ID & FD	299.1497	25.93
	Opensim	460.7948	39.94
	Fm	382.3423	33.14
Lateral	ID & FD	88.8655	66.58
	Opensim	81.2163	60.85
	Fm	98.6688	73.92

As expected, the RMSEs of 'ID & FD' in longitudinal and vertical directions are less than those in the other two solutions. In the lateral direction, the RMSE of 'ID & FD' is slightly more than the one in 'Opensim' solution. The rRMSEs see that all the three methods predict the best results in the vertical direction but the worst results in the lateral direction.

During human walking, the most important component of contact force at each joint is vertical contact force. From the 'eKnee' force curves, we can see the average value of the vertical component is around 2 to 3 times of the longitudinal force, and about 10 times of the lateral component. Therefore, comparing the RMSEs in vertical and longitudinal directions is more important than in the lateral direction. It can be seen that, in vertical and longitudinal directions, the 'ID&FD' method provides much better force prediction over the 'Opensim' method. Although the 'Fm' method gives better results than the 'Opensim' method, its prediction accuracy is still lower than the 'ID&FD' method. In the lateral direction, 'Opensim' method gives the best prediction among all three methods though its rRMSE is only slightly higher than the ID&FD method by 5.73%. Considering the RMSE and rRMSE of all three methods in all three directions, we conclude that 'ID&FD' method is the best method on predicting

individual muscle force and contact force at the knee joint among all three methods tested in this study.

6.6 Conclusions

In this study, a novel method to evaluate individual muscle forces during walking was proposed by using a combine inverse dynamics with forward dynamics optimizations method. 19 individual muscle forces and muscle fibre lengths are optimized. The muscle model used to construct our neuromusculoskeletal model in the optimization scheme was the muscle model we presented in Chapter 3, where more physiological characteristics and intrinsic properties were involved. The calibration process was conducted to find out the best muscle parameters used in the optimization scheme. The EMG data collected in the Grand Challenge Competition was treated as the initial guess of the optimal variables in our method, which proved the EMG data could help the algorithm efficiently find out the right searching direction, and it would inspire us in ways that how to take advantage of the EMG data for further research. The simulation results were compared with the results from conventional optimization method, the commercial software and the experimental data. The comparison shows our results have a good agreement with the experimental data rather than the other two ways.

Before evaluating the individual muscle forces, the maximum isometric muscle force and the slack tendon length of each muscle were calibrated by using a set of novel optimization approaches. Not only did the calibration process provide better parameters for constructing the human neuromusculoskeletal model during walking, but also it proved the parameters sensitivity in muscle force estimation during walking.

The calibrated muscle parameters made the optimization algorithm more efficient and accurate.

The muscle resultant forces were calculated by using the optimized individual muscle forces. The joint resultant forces obtained from the inverse dynamics in conjunction with the muscle resultant forces were used to calculate the knee joint contact forces.

An experimental validation was conducted by comparing the results of the optimization scheme proposed by us, the results of the conventional static optimization method and the results of the OpenSim software against the measured joint contact forces in all three directions. The results of the method we presented agreed the experimental data better than the others. Some of the discrepancies between our result and the experimental data are due to the model simplification and limitation of current understanding of physiology. Also, the muscle's parameters, other passive tissue and the cost function may also influence the results based on our method. The experiment error could have influenced the measurement data, which makes our method more reasonable and reliable.

Chapter 7. Conclusions and Future Work

7.1 Overview of the Thesis

The objective of the study in this thesis is to develop and validate the computational techniques, which is for quantitatively investigating the mechanical loadings in the musculoskeletal system during human standing and walking. The computational models can be employed to calculate the individual muscle forces prior to the physical measurements, if the physiological characteristics and the dynamic couplings are considered during computer simulation. This can lead to a better understanding of the dynamic performances of the musculoskeletal system during standing and locomotion, and hence provide sound scientific foundation for clinical diagnosis, treatment and rehabilitation intervention development. The research work in this thesis includes four major parts: modelling the representation of the mechanical behaviour of a single skeletal muscle group; analysing the musculoskeletal performance during standing, which includes the influence of the muscle intrinsic properties on dynamic stability and the interplay between stability and energy expenditure; constructing a three-dimensional musculoskeletal model to simulate human walking; developing a novel framework to assess the individual muscular loading during human walking and an experimental validation using the Grand Challenge Competition database.

In Chapter 3, an improved Hill-type model has been developed to represent the mechanical behaviour of skeletal muscles from neural input through to muscular force production by integrating the latest knowledge based on muscle physiology. The

muscle dynamic process is divided into the activation dynamics and the contraction dynamics. In the activation dynamics, two continuous first order dynamic systems representing the neural excitation and the muscle activation processes were represented using discretization functions in exponential form. The time constant for the increasing active state was set bigger than that for the decreasing active state in muscle activation process. In the contraction dynamics, an assumption about muscle fibre deformation during contraction was proposed, where the muscle force-length relationship was directly linked to the time dependent pennation angle. We used a continuous function to represent muscle fibre's force-velocity relationship, which can make the force generated by the muscle contractile element continuous when muscle fibre contraction velocity changes direction. Moreover, a function which can better reflect the non-linear force-length relationship of the tendon was used. A set of isometric contraction simulations was conducted, and reasonable results of dynamic muscle responses were reproduced compared with literature data.

In Chapter 4, we firstly investigated the influence of muscle intrinsic properties on the musculoskeletal system stability, and an inverted pendulum model activated by a pair of antagonistic muscles was developed to simulate human standing balance. In the simulation study, the CE's force-length relationship, the CE's force-velocity relationship, the parallel elastic element and the series elastic element were removed separately to examine their effects on the system response to external perturbation. The simulation results suggested that the muscle fibre pennation angle had little effect on the system performance while the CE's force-velocity relationship had the largest effects on the musculoskeletal system stability. Another investigation was to assess the interplay between stability and energy during human standing balance using a

musculoskeletal model with 6 ankle extensor and flexor muscles. A multiple optimization scheme was used based on four different criteria: minimizing the change of potential energy, minimizing the change of ankle angle excursion, minimizing the mechanical expenditure and minimizing the metabolic energy cost. The results indicated that there was a strong dependence between energy consumption and system stability, where any strategy attempting to reduce energy cost would decrease the system stability level. Additionally, it appeared that minimizing energy expenditure was more important than maximising system stability during standing balance.

In Chapter 5, a three-dimensional musculoskeletal model with 13 body segments and 98 muscles was constructed using OpenSim software package to simulate human walking. The gait measurement database provided by the Grand Challenge Competition was used to support and validate the model. The existing whole body human musculoskeletal model in OpenSim was scaled by using the static standing trails to fit the subject-specific anthropometric data, and the generalized coordinates that 'best match' the measured marker data were calculated by using an inverse kinematics approach. The muscle moment arms of 19 major muscle groups on the right leg over an entire gait cycle were calculated. Whereas, based on the recorded ground reaction forces and gait motions, the net muscle moments at the three lower limb joints: ankle, knee and hip over a complete gait cycle were calculated using the inverse dynamics method. Compared to literature data, the results are reasonable in terms of both magnitude and trend.

To evaluate the individual muscle forces during walking, a novel optimization based computational framework was developed in Chapter 6. Before the optimization, a

specially designed calibration process was performed to identify the key model parameters for each muscle group, which included the maximum isometric muscle force and the slack tendon length. The optimization scheme was conducted on a human lower limb neuromusculoskeletal model with 19 prime movers within right leg's stance phase. Based on the calibrated model parameters, an optimization scheme was used to estimate the mechanical loadings at each muscle group. Differing from conventional methods for solving the load sharing problem, the proposed new scheme integrated a dynamic time-dependent process to represent the muscle contraction mechanics into an inverse dynamics based static optimization formulation. The optimization scheme was applied to a three-dimensional musculoskeletal model to assess the dynamic forces at 19 major leg muscles during walking gait. The experimental validation suggested that the new approach proposed here provided more accurate estimation of the individual muscular forces than the conventional static optimization method and also the OpenSim software package.

7.2 Conclusions and Original Contributions

In this thesis, many original and novel works have been conducted to improve our understanding of musculoskeletal biomechanics. Firstly, an improved Hill-typed muscle model was developed to represent the mechanical behaviour of the skeletal muscles in response to the neural stimulations, which involved two dynamic processes from neural inputs to muscle activations and also a subsequent process to represent muscle contraction dynamics using contractile element, series and parallel elastic elements. Compared to the previous muscle models, this model has several improved representations.

A novel investigation was conducted to assess the effects of muscle intrinsic properties on the musculoskeletal system stability during standing. An inverted pendulum model regulated by a pair of antagonistic muscles was developed to simulate human standing in the sagittal plane. It was used to predict changes of system stability level due to muscle property changes. It was found that pennation angle had no effect on dynamic stability, whereas the force-velocity relationship of the contractile element demonstrated the largest effects on system stability.

Furthermore, a novel investigation was also performed to evaluate the interplay between the energy cost and the body stability in the musculoskeletal system during standing. A musculoskeletal model with six ankle flexor and extensor muscles was used to predict the human body dynamic responses subjected to an external perturbation. A multi-objective optimization scheme involving both energy and stability criteria has been used. The results suggested that highly dependent relationship existed between energy cost and system stability.

To investigate the musculoskeletal performance during walking, a three-dimensional model with 13 body segments and 98 muscle groups was constructed using OpenSim software package. A series of calculation was used to make the model fit the subject-specific anthropometric and kinematic database.

Finally, a novel computational framework for individual muscle force evaluation has been proposed, which involves the combined use of dynamic integration of muscle contraction mechanics, inverse dynamics method and stress-based static optimization scheme. The experimental validation suggested that the new method provided more

accurate muscle force estimations than the conventional static optimisation method and the OpenSim software.

7.3 Future Work

In order to obtain a thorough understanding of the musculoskeletal system performance during human standing and walking, more in-depth experimental and computer simulation works are required. The works include further experimental investigation on the mechanics of musculotendon units, more experimental studies on the human postural balance and walking dynamics, the development of more efficient muscle parameters calibration algorithm, the exploration of dynamic neural constraints for solving load sharing problem during walking, and more efficient and accurate methods to further investigate the physiological and biomechanical factors involved in mechanical loading evaluation during standing and walking.

The musculotendon unit model proposed in this thesis focused on the deformation of the muscle along its contraction direction while in muscle cross-sectional plane, the thickness was a constant value during contraction. In future work, three-dimensional deformation should be considered. In our study, the muscle fibre's force-velocity relationship is the relationship between normalized force and normalized velocity. We have chosen three parameters to normalize the muscle contraction velocity, where only one parameter is a muscle-specific parameter (F_{mo}, the maximum isometric muscle force). In the future, we will figure out the other two parameters to express the muscle fibre's force–velocity relationship accurately and satisfy the physiological requirement. In addition, the muscle force-length and force-velocity relationships were based on other people's empirical functions, and we could employ Ultrasound or

Magnetic Resonance Imaging techniques to measure the muscle fibre's length and its contraction velocity in the future.

The musculoskeletal model of human standing we used was a two-dimensional model, and the number of muscle was less than the number of muscle around the real ankle joint. Also, if the muscles' EMG data and motion data could be recorded during standing, they could provide a reliable resource to assist the analysis of muscle dynamic response as well as to validate the model we constructed. We will develop a three-dimensional musculoskeletal model of human standing in the future.

Due to the complexity of the human neuromusculoskeletal system, much work still needs to be conducted on computational modelling. A large scale three-dimensional walking model with more complex joint rotations and more muscle groups would provide greater insight into joint kinetics, muscle mechanics. Furthermore, due to the time consuming calibration algorithm we used, it would take three days to finish one computational cycle. We should develop a more efficient and robust strategy to calibrate the muscle parameters for modelling in the future. The exploration of dynamic neural constraints would be a fantastic work in the future. It could be simply described that at each time step, the optimal muscle force would be constrained by the neural inputs in the previous time steps. The lower bound and upper bound of the muscle force would be the force values corresponding to the neural inputs as 0 and 1.

Last, but not least, more experimental studies are needed to provide comprehensive in-vivo physiological and biomechanical database and validate the computational

frameworks in the future.

Appendix A. Publications Arising from This Thesis Work

Peer-reviewed Conference:

Lei Chen and Lin Ren. The Influence of Intrinsic Muscle Properties on Musculoskeletal System Stability : a Modelling Study. The 3rd International Conference of Bionic Engineering, Zhuhai, September, 2010.

Lei Chen and Lei Ren, The Interplay between Stability and Energy Expenditure in Postural Control: a Modelling Study. International Society of Biomechanics Congress XXIII, Brussels, July, 2011.

Peer-reviewed Journal:

Lin Chen and Lei Ren. (2010). The Influence of Intrinsic Muscle Properties on Musculoskeletal System Stability : a Modelling Study. Journal of Bionic Engineering, Vol. 7, pp. S158-S165

Lin Chen and Lei Ren. (2012). The Dynamic Performance of Musculoskeletal System in Standing Postural Control: Balance between Energy Cost and Body Stability. Proceedings of the IMechE, Part H: Journal of Engineering in Medicine (To be submitted)

Lin Chen and Lei Ren (2012). A New Formulation to Solve the Loading Sharing Problem in Musculoskeletal Biomechanics. Medical Physics and Engineering (To be submitted)

Appendix B. Matlab files in the thesis

Matlab file name	Function
Chapter 3	
Neuroex.m	Calculate muscle neural excitation
Muscleac.m	Calculate muscle activation
Musclefl.m	Calculate muscle fibre force from force-length relationship
Musclefv.m	Calculate muscle fibre force from force-velocity relationship
Musclefp.m	Calculate muscle fibre parallel element force
Muscleft.m	Calculate muscle tendon force
Muscleunit.m	Musculotendon unit model
Musclessw.m	Calculate dynamic response of musculotendon stimulated by single square wave neural input
Musclepsw.m	Calculate dynamic response of musculotendon stimulated by periodic square wave neural input
Chapter 4	
Stabilityfull.m	Calculate the dynamic response of the musculoskeletal system with full intrinsic properties to the perturbation
Stabilitypennation.m	Calculate the dynamic response of the musculoskeletal system with different pennation angle to the perturbation
Stabilityfl.m	Calculate the dynamic response of the

	musculoskeletal system without force-length relationship to the perturbation
Stabilityfv.m	Calculate the dynamic response of the musculoskeletal system without force-velocity relationship to the perturbation
Stabilitype.m	Calculate the dynamic response of the musculoskeletal system without parallel element to the perturbation
Stabilityse.m	Calculate the dynamic response of the musculoskeletal system without tendon to the perturbation
Stabilitya.m	Calculate the dynamic response of the musculoskeletal system under different muscle activation levels to the perturbation
Standmain.m	Main function for analyzing dynamic response of human neuromusculoskeletal system subjects to perturbation during walking
Standca.m	Calculate the dynamic response of human neuromusculoskeletal system in Criterion 1
Standcb.m	Calculate the dynamic response of human neuromusculoskeletal system in Criterion 2
Standcc.m	Calculate the dynamic response of human neuromusculoskeletal system in Criterion 3
Standcd.m	Calculate the dynamic response of human neuromusculoskeletal system in Criterion 4
Standmulti.m	Calculate the dynamic response of human neuromusculoskeletal system in both Criterion 1 and Criterion 3
Standmeta.m	Calculate the metabolic energy expenditure
Standmuscle.m	Calculate the muscle work

Chapter 5	
Resamples.m	Resample the experimental data
Filters.m	Filter the experimental data
Transformation.m	Coordination system transformation
Chapter 6	
Fmomain.m	Main function for maximum isometric muscle fibre force calibration
Fmofun.m	Objective function for maximum isometric muscle fibre force calibration
Fmocon.m	Constraints function for maximum isometric muscle fibre force calibration
Lstmain.m	Main function for slack tendon length calibration
Lstfun.m	Outer layer objective function for slack tendon length calibration
Lstcon.m	Outer layer constraints function for slack tendon length calibration
Lstfunna.m	Inner layer initial step objective function for slack tendon length calibration
Lstconna.m	Inner layer initial step constraints function for slack tendon length calibration
Lstfunnb.m	Inner layer objective function for slack tendon length calibration
Lstconnb.m	Inner layer constraints function for slack tendon length calibration
Fmfmomain.m	Main function for calculation of individual muscle forces based on optimization scheme based on muscle force only
Fmfmofun.m	Objective function for calculation of

	individual muscle forces based on optimization scheme based on muscle force only
Fmfmocon.m	Constraints function for calculation of individual muscle forces based on optimization scheme based on muscle force only
Fmnovelmain.m	Main function for calculation of individual muscle forces based on optimization scheme based on muscle activation and contraction dynamics
Initialmain.m	Initial step main function for calculation of individual muscle forces based on optimization scheme based on muscle activation and contraction dynamics
Initialfun.m	Initial step objective function for calculation of individual muscle forces based on optimization scheme based on muscle activation and contraction dynamics
Initialcon.m	Initial step constraints function for calculation of individual muscle forces based on optimization scheme based on muscle activation and contraction dynamics
Fmnovelfun.m	Objective function for calculation of individual muscle forces based on optimization scheme based on muscle activation and contraction dynamics
Fmnovelcon.m	Constraints function for calculation of individual muscle forces based on optimization scheme based on muscle activation and contraction dynamics
Inversev.m	Inverse force-velocity function (used in chapter 3 as well)
Transform.m	Muscle origin and insertion transformation
Incersedyn.m	Calculate joint resultant forces at knee joint
Contactmain.	Main function for joint contact forces calculation

Appendix C The Origin and Axis Directions of the Coordinate System of the eKnee

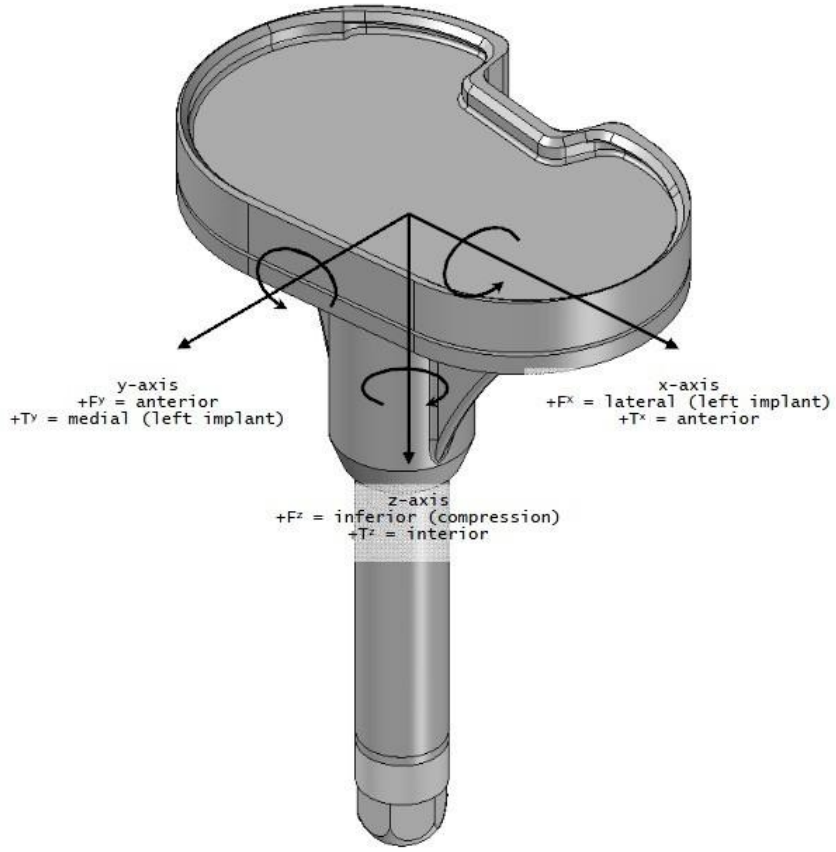

The origin of the coordinate system is located at the stem centre and the surface of tray. The figure shows the coordinate system of the eKnee implanted in the left knee joint. For the right knee implant, the coordinate system are the same as it except that the x-axis points medially instead.

Appendix D Java Applet files in thesis

File name	Function
Subject01_Setup_Scale.xml	Main file for scaling.
gait_Scale_Markerset.xml	Marker set for scaling. It contains the set of virtual markers that are placed on the body segments of the model.
Subject01_Scale_Measurementset.xml	Measurement set for scaling. It contains pairs of experimental markers, the distance between which are used to scale the generic musculoskeletal model.
Subject01_Scale_Scaleset.xml	Scale set for the scaling. It contains a set of scale factors to be applied to the generic musculoskeletal model
Subject01_Scale_Tasks.xml	Inverse kinematics tasks for the scaling.
Subject01_Setup_IK.xml	Main file for inverse kinematics.
Subject01_IK_Tasks.xml	Set up each maker and coordinate weight
Subject01_Setup_InverseDynamics.xml	Main file for inverse dynamics.

An example of scale setup file

<?xml version="1.0" encoding="UTF-8"?>

-<ScaleTool name="subject01">

<!--Mass of the subject in kg. -->

<mass> 67 </mass>

```
<!--Height of the subject in mm.).-->

 <height> 1720 </height>

<!--Age of the subject in years.-->

 <age> 30 </age>

<!--Specifies the name of the unscaled model (.osim) and the marker set.-->

 -<GenericModelMaker name="">

<!--Model file (.osim) for the unscaled model.-->

 <model_file> gait2354_simbody.osim </model_file>

<!--Set of model markers used to scale the model..-->

 <marker_set_file> gait_Scale_Markerset.xml </marker_set_file>
</GenericModelMaker>

<!--Specifies parameters for scaling the model.-->

 -<ModelScaler name="">

<!--Specifies the scaling method and order.-->

 <scaling_order> measurements </scaling_order>

<!--Specifies the measurements by which body segments are to be scaled.-->

 <MeasurementSet file=" Subject01_Scale_Measurementset.xml "/>

<!--TRC file (.trc) containing the marker positions used for measurement-based
scaling.-->

 <marker_file> phd02_static.trc </marker_file>

<!--Time range over which to average marker-pair distances in the marker file
(.trc) for measurement-based scaling.-->

 <time_range> 0.05 1.90 </time_range>

<!--Flag (true or false) indicating whether or not to preserve relative mass
between segments.-->

 <preserve_mass_distribution> true </preserve_mass_distribution>

<!--Name of SIMM joint file to write when done scaling-->
```

```
 <output_joint_file> subject01_scaledOnly.jnt </output_joint_file>

<!--Name of SIMM muscle file to write when done scaling.-->

 <output_muscle_file> subject01_scaledOnly.msl </output_muscle_file>

<!--Name of OpenSim model file (.osim) to write when done scaling.-->

 <output_model_file> subject01_scaledOnly.osim </output_model_file>

<!--Name of file to write containing the scale factors that were applied to the
unscaled model-->

 <output_scale_file> subject01_scaleSet_applied.xml </output_scale_file>

 </ModelScaler>

<!--Specifies parameters for placing markers on the model once a model is
scaled.-->

 -<MarkerPlacer name="">

<!--TRC file (.trc) containing the time history of experimental marker.-->

 <marker_file> subject01_static.trc </marker_file>

<!--Task set used to specify weights used in the IK computation of the static
pose.-->

 <IKTaskSet file=" Subject01_Scale_Tasks.xml"/>

<!--Time range over which the marker positions are averaged.-->

 <time_range> 0.05 1.90 </time_range>

</MarkerPlacer>

 </ScaleTool>
```

Reference

Ackland, D. C., Lin, Y. C., and Pandy, M. G. (2012) Sensitivity of model predictions of muscle function to changes in moment arms and muscle-tendon properties: a Monte-Carlo analysis, Journal of biomechanics, 45(8).p.1463-1471

Amarantini, D. and Martin, L. (2004) A method to combine numerical optimization and EMG data for the estimation of joint moments under dynamic conditions,Journal of Biomechanics, 37(9).p.1394-1404

Anderson, F. C. and Pandy, M. G. (2001) Dynamic optimization of human walking, Journal of Biomechanical Engineering-Transactions of the ASME, 123(5).p.381-390

Andriacchi, T. P., Alexander, E. J., Toney, M. K. and Dyrby, C. (1998) A point cluster method for invivo motion analysis: Applied to a study of knee kinematics, Journal of Biomechanical Engineering-Transactions of the ASME, 120(6).p.743-749

Arnold, A. S., Asakawa, D. J. and Delp. S. L. (2000) Do the hamstrings and adductors contribute to excessive internal rotation of the hip in persons with cerebral palsy? Gait and Posture. 11(3). p.181-190

Arnold, A. S., Blemker. S. S. and Delp. S. L. (2001) Evaluation of a deformable musculoskeletal model for estimating muscle-tendon lengths during crouch gait. Annals of Biomedical Engineering.29(3). p.263-274

Arnold, A. S. and Delp. S. L. (2001) Rotational moment arms of the medial hamstrings and adductors vary with femoral geometry and limb position: implications for the treatment of internally-rotated gait. Journal of Biomechanics. 34(4). p.437-447

Baratta, R. and Solomonow, M. (1990) The dynamic-response model of 9 different skeletal-muscles, IEEE Transactions on Biomedical Engineering, 37(3).p.243-251

Bartlett, R (1997) Introduction to sports biomechanics: analysing human movement patterns, New York, NY: Routledge.

Benedetti, A and Cappozzo (1994) Anatomical landmark definition and identification in computer aided movement analysis in a rehabilitation context II (Internal Report).

Benninghoff A and Rollhauser H. (1952).ZurinnerenMechanik des gefiedertenMuskels. Pflugers Arch 254(6). p.527–548.

Bernotas, L. A., Crago, P. E. and Chizeck, H. J. (1986) A discrete-time model of

electrically stimulated muscle, IEEE Transactions on Biomedical Engineering, 33(9).p.829-838

Bisi, M. C., Stagni, R., Gnudi, G. (2012) Sensitivity analysis of an energetic muscle model applied at whole body level in recumbent pedalling, Computer Methods in Biomechanics and Biomedical Engineering, 15(5). p.527-538

Blemker, S. S. and Delp, S. L. (2005) Three-dimensional representation of complex muscle architectures and geometries. Annals of Biomedical Engineering 33(5) p.661-673.

Bobet, J., Gossen, E. R. and Stein, R. B. (2005) A comparison of models of force production during stimulated isometric ankle dorsiflexion in humans, IEEE Transactions on Neural Systems and Rehabilitation Engineering, 13(4).p.444-451

Brown, E, I., Scott, H, S., Loeb and E, G. (1995) Preflexes – programmable, high-gain, zero-delay intrinsic responses to perturbed musculoskeletal systems. Society of Neuroscience Abstract, 21:1433 (Abstract)

Brown, I. E. and Loeb, G. E. (2000) A reductionist approach to creating and using neuromusculoskeletal models, Biomechanics and neural control of posture and movement. New York, NY: Springer. p.148-163

Bullimore, S. R. and Burn, J. F. (2007) Ability of the planar spring-mass model to predict mechanical parameters in running humans. Journal of Theoretical Biology 248(4). p.686-695.

Burkitt, H. G., Young, B. and Heath, J. W. (1993) Wheater's Functional Histology, Third Edition. Edinburgh: Churchill Livingstone.

Cacioppo, J, T., Tassinary, L, G., and Vanman, E. J. (2007) Handbook of Psychophysiology,The Skeletomotor system: surface electromyography, Third Edition., Cambridge: Cambridge University Press.

Casadio, M., Morasso, P. G. and Sanguineti, V. (2005) Direct measurement of ankle stiffness during quiet standing: implications for control modelling and clinical application. Gait & Posture. 21(4). p.410-424.

Chapman, A. E. and Harrower, P. T. (1977) Linear approximations of muscle mechanics in isometric contraction, Biological Cybernetics, 27(1).p.1-7

Chen, L. and Ren, L. (2010). The Influence of Intrinsic Muscle Properties on Musculoskeletal System Stability: a Modelling Study. Journal of Bionic Engineering, Vol. 7, S158-S165

Cheng, K. B. and Hubbard, M. (2004) Optimal jumping strategies from compliant surfaces: A simple model of springboard standing jumps. Human Movement Science 23(1). p.35-48.

Cheng, K. B. and Hubbard, M. (2005). Optimal compliant-surface jumping: a multi-segment model of springboard standing jumps. Journal of Biomechanics 38(9) p.1822-1829.

Chia, T. L., Chow, P. C. and Chizeck, H. J. (1991) Recursive parameter-identification of constrained system – an application to electrically stimulated muscle, IEEE Transactions on Biomedical Engineering, 38(5).p.429-442

Redl, C., Gfoehler, M. and Pandy, M. G. (2007) Sensitivity of muscle force estimates to variations in muscle-tendon properties, Human Movement Science, 26 (2), p.306-319

Collins, J.J., (1995) The redundant nature of locomotor optimization laws. Journal of Biomechanics.28(3).p.251-267

Crowninshield, R. D. (1978) Use of optimization techniques to predict muscle forces, Journal of Biomechanical Engineering-Transactions of the ASME, 100(2).p.88-92

Crowninshield, R. D. and Brand, R. A. (1981) A physiologically based criterion of muscle force prediction in locomotion, Journal of Biomechanics, 14(11).p.793-801

Delp, S. L., Anderson, F. C., Arnold, A. S., Loan, P., Habib, A., John, C. T., Guendelman, E. and Thelen, D. G. (2007) OpenSim: Open-Source Software to Create and Analyze Dynamic Simulations of Movement. IEEE Transaction on biomedical engineering. 54(11). p.1940-1950

Dennerlein, J. T. (2005) Finger flexor tendon forces are a complex function of finger joint motions and fingertip forces, Journal of hand therapy, 18(2).p.120-127

Dennerlein, J. T., Diao, E., Mote, C. D. and Rempel, D. M. (1998) Tensions of the flexor digitorumsuperficialis are higher than a current model predicts, Journal of Biomechanics, 31(4).p.295-301

Dennerlein, J. T., Diao, E., Mote, C. D. and Rempel, D. M. (1999) In vivo finger flexor tendon force while tapping on a keyswitch, Journal of Orthopaedic Research, 17(2).p.178-184

Ding, J., Wexler, A. S. and Binder-MacLeod, S. A. (2002) A mathematical model that predicts the force-frequency relationship of human skeletal muscle, Muscle & Nerve, 26(4).p.477-485

Durfee, W. K. and Maclean, K. E. (1989) Methods for estimating isometric recruitment curves of electrically stimulated muscle, IEEE Transactions on Biomedical Engineering, 36(7).p.654-667

Erdemir, A., McLean, S., Herzog, W. and van den Bogert, A. J. (2007) Model-based estimation of muscle forces exerted during movements, Clinical Biomechanics, 22(2).p.131-154

Erdemir, A. and Piazza, S. J. (2004) Changes in foot loading following plantar fasciotomy: a computer modelling study, Journal of Biomechanical Engineering-Transactions of the ASME, 126(2).p.237-243

Fenn, W. O. and Marsh, B. S. (1935) Muscular force at different speeds of shortening, Journal of Physiology-London, 85(3).p.277-297

Fernandez, J. W. and Pandy, M. G. (2006) Integrating modelling and experiments to assess dynamic musculoskeletal function in humans, Experimental Physiology 91(2). p.371-382.

Finni, T., Komi, P. V. and Lukkariniemi, J. (1998) Achilles tendon loading during walking: application of a novel optic fiber technique, European Journal of Applied Physiology and Occupational Physiology, 77(3).p289-291

Fleming, B. C. and Beynnon, B. D. (2004) In vivo measurement of ligament/tendon strains and forces: a review, Annals of Biomedical Engineering, 32(3).p.318-328

Friederich, J. A. and Brand, R. A. (1990) Muscle fibre architecture in the human lower limb, Journal of Biomechanics, 23(1).p.91-95

Fung, Y. C. (1971) Comparison of different models of the heart muscle, Journal of Biomechanics, 4(4).p.289-295

Ghigliazza, R. M. and Holmes, P. (2005) Towards a neuromechanical model for insect locomotion: Hybrid dynamical systems, Regular & Chaotic Dynamics, 10(2).p.193-225

Glitsch, U. and Baumann, W. (1997) The three-dimensional determination of internal loads in the lower extremity, Journal of Biomechanics, 30(11-12).p.1123-1131

Gordon, A. M., Huxley, A. F. and Julian, F. J. (1966) The variation in isometric tension with sarcomere length in vertebrate muscle fibres, Journal of Physiology-London, 184(1).p.170-192

Hallemans, A., Aerts, P., Otten, B., De Deyn, P. P. and De Clercq, D. (2004)

Mechanical energy in toddler gait - A trade-off between economy and stability?, Journal of Experimental Biology, 207(14).p.2417-2431

Happee, R. (1994) Inverse dynamic optimization including muscular dynamics, a new simulation method applied to goal-directed movement, Journal of Biomechanics, 27(7). p. 953-960

Harrison, A. J., Keane, S. P. and Coglan, J. (2004) Force-velocity relationship and stretch-shortening cycle function in sprint and endurance athletes, Journal of Strength and Conditioning Research, 18(3).p.473-479

Hatze, H. (1977) Amyocybernetic control model of skeletal muscle, Biological Cybernetics, 25(2).p.103-119

Hatze, H. (1981) A comprehensive model for human motion simulation and its application to the take-off phase of the long jump, Journal of Biomechanics, 14(3). p.135-142

Hill, A. V. (1938) The heat of shortening and the dynamic constants of muscle, Proceedings of the Royal Society B-Biological Sciences, 126(843).p.136-195

Hogan, N. (1984) Adaptive-control of mechanical impedance by coactivation of antagonist muscles, IEEE Transactions on Automatic Control, 29(8).p.681-690

Holmes, M. W. and Keir, P. J. (2012) Posture and hand load alter muscular response to sudden elbow perturbations. Journal of Electromyography and Kinesiology. 22(2). p.191-198.

Houdijk, H., Fickert, R., Van Velzen, J. and Van Bennekom, C. (2009) The energy cost for balance control during upright standing, Gait & Posture, 30(2).p.150-154

Houdijk, H., terHoeve, N., Nooijen, C., Rijntjes, D., Tolsma, M. and Lamoth, C. (2010) Energy expenditure of stroke patients during postural control tasks, Gait & Posture, 32(3).p.321-326

Hunt, K. J., Munih, M., Donaldson, N. N. and Barr, F. M. D. (1998) Investigation of the Hammerstein hypothesis in the modeling of electrically stimulated muscle, IEEE Transactions on Biomedical Engineering, 45(8).p.998-1009

Huxley, A. F. (1957) Muscle structure and theories of contraction, Progress in Biophysics and Biophysical Chemistry, 7.p.255-318

Jindrich, D. L. and Full, R. J. (2002) Dynamic stabilization of rapid hexapedal locomotion, Journal of Experimental Biology, 205(18).p.2803-2823

Kaufman, K. R., An, K. W.,Litchy, W. J. and Chao, E. Y. (1991) Physiological prediction of muscle forces-I. theoretical formulation, Neuroscience 40(3), p.781-792

Koo, T. K. and Mak, A. F. (2005) Feasibility of using EMG driven neuromusculoskeletal model for prediction of dynamic movement of the elbow, Journal of Electromyography and Kinesiology, 15(1).p.12-26

Kutz, M., Standard (2003) Handbook of Biomedical Engineering and Design, McGraw-Hill Professional Publishing

Lakie, M., Caplan, N. and Loram, I. D. (2003) Human balancing of an inverted pendulum with a compliant linkage: neural control by anticipatory intermittent bias. Journal of Physiology. 551(Pt 1). p.357-370.

Lappin, A. K., Monroy, J. A., Pilarski, J. Q., Zepnewski, E. D., Pierotti, D. J. and Nishikawa, K. C. (2006) Storage and recovery of elastic potential energy powers ballistic prey capture in toads, Journal of Experimental Biology, 209(13).p.2535-2553

Lloyd, D. G. and Besier, T. F. (2003) An EMG-driven musculoskeletal model to estimate muscle forces and knee joint moments in vivo, Journal of Biomechanics, 36(6).p.765-776

Loram, I. D., Maganaris, C. N. and Lakie, M. (2004) Paradoxical muscle movement in human standing. Journal of Physiology. 556(Pt 3). p.683-689

Loram, I. D., Maganaris, C. N. and Lakie, M. (2005) Active, non-spring-like muscle movements in human postural sway: how might paradoxical changes in muscle length be produced? Journal of Physiology. 564(Pt 1). p.281-293.

Loram, I. D., Maganaris, C. N. and Lakie, M. (2006) Use of ultrasound to make noninvasive in vivo measurement of continuous changes in human muscle contractile length. Journal of Applied Physiology. 100(4). p.1311-1323.

Mcmahon, T. A. (1984) Muscles, reflex, and locomotion. Princeton University Press, New Jersey

Mannard, A. and Stein, R. B. (1973) Determination of the frequency response of isometric soleus muscle in the cat using random nerve stimulation, Journal of Physiology-London, 229(2).p.275-296

Martin, B. (23 October 1999). A Genealogy of Biomechanics.23rd Annual Conference of the American Society of Biomechanics.

Martin, P. E., Rothstein, D. E. and Larish, D. D. (1992) Effects of age and physical activity status on the speed-aerobic demand relationship of walking, Journal of

Applied Physiology, 73(1).p.200-206

Mason, S. F (1962) A History of the Sciences, New York, NY: Collier Books.

McGinniS, P. M. (1999) Biomechanics of Sport and Exercise, Third Edition, Champaign, IL.: Human Kinetics.

McLean, S.G., Huang, X., Su, A., van den Bogert, A.J.(2004) Sagittal plane biomechanics cannot injure the ACL during sidestep cutting, Clinical Biomechanics, 19 (8). p.828-838

McLean, S.G., Su, A., van den Bogert, A.J. (2003). Development and validation of a 3-D model to predict knee joint loading during dynamic movement, Journal of Biomechanical Engineering, 125 (6).p.864-874

Morasso, P. G. and Sanguineti, V. (2002) Ankle muscle stiffness alone cannot stabilize balance during quiet standing, Journal of Neurophysiology, 88(4).p.2157-2162

Mutungi, G. and Ranatunga, K. W. (2000) Sarcomere length changes during end-held (isometric) contractions in intact mammalian (rat) fast and slow muscle fibres. Journal of Muscle Research and Cell Motility 21(6). p.565-575.

Nagano, A., Umberger, B. R., Marzke, M. W. and Gerritsen, K. G.(2005) Neuromusculoskeletal computer modeling and simulation of upright, straight-legged, bipedal locomotion of Australopithecus afarensis (AL 288-1). American Journal of Physical Anthropology 126(1). p.2-13.

Nakazawa, K., Kawashima, N., and Akai, M. (2009) Effect of different preparatory states on the reflex responses of ankle flexor and extensor muscles to a sudden drop of support surface during standing in humans. Journal of Electromyography and Kinesiology. 19(5). p.782-788

Neptune, R. R. and Hull, M. L. (1999) A theoretical analysis of preferred pedaling rate selection in endurance cycling, Journal of Biomechanics, 32(4).p.409-415

Nigg B.M., and Herzog W. (1999) Biomechanics of the Musculo-Skeletal system. Third Edition ,Chichester :Wiley.

Ohta, K., Svinin, M.M., Luo, Z., Hosoe, S., Laboissiere, R. (2004) Optimal trajectory formation of constrained human arm reaching movements, Biological Cybernetics, 91(1). p.23-36

Pedersen, D.R., Brand, R.A., Cheng, C., Arora, J.S. (1987) Direct comparison of muscle force predictions using linear and nonlinear programming, Journal of Biomechanical Engineering, 109(3). p.192-199

Pandy, M. G. (2001). Computer modeling and simulation of human movement. Annual Review of Biomedical Engineering 3. p.245-273.

Pandy, M. G. (2003). Simple and complex models for studying muscle function in walking.Philosophical Transactions of the Royal Society of London Series B-Biological Sciences358(1437). p.1501-1509.

Pandy, M. G., Anderson, F. C. and Hull, D. G. (1992) A parameter optimization approach for the optimal control of large-scale musculoskeletal system, Journal of Biomechanical Engineering-Transactions of the ASME, 114(4).p.450-460

Pandy, M. G., Lin, Y. C. and Kim, H. J. (2010) Muscle coordination of mediolateral balance in normal walking, Journal of Biomechanics, 43(11). p.2055-2064

Patriarco, A. G., Mann, R. W., Simon, S. R. and Mansour, J. M. (1981) An evaluation of the approaches of optimization models in the prediction of muscle forces during human gait, Journal of Biomechanics, 14(8).p.513-525

Piazza, S. J. and Delp, S. L. (1996) The influence of muscles on knee flexion during the swing phase of gait, Journal of Biomechanics, 29(6).p.723-733

Rassier, D. E. and Herzog, W. (2004) Considerations on the history dependence of muscle contraction, Journal of Applied Physiology, 96(2).p.419-427

Redl, C., Gfoehler, M. and Pandy, M. G. (2007) Sensitivity of muscle force estimates to variations in muscle-tendon properties, Human Movement Science, 26(2). p306-319

Ren L, Jones R. K. and Howard D. (2008) Whole-body inverse dynamics over a complete gait cycle based only on measured kinematics.Journal of Biomechanics.41(12). p. 2750-2759.

Richardson, A. G., Slotine, J. J. E., Bizzi, E. and Tresch, M. C. (2005) Intrinsic musculoskeletal properties stabilize wiping movements in the spinalized frog, Journal of Neuroscience, 25(12).

Riener, R. and Quintern, J. (1997) A physiologically based model of muscle activation verified by electrical stimulation, Bioelectrochemistry and Bioenergetics, 43(2). p. 257-264

Robilliard, J. J. and Wilson, A. M. (2005) Prediction of kinetics and kinematics of running animals using an analytical approximation to the planar spring-mass system. Journal of Experimental Biology, 208(23) p.4377-4389.

Rohrle, H., Scholten, R., Sigolotto, C., Sollbach, W. and Kellner, H. (1984) Joint forces in the human pelvis leg skeleton during walking, Journal of Biomechanics, 17(6).p.409-424

Ross, W. D. and Smith, J. A. (1912) On the Motion of Animals. Oxford: Clarendon Press

Runge, C. F., Shupert, C. L., Horak, F. B. and Zajac, F. E.(1999) Ankle and hip postural strategies defined by joint torques. 10(2). p.161-170.

Saha, D., Gard, S., Fatone, S. and Ondra, S. (2007) The effect of trunk-flexed postures on balance and metabolic energy expenditure during standing, Spine, 32(15).p.1605-1611

Schouten, A.C., de Vlugt, E., van der Helm, F.C., Brouwn, G.G. (2001) Optimal posture control of a musculo-skeletal arm model, Biological Cybernetics, 84(2). p.143-152

Schutte, L.M., Rodgers, M.M., Zajac, F.E. (1993) Improving the efficacy of electrical stimulation-induced leg cycle ergometry: an analysis based on a dynamic musculoskeletal model, IEEE Transactions on Rehabilitation Engineering, 1(2).p.109-125.

Shwedyk, E., Balasubramanian, R. and Scott, R. N. (1977) A Nonstationary model for electromyogram, IEEE Transactions on Biomedical Engineering, 24(5).p.417-424

Syme, D. A., Gollock, M., Freeman, M. J. and Gamperl, A. K. (2008) Power isn't everything: Muscle function and energetic costs during steady swimming in Atlantic cod, Physiological and Biochemical Zoology, 81(3). p. 320-335

Thelen, D. G. (2003) Adjustment of muscle mechanics model parameters to simulate dynamic contractions in older adults, Journal of Biomechanical Engineering-Transactions of the ASME, 125(1).p.70-77

Thelen, D.G., Anderson, F.C., and Delp, S.L. (2003) Generating dynamic simulations of movement using computed muscle control, Journal of Biomechanics, 36. p.321–328.

Ting, L. H., Blickhan, R. and Full, R. J. (1994) Dynamic and static stability in hexapedal runners, Journal of Experimental Biology, 197.p.251-269

Tsirakos, D., Baltzopoulos, V. and Bartlett, R. (1997) Inverse optimization: functional and physiological considerations related to the force-sharing problem, Critical

Reviews in Biomedical Engineering, 25(4-5).p.371-407

Umberger, B. R., Gerritsen, K. G. and Martin, P. E. (2003) A model of human muscle energy expenditure, Computer Methods in Biomechanics and Biomedical Engineering, 6(2).p.99-111

van der Helm, F. C. T. (1994) A finite element musculoskeletal model of the shoulder mechanism. Journal of Biomechanics. 27(5). p. 551-569

van Zandwijk, J. P., Bobbert, M. F., Baan, G. C. and Huijing, P. A. (1996) From twitch to tetanus: performance of excitation dynamics optimized for a twitch in predicting tetanic muscle forces. Biological Cybernetics. 75(5). p.409-417

van Zandwijk, J. P., Bobbert, M. F., Harlaar, J. and Hof, A. L. (1998) From twitch to tetanus for human muscle: experimental data and model predictions for m-triceps surae, Biological Cybernetics, 79(2).p.121-130

Viceconti, M., Testi, D., Taddei, F., Martelli, S., Clapworthy, G. J. and Jan, S. V. S. (2006). Biomechanics modelling of the musculoskeletal apparatus: Status and key issues. Proceedings of the IEEE. 94(4). p.725-739

Wagner, H. and Blickhan, R. (1999) Stabilizing function of skeletal muscles: an analytical investigation, Journal of Theoretical Biology, 199(2).p.163-179

Wagner,H. and Blickhan, R. (2003) Stabilizing function of antagonistic neuromusculoskeletal systems: an analytical investigation, Biological Cybernetics, 89(1).p.71-79

Waters, R. L., Lunsford, B. R., Perry, J. and Byrd, R. (1988) Energy-speed relationship of walking: standard tables, Journal of Orthopaedic Research, 6(2).p.215-222

Winter, D. A., Patla, A. E., Rietdyk, S. and Ishac, M. G. (2001) Ankle Muscle Stiffness in the Control of Balance During Quiet Standing, Journal of Neurophysiology, 85(6).p.2630-2633

Winter, D. A. (2009) Biomechanics and Motor Control of Human Movement, John Wiley & Sons, Inc, Hoboken, New Jersey

Winters and Woo (1990) Multiple muscle systems: Biomechanics and movement organization, Springer-Verlag, New York

Winters, J. M., Stark, L (1985) Analysis of fundamental human movement patterns through the use of in-depth antagonistic muscle models, IEEE Transactions on

Biomedical Engineering, 32(10). p.826-839

Yamaguchi, G. T. and Zajac, F. E. (1990) Restoring unassisted natural gait to paraplegics via functional neuromuscular stimulation: a computer-simulation study, IEEE Transactions on Biomedical Engineering, 37(9).p.886-902

Yamaguchi, G.T., Moran, D.W. and Si, J. (1995) A computationally efficient method for solving the redundant problem in biomechanics, Journal of Biomechanics, 28(8).p.999-1005

Zajac, F. E. (1989) Muscle and tendon: properties, models, scaling and application to biomechanics and motor control, Critical Reviews in Biomedical Engineering, 17(4).p.359-411

Zajac, F. E., Neptune, R. R. and Kautz, S.A. (2002) Biomechanics and muscle coordination of human walking: Part I: Introduction to concepts, power transfer, dynamics and simulations. Gait & Posture 16(3). p.215-232.

Zajac, F.E., Neptune, R.R. and Kautz, S.A. (2003) Biomechanics and muscle coordination of human walking: Part II: Lessons from dynamical simulations and clinical implications, Gait &Posture, 17(1). p.1-17

Zakotnik, J., Matheson, T. and Durr, V. (2006) Co-contraction and passive forces facilitate load compensation of aimed limb movements, Journal of Neuroscience, 26(19). p.4995-5007